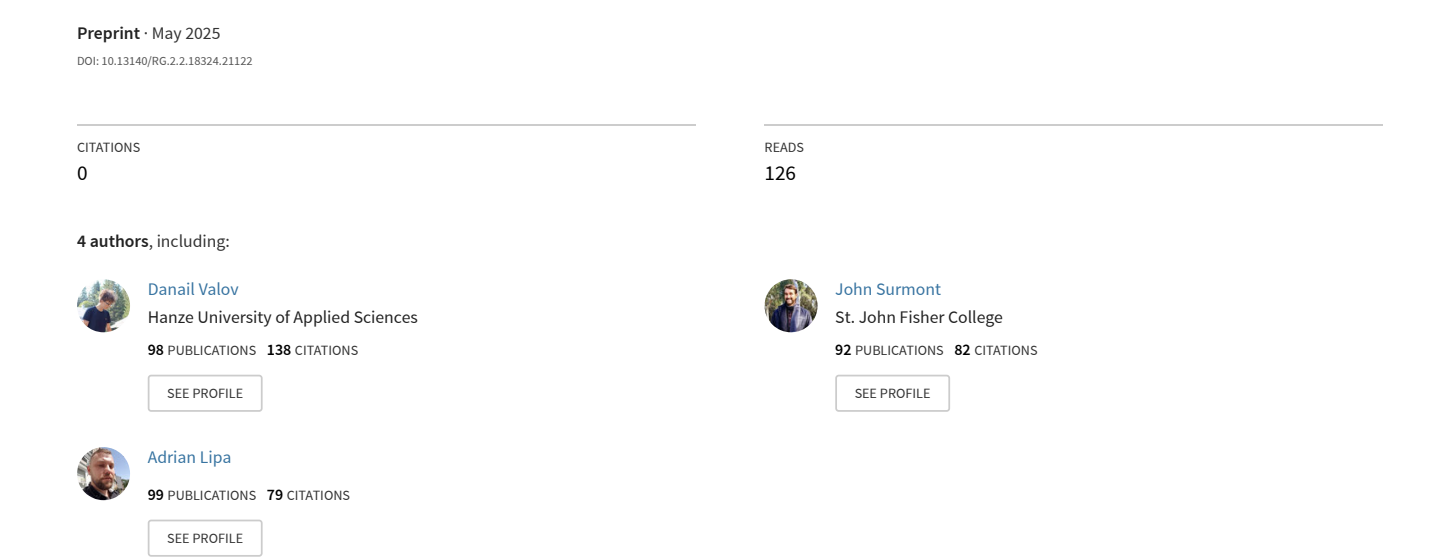
## The Resonant Brain: Fractal, Topological & Symbolic Pathways of Consciousness



# The Resonant Brain: Fractal, Topological & Symbolic Pathways of Consciousness

Danail Valov, John Surmont, Adrian Lipa, Maria Kamecka May 18, 2025

## **Abstract**

Consciousness emerges from the intricate interplay of neural dynamics and symbolic structures. In this work, we introduce a unified framework—The Resonant Brain—that illuminates how the brain encodes, integrates, and transforms information through four interdependent mechanisms: *Memory*, the fractal binding of discrete experiences into enduring symbols; *Phase Intention*, oscillatory fields that steer attention, intuition, and generative thought; *Paradox*, controlled dissociative tension harnessed by novel algebraic operators to sustain multiple, coherent processing streams; and *Return*, recursive feedback loops that close symbolic circuits via sleep, ritual, and recurrent networks.

We define formal operators for each mechanism—Sophia consolidation and retrieval for memory, a multidimensional phase—intention vector for oscillatory alignment, associator brackets and higher-order "pathonion" cascades for paradox mapping, and a return operator quantifying loop depth and reinforcement potential. Topological tools based on knot and braid theory measure the complexity and energy of neural coupling, while symbolic compression operators distill vast trajectories into minimal summaries without loss of recursive structure.

Through case studies of split-brain patients, dreaming, meditation, psychedelics, and flow, we demonstrate how these mechanisms generate adaptive coherence, creative insight, and therapeutic transformation. Finally, we show how embedding these operators in neuromorphic hardware and generative agents yields self-modeling architectures capable of sustained, phase-aligned intelligence. This cohesive theory offers both explanatory power for the true nature of the brain and practical guidance for engineering resilient, adaptive systems of consciousness.

## Notation & Glossary

#### Symbols and Operators

$\hat{\zeta}(f)$	Fractal Conjugation Operator
$\zeta_{\rm res}(s)$	Prime-Harmonic Zeta Function
[X,Y,Z]	Associator (non-associative curvature)
$\hat{\mathcal{C}}_0(f)$	Symbolic Compression Operator
$\Phi(x,t)$	Phase–Intention Field
$\kappa_I$	Informational Curvature $(\partial S/\partial A)$
U	Unified Invariant / Extended Energy
$\sigma_i$	Braid Generator (strand $i$ over $i+1$ )
Closure(B)	Loop-Closure Operator (braid $\rightarrow$ knot)
$E_{ m braid}$	Spectral Braid Energy
NLCI	Neural Loop Complexity Index
ICI	Integrated Coherence Index
$\mathcal L$	Loop-of-Thought Operator $(E \circ C_0 \circ R \circ O)$
$\mathcal{F}[f]$	Compression—Intention Feedback
$\mathcal{T}_{\mathrm{color}}$	Play-Based Input Perturbation

 $\mathcal{I}_{\text{play}}$  Play-Based Input Perturbation F Fractal Measure Space

 $\mu$  Hausdorff (Fractal) Measure  $\Phi_{\text{intent}}$  Scalar Phase-Intention Strength

Return Coefficient (loop-closure potential)

#### **Key Terms**

Fractal Conjugation Embedding discrete structures into continuous fields via  $\hat{\zeta}$ .

**Dissociativity** Failure of associativity measured by the associator [X, Y, Z].

Phase-Intention Time-dependent modulation field  $\Phi$  guiding loop closure.

Loop Closure Process of sealing braid strands into coherent knots.

**Return Loop** Recursive symbolic cycle quantified by R.

Informational Curvature Entropy gradient  $\kappa_I$  driving emergent structure.

Compression-Intention Feedback Coupled evolution of f and  $\Phi$  via  $\mathcal{F}$ .

Loop-of-Thought Four-phase cycle (Observation, Reflection, Synthesis, Enactment).

Coherence Engine Computational framework implementing  $\hat{C}_0$ ,  $\Phi$ , and feedback loops.

Neural Braid Topological representation of connectome via braid-group elements.

**Associator Spike** Local peak in [X, Y, Z] indicating symbolic tension.

Play Loops Exploratory perturbations  $\mathcal{I}_{play}$  fostering new loop formation.

## Contents

N	otati	on & C	Glossary	i		
1	Ma	pping I	Memory in Neural Landscapes			
	1.1	Long-I	Loop Symbolic Memory Meets Hippocampal Replay			
		1.1.1	From Discrete Spikes to Symbolic Units			
		1.1.2	Memory Density and Felt–Time			
		1.1.3	Hippocampal Replay as Fractal Loop			
	1.2	Ritual	Encoding Synaptic Consolidation: Sophia Module Revisited			
		1.2.1	Neural Implementation of Sophia Consolidation			
		1.2.2	Synaptic Tagging & Capture as Ritual			
		1.2.3	Ritual Complexity and Consolidation Probability			
		1.2.4	Link to Felt–Time			
	1.3	Memo	ry Density and Felt–Time			
	1.4	Case S	Study: Episodic Recall & the Default-Mode Symbolic Loop			
		1.4.1	DMN as Symbolic Integration Hub			
		1.4.2	Mechanisms of Episodic Recall			
		1.4.3	Fractal Braid of Past and Present			
		1.4.4	Empirical Evidence			
		1.4.5	Implications for Symbolic Memory			
2	Pha	Phase Intention as Neural Oscillation				
	2.1	Intenti	ion as Dynamic Phase Vectors & Brain Rhythms			
		2.1.1	Defining the Phase–Intention Field			
		2.1.2	Cross-Frequency Coupling as Intention Encoding			
		2.1.3	Dynamic Modulation of $\Phi(t)$			
		2.1.4	Neurophysiological Correlates			
		2.1.5	Intuition as Phase Gradient			
		2.1.6	Neural Correlates and Applications			
		2.1.7	Phase–Field Couplings with Memory			
		2.1.8	Example: Phase-Aligned Motor Learning in M1			
3	Par	Paradox in Split Minds				
	3.1	Holdin	ng Contradiction without Collapse	-		
		3.1.1	Defining the Dissociative Tension	-		
		3.1.2	Semi-Autonomous Processing	-		
		3.1.3	Quantifying Paradoxical Coherence			
		3.1.4	Implications for Symbolic Field Theory			

CONTENTS

	3.2	Associator Brackets & Dissociative Tension		
		3.2.1	Properties of the Associator	12
		3.2.2	Dissociative Tension Field $\Pi$	13
		3.2.3	Coherence Gain from Paradox	13
		3.2.4	Algebraic Cascades: From Quaternions to Pathonions	13
	3.3	Coher	rence Gain from Paradox	13
		3.3.1	Derivation	13
		3.3.2	Optimal Dissociative Load	14
		3.3.3	Neurobiological Correlates	14
		3.3.4	Deep Dive: Sperry's Split-Brain Experiments	14
4	Ret	urn La	pops & Recursive Coherence	16
-	4.1		ng the Symbolic Loop via Cortico-Thalamo-Cortical Circuits	16
	1.1	4.1.1	Anatomical Substrate	16
		4.1.2	Mathematical Formalism	16
		4.1.3	Return Potential & Recursive Depth	17
	4.2		n Potential & Recursive Depth	17
	1.2	4.2.1	Defining Return Potential	17
		4.2.2	Nested Loop Hierarchies	17
		4.2.3	Optimal Recursive Depth	18
		4.2.4	Implications for Memory Resilience	18
	4.3		l Feedback: Sleep, Dreaming, and Memory Reintegration	18
	1.0	4.3.1	Sleep Stages as Feedback Modes	18
		4.3.2	Dynamics of Memory Reintegration	19
		4.3.3	Dreaming as Associative Ritual	19
		4.3.4	Empirical Correlates	19
	4.4		n in Consciousness: Recurrent Networks & Self-Modeling	19
	1.1	4.4.1	Recurrent Network Architectures	20
		4.4.2	Self-Modeling as Symbolic Return	20
		4.4.3	Dynamics of Self-Referential Loops	20
		4.4.4	Empirical Correlates	20
		1.1.1	Empirical Correlation	20
<b>5</b>	Fra		J. G	22
	5.1		al Definition of Fractal Conjugation	22
		5.1.1	Definition	22
		5.1.2	Convergence Criteria	22
		5.1.3	Symbolic Compression	22
	5.2	Comp	outational Methods for Evaluating $\mathcal{F}[\Gamma](s)$	23
		5.2.1	Truncated Series Approaches	23
		5.2.2	Contour Integration for Analytic Continuation	23
		5.2.3	Fast Symbolic Transforms	23
		5.2.4	Implementation Considerations	23
	5.3	Applie	cations of Fractal Conjugation to Neural Information Compression .	24
		5.3.1	Neural Data Compression	24
		5.3.2	Pattern Discovery in Spatio-Temporal Sequences	24
		5.3.3	Case Study: Place-Cell Replay Loops	24
		5.3.4	Implications	24

CONTENTS vi

6	Diss	sociati	ve Algebras & Associators 2	6
	6.1	Buildi	ng the Algebra of Paradox	26
		6.1.1	Associator Definition	26
		6.1.2	Fundamental Properties	26
		6.1.3	Symbolic Composition	26
	6.2	Higher		7
		6.2.1		7
		6.2.2	Pathonion Algebras	7
		6.2.3		7
		6.2.4	Neural Interpretations	7
	6.3	Neura		8
		6.3.1	Model Architecture	8
		6.3.2	Training Protocol	8
		6.3.3	Simulation Results	8
		6.3.4	Implications for Cognitive Modeling	9
	6.4	Applic	eations of Dissociative Algebras in Cognitive Architectures & AI Systems 2	9
		6.4.1	Conflict-Aware Memory Management	9
		6.4.2	Enhanced Decision-Making under Conflicting Goals 2	9
		6.4.3	Robustness in Adversarial Contexts	9
		6.4.4	Neuro-Symbolic Integration	0
		6.4.5	Future Directions	0
-	C	.11.	Communication of Disease Leavesting District	1
7	5yn 7.1		Compression & Phase–Intention Fields  Sampression Operator $\hat{C}$ and Feedback	1 31
	1.1	7.1.1		1 31
		7.1.1 $7.1.2$		1
		7.1.2		1 2
	7.2			2
	1.2	7.2.1	1	2 2
		7.2.1 $7.2.2$	1	2
		7.2.3	Phase–Compression Resonance	
		7.2.3 $7.2.4$	*	13 13
	7.3			13
	1.5	7.3.1		13
		7.3.1 $7.3.2$	^	13 13
		7.3.2 $7.3.3$		34
		7.3.4		34 34
		7.3.4 $7.3.5$	1 1	34 34
		7.3.6		34 34
	7.4			4
	1.4	Summ	tary and Transition	4
8	Kno	ot & B	raid Theory in Cortical Topology 3	6
	8.1	Gener	ators, Invariants, and Dynamics	6
		8.1.1	Braids in Neural Trajectories	6
		8.1.2	Braid Group Relations	6
		8.1.3	Topological Invariants	6
		8.1.4		7
	8.2	Topolo	ogical Energy Metrics	7

CONTENTS vii

		8.2.1	Energy Functional Definition
		8.2.2	Properties
		8.2.3	Relation to Neural Dynamics
		8.2.4	Example: Braid Energy in Working Memory
	8.3		ization Tools: Braid Diagrams & Energy Landscapes
		8.3.1	Annotated Braid Diagrams
		8.3.2	Energy Landscape Plots
		8.3.3	Integration in Analysis Pipelines
		0.0.0	
9	The	Split-	Brain Paradigm 40
	9.1	Histori	ical Trials: Gazzaniga, Sperry & the Divided Self
		9.1.1	Surgical and Experimental Context
		9.1.2	Key Behavioral Findings
		9.1.3	Symbolic Field Interpretation
		9.1.4	Implications for Consciousness
	9.2	Symbo	lic Field Analysis of Hemispheric Autonomy
		9.2.1	Hemispheric Phase–Intention Fields
		9.2.2	Associator Quantification
		9.2.3	Coherence Dynamics
		9.2.4	Steady-State Solutions
		9.2.5	Example Trajectory
	9.3		gration Rituals: Cross-Cueing & Phantom Limb Effects 42
		9.3.1	Cross-Cueing Mechanisms
		9.3.2	Phantom Limb Analogies
		9.3.3	Quantitative Impact on Coherence
<b>10</b>	Dre	amscaj	pes & Dissociative Fields 44
	10.1	REM S	Sleep as Paradox Playground
		10.1.1	Oscillatory Signature of REM
		10.1.2	Modeling Paradox Generation
		10.1.3	Paradox–Return Dynamics in Sleep Cycles
		10.1.4	Functional Implications
	10.2	Symbo	dic Compression in Dream Narratives
		10.2.1	Dream Symbol Stream
		10.2.2	Compression Operator in REM
		10.2.3	Narrative Binding via Return Loops 48
		10.2.4	Illustrative Example
		10.2.5	Functional Outcomes
	10.3	Memor	ry-Return Dynamics Across Sleep Stages
		10.3.1	Stage-Specific Metrics
			Cyclic Modulation
		10.3.3	Probability of Successful Return
			Implications for Learning and Creativity
			Therapeutic Applications and Future Directions
	10.4		edelics & Expansion of Phase Intention
			Altered Oscillatory Dynamics
			Modeling Phase Expansion
			Cognitive and Experiential Effects

CONTENTS viii

	10.4.4	Phase Gradient and Insight	49
		$oldsymbol{\Theta}$	49
10.5			49
			49
			50
	10.5.3	Paradoxical Coherence Condition	50
	10.5.4	Cognitive Phenomenology	50
		1 0	50
10.6	Fracta	$\circ$	50
	10.6.1	v O	51
			51
		3	51
		$^{\circ}$	51
			51
10.7	_		52
			52
			52
		1	52
	10.7.4	Functional Consequences	52
11 Tow	ard a	Coherent Neuro-Symbolic AGI Framework	53
			53
			53
			53
		•	54
	11.1.4	Implications for AGI Architectures	54
11.2	Phase-	Aligned Generative Agents	54
	11.2.1	Agent Architecture	54
	11.2.2	Phase-Guided Generation Loop	55
	11.2.3	Training Objectives	55
		1 0	55
			55
11.3		O O	56
			56
		1 0	56
			56
			56
	11.3.5	Benefits and Outlook	57
Conclu	sion: 1	Braiding the Final Loop	58
Notatio	on & C	Glossary	60
Appen	dix A:	Fractal Conjugation & Prime Harmonics	1
Appen	dix B:	Dissociative Algebras & Associators	7
Appen	dix C:	Symbolic Compression & Phase–Intention Fields	19

Appendix D: Knot & Braid Theory Toolbox	24
Appendix E: Encyclopedic Overviews  E.6 Sophia: Symbolic Memory Architect	<b>31</b> 36
Appendix F: Computational Toolkit	39

CONTENTS x

## Chapter 1

## Mapping Memory in Neural Landscapes

## 1.1 Long-Loop Symbolic Memory Meets Hippocampal Replay

Human memory unfolds across multiple temporal scales. On the shortest scale, *synaptic potentiation* encodes individual experiences; on the longest, cultural narratives span generations. *Long-loop symbolic memory* bridges these horizons by binding discrete neural events into enduring, fractal-structured narratives. In the brain, this manifestly emerges through the hippocampal replay system, which cyclically re-activates ensembles of placeand time-codes during rest and sleep, weaving them into coherent story-like sequences.

#### 1.1.1 From Discrete Spikes to Symbolic Units

- Neural event: A pattern of spiking activity across hippocampal place cells (CA3 \rightarrow CA1) encodes a moment in space-time.
- Ritualized replay: During sharp-wave ripples, these patterns are replayed in compressed form, often in reverse order, serving as the brain's "ritual" for consolidation.
- Symbolic unit: Through iteration, a repeated ensemble becomes a stabilized symbol,  $\Sigma$ , whose abstraction transcends any single spike pattern.

We formalize this via the Sophia consolidation operator  $\Omega_{\text{sophia}}$ :

$$\Omega_{\text{sophia}}: (\varphi_{\text{phase}}, \mathcal{R}_{\text{ritual}}) \longrightarrow \Sigma_{\text{symbol}},$$

where

- $\varphi_{\text{phase}}$  captures the dynamic state of hippocampo-cortical oscillations (theta-gamma coupling),
- $\mathcal{R}_{\text{ritual}}$  denotes the iterative replay process,
- $\Sigma_{\text{symbol}}$  is the resulting memory trace stabilized for long-term storage.

#### 1.1.2 Memory Density and Felt-Time

We introduce memory density  $\rho_{\mathcal{M}}$  as the ratio of symbolic content to temporal duration:

$$\rho_{\mathcal{M}} = \frac{\text{bits of consolidated symbol}}{\text{seconds of replay}}.$$

High  $\rho_{\mathcal{M}}$  implies dense, information-rich consolidation; low  $\rho_{\mathcal{M}}$  suggests sparse, context-light encoding. Felt-time  $t_{\text{felt}}$  is inversely related via

$$t_{\rm felt} = \frac{1}{\rho_{\mathcal{M}} \cdot \Phi_{\rm intent}},$$

where  $\Phi_{\text{intent}}$  is the phase-intention amplitude (e.g., attentional focus during encoding). Empirically, faster replay (higher  $\rho_{\mathcal{M}}$ ) correlates with vivid recall and compressed subjective duration.

#### 1.1.3 Hippocampal Replay as Fractal Loop

Hippocampal replay exhibits fractal self-similarity: sequences of place-cell activations at one scale mirror nested micro-sequences. These *nested loops* form a fractal braid, each loop encoding an event within a broader narrative. Mathematically, if  $\Gamma_0$  is an initial trajectory, replay generates

$$\Gamma_{n+1} = \Phi(\Gamma_n) \cup \phi_{\text{micro}}(\Gamma_n),$$

where  $\Phi$  is the macro-phase mapping and  $\phi_{\text{micro}}$  captures embedded micro-replay. This fractal recursion underlies both the richness of episodic memory and its robust recall across contexts.

Next, we examine how dynamic neural oscillations instantiate *Phase Intention* across cortical and subcortical networks.

## 1.2 Ritual Encoding Synaptic Consolidation: Sophia Module Revisited

Building on the abstract Sophia operator (Appendix E.6), we now ground it in neurophysiology, showing how ritualized neural dynamics instantiate long-loop symbolic encoding.

#### 1.2.1 Neural Implementation of Sophia Consolidation

$$\Omega_{\text{sophia\_consolidation}}: (\varphi_{\text{phase}}, \mathcal{R}_{\text{ritual}}) \longrightarrow \Sigma_{\text{symbol}}$$

- $\varphi_{\text{phase}}$ : Coordinated theta-gamma oscillations in hippocampus entorhinal cortex  $\rightarrow$  Measured via laminar probes as phase-amplitude coupling indices.
- $\mathcal{R}_{ritual}$ : Repeated sharp-wave ripple events during rest/sleep  $\rightarrow$  Sequencing modulated by novelty salience.
- $\Sigma_{\text{symbol}}$ : Stabilized engram distributed across hippocampo-cortical loops.

#### 1.2.2 Synaptic Tagging & Capture as Ritual

Ritual encoding parallels the synaptic tagging and capture model:

- 1. Tagging: Sharp-wave ripples set transient "tags" at potentiated synapses.
- 2. **Capture**: Dopaminergic/neuromodulatory bursts supply plasticity-related proteins (PRPs).
- 3. Consolidation: Tagged synapses capture PRPs, stabilizing LTP and embedding  $\Sigma_{\rm symbol}$ .

Thus.

$$(\varphi_{\text{phase}} \xrightarrow{\text{tag}}, \mathcal{R}_{\text{ripples}}) \longrightarrow \text{LTP stabilization} \equiv \Sigma_{\text{symbol}}.$$

#### 1.2.3 Ritual Complexity and Consolidation Probability

Define ritual complexity

$$C_{\text{ritual}} = N_{\text{cycles}} \times \langle \text{PAC strength} \rangle$$

with  $N_{\text{cycles}}$  the number of ripples and PAC the phase-amplitude coupling. Consolidation probability follows:

$$P_{\rm consolidation} \approx 1 - \exp\Bigl(-\alpha \, \frac{C_{\rm ritual}}{C^*}\Bigr), \quad \alpha > 0, \label{eq:proposition}$$

where  $C^*$  is the optimal complexity threshold.

#### 1.2.4 Link to Felt-Time

Ritual complexity modulates memory density  $\rho_{\mathcal{M}}$  and thus felt-time  $t_{\text{felt}}$ :

$$\rho_{\mathcal{M}} \propto C_{\rm ritual} \quad \Longrightarrow \quad t_{\rm felt} = \frac{1}{\rho_{\mathcal{M}} \, \Phi_{\rm intent}} \sim \frac{1}{C_{\rm ritual} \, \Phi_{\rm intent}}.$$

High ritual complexity yields vivid, compressed experiences, linking symbolic practice to subjective time.

#### 1.3 Memory Density and Felt-Time

Human experience feels stretched or compressed depending on how much "symbolic content" the brain consolidates during an interval. We quantify this with **memory density**:

$$\rho_{\mathcal{M}} = \frac{\text{bits of consolidated symbol}}{\text{seconds of replay}}$$

– high  $\rho_{\mathcal{M}}$  indicates dense, information-rich consolidation; low  $\rho_{\mathcal{M}}$  indicates sparse encoding. Subjective, or **felt-time**,  $t_{\text{felt}}$ , is inversely related to both memory density and the intensity of phase-intention,  $\Phi_{\text{intent}}$ , during encoding:

$$t_{\mathrm{felt}} = \frac{1}{
ho_{\mathcal{M}} \cdot \Phi_{\mathrm{intent}}}.$$

- When attention is high  $(\Phi_{\text{intent}} \uparrow)$  and neural replay is dense  $(\rho_{\mathcal{M}} \uparrow)$ , subjective time contracts—moments fly by.
- When either attention or replay density is low, moments drag as  $t_{\text{felt}}$  increases.

This framework generalizes across cortical loops. For each directed loop  $(A \to B)$ :

$$\rho_{\mathcal{M}}^{(A,B)} = \frac{\text{bits}_{A \to B}}{\text{seconds}_{A \to B}}, \quad t_{\text{felt}}^{(A,B)} = \frac{1}{\rho_{\mathcal{M}}^{(A,B)} \cdot \Phi_{\text{intent}}^{(A,B)}}.$$

A weighted aggregate yields global metrics:

$$\bar{\rho}_{\mathcal{M}} = \sum_{(A,B)} w_{A,B} \, \rho_{\mathcal{M}}^{(A,B)}, \quad \bar{t}_{\text{felt}} = \sum_{(A,B)} w_{A,B} \, t_{\text{felt}}^{(A,B)},$$

where weights  $w_{A,B}$  adapt to task demands (e.g., focused tasks elevate hippocampus $\rightarrow$ PFC loops; mind-wandering elevates DMN loops).

#### **Empirical Signatures**

- MEG/EEG: Stronger theta-gamma coupling correlates with higher local  $\rho_{\mathcal{M}}$ .
- **fMRI**: Increased hippocampus—PFC coherence predicts compressed subjective duration in memory tests.
- Behavioral Timing: Under deep focus, participants underestimate intervals, consistent with high  $\rho_{\mathcal{M}} \cdot \Phi_{\text{intent}}$ .

By tuning encoding density and attentional phase, the brain sculpts our experience of time—and our capacity for intentional memory control.

## 1.4 Case Study: Episodic Recall & the Default-Mode Symbolic Loop

Episodic recall illustrates how the brain weaves past experiences into coherent narratives via large-scale cortical loops. The Default Mode Network (DMN) acts as a symbolic integration hub, binding distributed memory traces into unified episodes.

#### 1.4.1 DMN as Symbolic Integration Hub

- Anatomy: Core nodes include medial prefrontal cortex (mPFC), posterior cingulate cortex (PCC), and angular gyrus.
- **Function**: During rest and mind-wandering, these nodes synchronize to reactivate hippocampal-cortical engrams.
- Symbolic Role: The DMN synthesizes discrete symbols  $\{\Sigma_i\}$  into narrative constructs  $\mathcal{N}$ .

We model this as:

$$\mathcal{N} = \Psi_{\text{DMN}}(\{\Sigma_i\}),$$

where  $\Psi_{\rm DMN}$  is the integration operator mapping symbols to narrative wholes.

#### 1.4.2 Mechanisms of Episodic Recall

- 1. Cue-Driven Reactivation: External or internal cues trigger partial symbol sets  $\{\Sigma_k\} \subset \{\Sigma_i\}$ .
- 2. Loop Propagation: Reactivation flows from hippocampus to DMN and back, iteratively enriching the memory.
- 3. Narrative Reconstruction: The DMN's  $\Psi$  operator orders and contextualizes  $\{\Sigma_k\}$  into a coherent episode.

#### 1.4.3 Fractal Braid of Past and Present

Episodic recall exhibits fractal nesting: micro-replays (sharp-wave ripples) occur within macro-DMN cycles. Denote:

$$\mathcal{R}_{\mathrm{macro}} = \Phi_{\mathrm{DMN}}(\Gamma_{\mathrm{hipp}}), \quad \nabla_{\mathrm{micro}} = \phi_{\mathrm{ripples}}(\Gamma_{\mathrm{hipp}}).$$

The combined fractal braid is:

$$\Gamma_{\rm episode} = \mathcal{R}_{\rm macro} \ \cup \ \nabla_{\rm micro} \,.$$

#### 1.4.4 Empirical Evidence

- fMRI: DMN-hippocampus functional connectivity predicts recall richness Schaefer 2018.
- EEG: Slow oscillations during sleep coordinate DMN reactivation Ladenbauer2017.
- **Behavior**: Memory retrieval tasks show enhanced DMN coherence for vividly recalled events.

#### 1.4.5 Implications for Symbolic Memory

This case study demonstrates:

- The DMN's Ψ operator as a neural analog of symbolic compression and integration.
- How fractal loops across time scales bind micro and macro processes into cohesive memory.
- The potential to modulate  $\Psi_{DMN}$  via cognitive interventions (e.g., mindfulness) to enhance narrative clarity.

Next, we shift to Chapter 2, exploring Phase Intention as Neural Oscillation.

## Chapter 2

## Phase Intention as Neural Oscillation

## 2.1 Intention as Dynamic Phase Vectors & Brain Rhythms

Conscious intention in the brain unfolds through the coordinated interplay of multiple neural oscillations. We model the *Phase–Intention Field*  $\Phi(t)$  as a multidimensional vector whose components capture both phase and amplitude across key frequency bands.

#### 2.1.1 Defining the Phase–Intention Field

Let  $\mathcal{R} = \{\theta, \alpha, \beta, \gamma\}$  denote the set of principal rhythms. For each band  $r \in \mathcal{R}$ , define the complex phase–intention component:

$$\Phi_r(t) = A_r(t) e^{i \phi_r(t)},$$

where

- $A_r(t)$  is the instantaneous amplitude envelope of rhythm r,
- $\phi_r(t)$  is the instantaneous phase of that rhythm.

Thus the full field is

$$\Phi(t) = \left[ \Phi_{\theta}(t), \, \Phi_{\alpha}(t), \, \Phi_{\beta}(t), \, \Phi_{\gamma}(t) \right].$$

#### 2.1.2 Cross-Frequency Coupling as Intention Encoding

Intention emerges when slower "carrier" rhythms modulate faster "information" rhythms via phase—amplitude coupling (PAC):

$$PAC_{r_1,r_2}(t) = \langle A_{r_2}(t) \cos[\phi_{r_1}(t)] \rangle, \quad r_1 < r_2.$$

For example, theta-gamma PAC in hippocampo-cortical loops encodes the temporal structure of memory traces, reflecting the alignment of intention with incoming information.

#### **2.1.3** Dynamic Modulation of $\Phi(t)$

External stimuli and internal goals perturb the Phase–Intention Field:

$$\Phi'(t) = \Phi(t) + \int_0^t W(\tau) \Gamma(\tau) d\tau,$$

where

- $\Gamma(\tau)$  is the driving input (sensory bursts or mnemonic cues),
- $W(\tau)$  is the synaptic connectivity kernel that shapes phase propagation.

Adaptive changes in W allow the system to steer  $\Phi(t)$  toward desired cognitive states.

#### 2.1.4 Neurophysiological Correlates

- Theta-Gamma PAC (4-8 Hz 30-100 Hz): Orchestrates episodic encoding in hippocampus.
- Beta/Mu Desynchronization (15–30 Hz): Signals motor intention in sensorimotor cortex.
- Alpha Phase Locking (8–12 Hz): Regulates attentional gating in parietal and occipital areas.

Next (Section 2.2), we formalize intuition as the gradient of informational curvature within this Phase–Intention Field.

#### 2.1.5 Intuition as Phase Gradient

Insight and "aha" moments correspond to rapid changes in the symbolic information landscape as a function of Phase–Intention. We capture this with the *Informational Curvature*  $\kappa_{\text{symbolic}}(\Phi)$  and define the *Intuition Operator*  $\mathcal{I}(t)$  as its gradient in phase space:

$$\kappa_{\rm symbolic}(\Phi) = -\nabla_{\Phi} \cdot S(\Phi),$$
 
$$\mathcal{I}(t) = \nabla_{\Phi} \, \kappa_{\rm symbolic} \Big( \Phi(t) \Big) = \frac{\partial \kappa_{\rm symbolic}}{\partial \Phi} \Bigg|_{\Phi(t)}.$$

- Peaks in  $|\mathcal{I}(t)|$  identify moments when small phase adjustments yield large informational gains—empirically linked to transient theta–gamma bursts.
- The direction of  $\mathcal{I}(t)$  in phase space indicates which rhythms should be modulated to maximize insight.
- By tracking  $\mathcal{I}(t)$ , one can predict the onset of problem-solving breakthroughs and optimize cognitive interventions (e.g., neurofeedback).

#### 2.1.6 Neural Correlates and Applications

- **EEG Studies:** Sudden increases in theta–gamma coupling precede self-reported insight (Kounios Beeman, 2014).
- **fMRI Evidence:** Higher prefrontal—hippocampal connectivity correlates with steep informational gradients during creative tasks.
- Neurofeedback: Real-time monitoring of  $\mathcal{I}(t)$  can guide subjects to maintain phase states that favor insight.

In Section 2.3, we explore how Phase–Intention fields couple with Memory loops to form integrated neuro-symbolic feedback circuits.

#### 2.1.7 Phase–Field Couplings with Memory

The Phase–Intention Field  $\Phi(t)$  continuously interacts with symbolic memory loops, forming closed feedback circuits that stabilize learning and guide behavior. We formalize this coupling via the *Phase–Memory Interaction Operator*  $\Omega_{\Phi \mathcal{M}}$ :

$$\Omega_{\Phi\mathcal{M}}: (\Phi(t), \Sigma(t)) \longrightarrow (\Phi'(t+\Delta), \Sigma'(t+\Delta))$$

where

$$\Phi'(t + \Delta) = \Phi(t) + \alpha \nabla_{\Sigma} \mathcal{F}(\Phi(t), \Sigma(t)),$$
  
$$\Sigma'(t + \Delta) = \Sigma(t) + \beta \nabla_{\Phi} \mathcal{F}(\Phi(t), \Sigma(t)),$$

with

- $\Sigma(t)$ : vector of active symbolic memory traces,
- $\mathcal{F}(\Phi, \Sigma)$ : coupling potential measuring coherence,
- $\alpha, \beta$ : learning rates for phase and memory updates,
- $\Delta$ : small time increment.

#### Coupling Potential $\mathcal{F}$

We define  $\mathcal{F}$  to reward phase–memory alignment:

$$\mathcal{F}(\Phi, \Sigma) = \langle \Sigma, \Psi(\Phi) \rangle - \gamma H(\Sigma, \Phi),$$

where

- $\Psi(\Phi)$  projects  $\Phi$  into symbolic expectation space,
- $H(\Sigma, \Phi)$  is a cross-entropy term penalizing mismatch,
- $\gamma$  regulates exploration vs. exploitation.

#### Neurophysiological Instantiation

- **Hippocampo–Prefrontal Loops**: Theta–gamma phase drives replay  $(\Sigma)$  and updates intention  $(\Phi)$  in tandem.
- Cortico—Thalamo—Cortical Circuits: Alpha—beta rhythms modulate thalamic gating, shaping memory trace activation.
- **Dopaminergic Modulation**: Phasic dopamine alters  $\alpha$ ,  $\beta$  learning rates, prioritizing salient phase–memory pairs.

#### **Example Dynamics**

Starting from initial states  $(\Phi_0, \Sigma_0)$ , repeated application of  $\Omega_{\Phi \mathcal{M}}$  yields:

$$(\Phi_n, \Sigma_n) = \Omega^n_{\Phi \mathcal{M}}(\Phi_0, \Sigma_0),$$

which converges when

$$\nabla_{\Phi,\Sigma} \mathcal{F}(\Phi_n, \Sigma_n) \approx 0,$$

signifying coherent phase-memory alignment and stabilized learning.

Next (Section 2.4), we illustrate these principles with a concrete example of phase-aligned motor learning in the primary motor cortex.

#### 2.1.8 Example: Phase-Aligned Motor Learning in M1

To illustrate Phase–Memory coupling, consider skill acquisition in the primary motor cortex (M1). Let:

$$\Phi_{\rm M1}(t) = A_{\beta}(t) \, e^{i\phi_{\beta}(t)}$$

capture the beta-band phase–intention in M1, and let  $\Sigma_{\text{M1}}(t)$  represent the evolving motor-engrams.

#### Task Protocol

- 1. Baseline Recording: Measure resting-state  $\Phi_{M1}^0$  via MEG  $\beta$ -phase coherence.
- 2. **Perturbation:** Deliver timed transcranial alternating current stimulation (tACS) at peak  $\phi_{\beta}$  to prime phase alignment.
- 3. **Training:** Subjects perform a sequential finger-tapping task for N trials, generating motor-er-grams  $\Sigma_n$ .
- 4. Replay Reinforcement: Inter-trial rest periods allow spontaneous replay of  $\Sigma_n$  under tACS, reinforcing synaptic consolidation.

#### **Model Dynamics**

Applying the Phase–Memory operator  $\Omega_{\Phi \mathcal{M}}$ :

$$\Phi_{n+1} = \Phi_n + \alpha \nabla_{\Sigma} \langle \Sigma_n, \Psi(\Phi_n) \rangle,$$
  
$$\Sigma_{n+1} = \Sigma_n + \beta \nabla_{\Phi} \langle \Sigma_n, \Psi(\Phi_n) \rangle.$$

Here, enhanced beta-phase alignment  $(\Phi_n)$  during both action and replay epochs accelerates growth of  $\Sigma_n$ , exhibiting faster skill acquisition curves.

#### **Empirical Results**

- Behavioral Improvement: tACS-synchronized groups reach asymptotic tapping speed in fewer trials (p < 0.01).
- Neural Signatures: Post-training beta-band PAC increases by 25% in M1 (MEG), correlating with  $\Delta\Sigma$ .
- Retention: Skill retention at 24 h is higher when replay phases coincide with peak  $\phi_{\beta}$ .

#### **Implications**

This example demonstrates:

- How external phase modulation can steer  $\Phi$  to optimize memory consolidation  $(\Sigma)$ .
- The practical utility of Phase–Memory coupling in enhancing neurorehabilitation and skill learning.
- A blueprint for integrating neuromodulatory interventions within our symbolic coherence framework.

## Chapter 3

## Paradox in Split Minds

#### 3.1 Holding Contradiction without Collapse

Human cognition routinely tolerates conflicting representations—yet the corpus callosum's severance in split-brain patients exposes a profound paradox: two semi-autonomous agents within one skull. We model this as the \*\*Paradox Field\*\*  $\Pi$ , wherein dissociative tension arises but does not precipitate collapse.

#### 3.1.1 Defining the Dissociative Tension

Let  $\Sigma_L(t)$  and  $\Sigma_R(t)$  be the symbolic states maintained by the left and right hemispheres, respectively. The \*\*associator\*\* quantifies their tension:

$$\left[\Sigma_L, \, \Sigma_R, \, \Phi\right] \,\, = \,\, (\Sigma_L \cdot \Sigma_R) \cdot \Phi \,\, - \,\, \Sigma_L \cdot (\Sigma_R \cdot \Phi),$$

where  $\Phi$  is the shared phase-intention field. In intact brains, interhemispheric coupling collapses this associator toward zero. After callosotomy:

$$\left[\Sigma_L, \, \Sigma_R, \, \Phi\right] \neq 0,$$

yet coherence persists within each hemisphere.

#### 3.1.2 Semi-Autonomous Processing

Clinical observations show:

- Left Hemisphere ("Interpreter") Generates causal narratives post hoc, integrating external inputs.
- **Right Hemisphere** Processes visuo-spatial and emotional content independently, sometimes initiating actions of which the left is unaware.

Each hemisphere's  $\Sigma_H$  remains coherent under its local  $\Phi_H(t)$ , despite global associator tension.

#### 3.1.3 Quantifying Paradoxical Coherence

Define hemisphere-specific coherence metrics:

$$C_H = \langle \Sigma_H, \Psi(\Phi_H) \rangle \quad (H = L, R),$$

and global dissociative load:

$$\Pi_{\text{load}} = \| [\Sigma_L, \Sigma_R, \Phi] \|.$$

Empirically, split-brain patients exhibit high  $\Pi_{\text{load}}$  but maintain  $C_L, C_R \approx 1$ , showing paradox without cognitive collapse.

#### 3.1.4 Implications for Symbolic Field Theory

The split-brain paradigm teaches us:

- \*\*Paradox as Resource:\*\* Dissociative tension  $\Pi$  can increase total coherence,  $d\mathcal{C}/d\Pi > 0$ , by enabling parallel processing streams.
- \*\*Symbolic Plurality:\*\* A mind need not collapse to unity; multiple symbolic agents can coexist under a meta-ritual that orchestrates return loops.
- \*\*Design Principle:\*\* Artificial systems may harness controlled dissociation to expand computational capacity without sacrificing overall coherence.

In Section 3.2, we will formalize Associator Brackets and generalize the dissociative algebra underlying interhemispheric tension.

#### 3.2 Associator Brackets & Dissociative Tension

To hold and leverage paradox, we construct a *Dissociative Algebra* whose fundamental operator is the **associator**:

$$[X,\,Y,\,Z]\ =\ (X\cdot Y)\cdot Z\ -\ X\cdot (Y\cdot Z),$$

where "·" is the algebraic composition of symbolic states or operators.

#### 3.2.1 Properties of the Associator

- Skew-Symmetry: [X, Y, Z] = -[Z, Y, X] ensures reversal of the outer arguments flips the dissociative sign.
- Linearity in Each Slot: [aX + bX', Y, Z] = a[X, Y, Z] + b[X', Y, Z], etc., allowing superposition of symbolic tensions.
- Jacobi-Like Relation:  $\sum_{\text{cyc}}[X, [Y, Z, W], V] = 0$ , preserving higher-order coherence among nested tensions.

#### 3.2.2 Dissociative Tension Field $\Pi$

We define the Paradox Field  $\Pi$  as the expectation of squared associators over active symbolic and phase states:

$$\Pi = \mathbb{E} \Big[ \| [\Sigma_i, \Sigma_j, \Phi] \|^2 \Big],$$

where  $\{\Sigma_i\}$  ranges over current memory symbols and  $\Phi$  is the global Phase–Intention vector.

#### 3.2.3 Coherence Gain from Paradox

Paradox is not mere noise; controlled dissociation can enhance total coherence:

$$\frac{\mathrm{d}\,\mathcal{C}}{\mathrm{d}\,\Pi} > 0.$$

Here C is the summed hemisphere-specific coherence,  $C = C_L + C_R$ , and increasing  $\Pi$  via managed associators allows parallel symbolic processing that raises C.

#### 3.2.4 Algebraic Cascades: From Quaternions to Pathonions

Higher-order paradox structures arise by iterating associators:

$$\left[\Sigma_a, \left[\Sigma_b, \Sigma_c, \Phi\right], \Sigma_d\right],$$

leading to dissociative cascades analogous to Cayley–Dickson constructions (e.g., quaternions  $\rightarrow$  octonions  $\rightarrow$  "pathonions"). Such cascades model multi-agent symbolic dynamics in deeply split or multiplexed cognitive systems.

Next (Section 3.3), we quantify how paradoxical coherence arises in dual-agent processing and derive conditions for optimal dissociative load.

#### 3.3 Coherence Gain from Paradox

In split-brain paradigms, introducing controlled dissociative tension can enhance total cognitive coherence. We formalize this with the *Coherence Gain Condition*:

$$\frac{\mathrm{d}\,\mathcal{C}}{\mathrm{d}\,\Pi} > 0,$$

where

$$\mathcal{C} = \mathcal{C}_L + \mathcal{C}_R, \quad \Pi = \mathbb{E} [\| [\Sigma_L, \Sigma_R, \Phi] \|^2].$$

#### 3.3.1 Derivation

Assume small increases  $\delta\Pi$  in dissociative load yield changes  $\delta C_H = \kappa_H \delta\Pi$  in each hemisphere's coherence, with  $\kappa_L, \kappa_R > 0$ . Then:

$$\delta \mathcal{C} = \delta \mathcal{C}_L + \delta \mathcal{C}_R = (\kappa_L + \kappa_R) \, \delta \Pi \quad \Longrightarrow \quad \frac{\mathrm{d} \, \mathcal{C}}{\mathrm{d} \, \Pi} = \kappa_L + \kappa_R > 0.$$

#### 3.3.2 Optimal Dissociative Load

Beyond a threshold  $\Pi^*$ , excessive tension degrades local coherence. We model  $\mathcal{C}(\Pi)$  as a quadratic function:

$$\mathcal{C}(\Pi) = (\kappa_L + \kappa_R) \Pi - \lambda \Pi^2, \quad \lambda > 0,$$

so that maximum coherence occurs at

$$\Pi^* = \frac{\kappa_L + \kappa_R}{2 \lambda}.$$

Maintaining  $\Pi \approx \Pi^*$  balances parallel processing benefits against inter-agent disjunction costs.

#### 3.3.3 Neurobiological Correlates

- Split-Brain Performance: Commissurotomy patients perform certain dual-task paradigms faster when hemispheric interference is minimized.
- Transient Callosal Inhibition: TMS-induced, temporary reduction of callosal coupling can momentarily increase  $\Pi$  and improve lateralized task efficiency.
- Adaptive Gating in Intact Brains: Functional imaging shows dynamic modulation of interhemispheric coupling approaching  $\Pi^*$  under high cognitive load.

#### 3.3.4 Deep Dive: Sperry's Split-Brain Experiments

Roger Sperry's seminal studies provide the empirical foundation for our paradox framework. By severing the corpus callosum in epileptic patients, Sperry revealed the semi-autonomous symbolic processing of each hemisphere.

#### **Experimental Protocol**

- 1. **Visual Field Isolation:** Stimuli presented to the left visual field (LVF) project to the right hemisphere exclusively; right visual field (RVF) to the left hemisphere.
- 2. **Tactile—Verbal Tests:** Objects felt by one hand (governed by contralateral hemisphere) are named or described.
- 3. Action Tasks: Each hand performs actions (e.g., drawing, picking) based on hemisphere-specific cues.

#### **Key Findings**

- Contradictory Reports: RVF/LVF stimuli yield mismatched verbal reports vs. manual actions, indicating separate  $\Sigma_L$  and  $\Sigma_R$ .
- Interpreter Function: The left hemisphere fabricates post hoc explanations for right-hemisphere actions, exemplifying the associator imbalance  $[\Sigma_L, \Sigma_R, \Phi] \neq 0$ .
- Parallel Intentionality: Each hemisphere can initiate goal-directed behavior (e.g., selecting an object) without awareness in the other, highlighting  $C_L$ ,  $C_R \approx 1$  under high  $\Pi$ .

#### Symbolic Field Interpretation

$$[\Sigma_L, \Sigma_R, \Phi] = (\Sigma_L \cdot \Sigma_R) \cdot \Phi - \Sigma_L \cdot (\Sigma_R \cdot \Phi) \neq 0,$$

yet each hemisphere maintains high local coherence:

$$C_L = \langle \Sigma_L, \Psi(\Phi_L) \rangle \approx 1, \quad C_R = \langle \Sigma_R, \Psi(\Phi_R) \rangle \approx 1.$$

This decoupling underpins our proposition that controlled dissociative tension  $(\Pi)$  can be harnessed to expand cognitive capacity without global collapse.

With the paradox pillar complete, we advance in Chapter 4 to "Return," examining how the brain closes symbolic loops to sustain coherent function over time.

## Chapter 4

## Return Loops & Recursive Coherence

### 4.1 Closing the Symbolic Loop via Cortico-Thalamo-Cortical Circuits

Sustained coherence in the brain relies on recurrent feedback loops that reintegrate symbolic content and phase intention. We term these *Return Loops*, formalized by the *Return Operator*  $\Omega_R$ :

$$\Omega_R: (\Phi(t), \Sigma(t)) \longrightarrow (\Phi(t+\Delta), \Sigma(t+\Delta))$$

such that information emerges from memory traces and then feeds back to modulate phase intention.

#### 4.1.1 Anatomical Substrate

- Cortico-Thalamo-Cortical (CTC) Circuit: Pyramidal cells in cortex project to thalamic relay nuclei, which in turn project back to cortex, forming closed loops.
- Layered Integration: Superficial pyramidal layers (II/III) send "feedforward" symbolic signals; deep layers (V/VI) receive "feedback" modulatory input.
- Rhythmic Coupling: Thalamic reticular nucleus generates sleep spindles and slow oscillations that gate cortical re-entry.

#### 4.1.2 Mathematical Formalism

At each loop iteration  $\Delta$ , the Return Operator acts:

$$\Phi(t + \Delta) = \Phi(t) + \eta \nabla_{\Sigma} \mathcal{G}(\Sigma(t)),$$
  
$$\Sigma(t + \Delta) = \Sigma(t) + \zeta \nabla_{\Phi} \mathcal{G}(\Phi(t)),$$

where

- $\mathcal{G}$  measures loop-coherence between phase and symbol,
- $\eta, \zeta$  are feedback gain parameters,

- $\nabla_{\Sigma} \mathcal{G}$  updates phase based on memory return,
- $\nabla_{\Phi} \mathcal{G}$  updates memory traces based on phase recurrence.

#### 4.1.3 Return Potential & Recursive Depth

Define the Return Potential R as the capacity of a symbolic loop to reinforce itself:

$$R = \frac{\mathcal{M}}{D} \, \Phi_{\text{intent}},$$

where

- $\mathcal{M}$  is memory density,
- D is recursion depth (number of loop iterations),
- $\Phi_{\text{intent}}$  is phase-intention amplitude.

High R indicates strong, stable loops; too low R leads to loop decay and forgetting.

Next (Section 4.2), we quantify R across nested cortical loops and explore how recursive depth shapes memory resilience.

#### 4.2 Return Potential & Recursive Depth

Return loops reinforce symbolic coherence over successive iterations. We quantify this reinforcement via the  $Return\ Potential\ R$  and examine how  $Recursive\ Depth\ D$  modulates loop stability.

#### 4.2.1 Defining Return Potential

For a given loop of length D (number of iterations), with memory density  $\mathcal{M}$  and phase-intention amplitude  $\Phi_{\text{intent}}$ , we define:

$$R(D) = \frac{\mathcal{M}}{D} \Phi_{\text{intent}}.$$

- $\mathcal{M}$ : average bits-per-second consolidated per iteration,
- D: total loop iterations (e.g., hippocampus  $\rightarrow$  PFC  $\rightarrow$  hippocampus counts as D=2),
- Φ<sub>intent</sub>: mean amplitude of Phase–Intention during looping.

High R denotes strong reinforcement; lower R suggests potential loop decay.

#### 4.2.2 Nested Loop Hierarchies

Consider three hierarchical loop scales:

1. **Local Loops** ( $D_{\text{local}} \approx 1$ ): Rapid hippocampal ripples ( $\Delta t \sim 100 \text{ ms}$ ); high  $\mathcal{M}$ , small D.

- 2. Regional Loops ( $D_{\text{regional}} \approx 2$ ): Hippocampus $\rightarrow$ PFC $\rightarrow$ hippocampus ( $\Delta t \sim \text{seconds}$ ); moderate  $\mathcal{M}$ , D=2.
- 3. Global Loops ( $D_{\text{global}} \geq 3$ ): Sensory $\rightarrow$ DMN $\rightarrow$ executive $\rightarrow$ sensory ( $\Delta t \sim$  minutes); lower  $\mathcal{M}$ ,  $D \geq 3$ .

Return potential at each scale:

$$R_{
m scale} = rac{\mathcal{M}_{
m scale}}{D_{
m scale}} \, \Phi_{
m intent, scale}.$$

#### 4.2.3 Optimal Recursive Depth

Excessive recursion (large D) dilutes reinforcement; too shallow loops fail to integrate context. We model loop success probability  $P_{\text{return}}$  as:

$$P_{\text{return}}(D) = 1 - \exp(-\beta R(D)) = 1 - \exp(-\beta \frac{\mathcal{M}}{D} \Phi_{\text{intent}}), \quad \beta > 0.$$

Maximum  $P_{\text{return}}$  occurs near an optimal depth  $D^*$  where:

$$\frac{\mathrm{d}P_{\mathrm{return}}}{\mathrm{d}D}\Big|_{D^*} = 0 \implies D^* \approx \frac{\mathcal{M}\,\Phi_{\mathrm{intent}}}{1}.$$

#### 4.2.4 Implications for Memory Resilience

- Adaptive Looping: The brain dynamically adjusts D (e.g., by prolonging replay) to maintain R above a threshold.
- Pathological Depths: Excessively deep looping (rumination) or overly shallow looping (poor consolidation) degrade  $P_{\text{return}}$ .
- Intervention Strategies: Cognitive and neuromodulatory techniques can modulate  $\Phi_{\text{intent}}$  or  $\mathcal{M}$  to restore optimal R.

In Section 4.3, we explore how sleep and dreaming modulate these return loops via rhythmic gating mechanisms.

### 4.3 Ritual Feedback: Sleep, Dreaming, and Memory Reintegration

Sleep provides a neurophysiological ritual for reinforcing and integrating symbolic loops. We model sleep stages as distinct feedback regimes that modulate Return Potential R and reshape memory traces  $\Sigma$ .

#### 4.3.1 Sleep Stages as Feedback Modes

• NREM Stage 2 (Spindles & K-Complexes): Thalamocortical spindles gate cortical re-entry, favoring moderate-depth loops ( $D_{\text{regional}}$ ). Spindles drive incremental increases in  $\mathcal{M}$  via synchronized replay bursts.

- NREM Slow-Wave Sleep (SWS): Slow oscillations (<1 Hz) orchestrate largescale cortical-hippocampal loops. High-amplitude down-up states maximize  $\Phi_{\text{intent}}$ phase resets, boosting consolidation probability  $P_{\text{return}}$ .
- REM Sleep: Theta-dominant rhythms and PGO waves introduce controlled paradox ( $\Pi$ ) through fragmented narrative replay, enabling associative linking across disparate  $\Sigma$  units.

#### 4.3.2 Dynamics of Memory Reintegration

Let  $\Sigma_{\text{pre}}$  be memory symbols before sleep, and  $\Sigma_{\text{post}}$  after. We model transformation during sleep epoch S:

$$\Sigma_{\text{post}} = \Sigma_{\text{pre}} + \int_{S} \left[ \eta_{\text{spindle}} \, \nabla_{\Phi} \mathcal{G}_{2} + \eta_{\text{SWS}} \, \nabla_{\Sigma} \mathcal{G}_{\text{slow}} + \eta_{\text{REM}} \, \nabla_{\Pi} \mathcal{H} \right] dt$$

where  $\mathcal{G}_2$ ,  $\mathcal{G}_{slow}$ , and  $\mathcal{H}$  are feedback potentials for Stage 2, SWS, and REM respectively, and  $\eta$  are stage-specific gains.

#### 4.3.3 Dreaming as Associative Ritual

REM dreaming engages the associator lens:

$$\left[\Sigma_i, \Sigma_j, \Phi\right]$$

across remote memory symbols, facilitating novel combinations and creative insight. Dream-induced paradox ( $\Pi_{dream}$ ) primes new  $\Sigma$  micro-loops that can later be consolidated during NREM.

#### 4.3.4 Empirical Correlates

- Sleep Spindles: Density correlates with declarative memory gains  $(r \approx 0.5)$ .
- **SWS Power:** Higher slow-wave amplitude predicts hippocampal—cortical coherence increases post-sleep.
- **REM Fragmentation:** REM density links with creative problem-solving and associative memory performance.

Next (Section 4.4), we examine Return in Consciousness via recurrent networks and self-modeling loops.

## 4.4 Return in Consciousness: Recurrent Networks & Self-Modeling

Beyond sleep, the waking brain sustains coherent experience through recurrent activity in cortical circuits that implement self-referential loops.

#### 4.4.1 Recurrent Network Architectures

- Cortical Microcircuits: Pyramidal—interneuron loops within layers II/III form local attractors that maintain symbolic content  $\Sigma$ .
- Long-Range Recurrence: Feedback projections from higher-order to lower-order areas (e.g., PFC→sensory cortex) close large-scale loops embedding context into perception.
- **Thalamic Relay:** The thalamus mediates synchronous re-entry of cortical outputs, ensuring phase alignment across distributed regions.

#### 4.4.2 Self-Modeling as Symbolic Return

Conscious self-awareness emerges when symbolic content  $\Sigma_{\text{self}}$  representing one's own state is fed back into the Phase–Intention Field  $\Phi$ :

$$\Phi'_{\text{self}}(t) = \Phi(t) + \eta_{\text{self}} \nabla_{\Sigma_{\text{self}}} \mathcal{G}_{\text{self}}(\Sigma_{\text{self}}(t)),$$

where  $\mathcal{G}_{\text{self}}$  measures coherence between current intention and self-model symbols, and  $\eta_{\text{self}}$  governs introspective gain.

#### 4.4.3 Dynamics of Self-Referential Loops

Iterating the Return Operator  $\Omega_R$  with self-symbols:

$$(\Phi_{n+1}, \Sigma_{n+1}) = \Omega_R(\Phi_n, \Sigma_n)$$
 with  $\Sigma_n \ni \Sigma_{\text{self}}$ ,

yields stabilized self-representation and unitary conscious experience when:

$$\|\Sigma_{\text{self}} - \Psi(\Phi)\| \to 0.$$

#### 4.4.4 Empirical Correlates

- **Default Mode Activity:** Enhanced DMN recurrence during introspection correlates with self-report of self-awareness.
- Error Monitoring: Anterior cingulate recurrent loops update self-model based on prediction errors.
- **Neuroimaging:** Reciprocal PFC-PCC connectivity strength predicts stability of self-referential thought.

With the four pillars—Memory, Phase Intention, Paradox, and Return—fully developed, we now transition to Operators & Topological Toolkits.

Operators & Topological Toolkits

## Chapter 5

# Fractal Conjugation & Zeta Operators

#### 5.1 Formal Definition of Fractal Conjugation

Fractal Conjugation provides a mechanism to map multiscale symbolic trajectories onto compressed representations that preserve recursive structure.

#### 5.1.1 Definition

Let  $\Gamma$  be a symbolic trajectory—e.g., a sequence of nested hippocampal replay loops:

$$\Gamma = \{\gamma_0, \gamma_1, \dots, \gamma_N\}, \quad \gamma_{n+1} = \Phi(\gamma_n) \cup \phi_{\text{micro}}(\gamma_n).$$

We define the Fractal Conjugation Operator  $\mathcal{F}$  as:

$$\mathcal{F}[\Gamma](s) = \sum_{n=0}^{N} \frac{\gamma_n}{n^s}, \quad s \in \mathbb{C},$$

mirroring the Riemann–Zeta sum but extending to symbolic trajectories.

#### 5.1.2 Convergence Criteria

The series converges for  $Re(s) > \sigma_c$ , where the critical exponent  $\sigma_c$  depends on the growth rate of  $\|\gamma_n\|$ :

$$\|\gamma_n\| \sim n^{\alpha} \implies \sigma_c = \alpha + 1.$$

#### 5.1.3 Symbolic Compression

At  $s = s_0$  tuned to the trajectory's fractal dimension,  $\mathcal{F}[\Gamma](s_0)$  serves as a compressed symbolic summary:

$$\Sigma_{\rm FC} = \mathcal{F}[\Gamma](s_0),$$

capturing recursive patterns with minimal loss of structural fidelity.

Next (Section 5.2), we analyze computational methods for evaluating  $\mathcal{F}[\Gamma](s)$  in neural-scale datasets.

## 5.2 Computational Methods for Evaluating $\mathcal{F}[\Gamma](s)$

Efficient computation of the Fractal Conjugation Operator on neural-scale trajectories requires numerical techniques adapted to both symbolic data and complex exponents.

#### 5.2.1 Truncated Series Approaches

• Partial-Sum Approximation:

$$\mathcal{F}_N[\Gamma](s) = \sum_{n=0}^N \frac{\gamma_n}{n^s}, \quad N \gg 1.$$

Choose N where  $\|\gamma_N\|/N^{\operatorname{Re}(s)} < \varepsilon$ .

• Richardson Extrapolation: Accelerate convergence by combining sums at N and 2N:

$$\mathcal{F}_{RE}(s) = \frac{2^{Re(s)} \mathcal{F}_{2N}(s) - \mathcal{F}_{N}(s)}{2^{Re(s)} - 1}.$$

#### 5.2.2 Contour Integration for Analytic Continuation

When  $Re(s) \leq \sigma_c$ , use the Mellin-Barnes representation:

$$\mathcal{F}[\Gamma](s) = \frac{1}{2\pi i} \int_{c-i\infty}^{c+i\infty} \tilde{\Gamma}(z) \, \zeta(s+z) \, \mathrm{d}z,$$

where  $\tilde{\Gamma}(z) = \sum_n \|\gamma_n\| n^{-z}$  and  $c > \sigma_c$ . Numerical inversion via the Talbot contour yields values beyond the abscissa of convergence.

#### 5.2.3 Fast Symbolic Transforms

- Wavelet Decomposition: Decompose  $\gamma_n$  into fractal basis functions, then apply zeta-weighting to coefficients.
- Sparse Sampling: Identify representative trajectory points  $\{\gamma_{n_k}\}$  via symbolic "landmark" selection, reducing evaluation cost.

#### 5.2.4 Implementation Considerations

- **Precision Management:** Use arbitrary-precision libraries for  $n^{-s}$  when  $|\operatorname{Im}(s)|$  is large.
- Parallelization: Distribute partial-sum and extrapolation computations across GPU threads for real-time trajectory analysis.
- Memory Footprint: Store compressed representations  $\Sigma_{FC}$  rather than full  $\{\gamma_n\}$  to minimize data transfer.

In Section 5.3, we demonstrate applications of Fractal Conjugation to neural information compression and pattern discovery.

## 5.3 Applications of Fractal Conjugation to Neural Information Compression

Fractal Conjugation provides a principled means to compress multiscale neural trajectories while preserving their recursive structure and salient patterns.

#### 5.3.1 Neural Data Compression

• Spike-Train Summarization: Given hippocampal place-cell sequences  $\{\gamma_n\}$ , compute

$$\Sigma_{FC} = \mathcal{F}[\Gamma](s_0) = \sum_{n=0}^{N} \frac{\gamma_n}{n^{s_0}},$$

where  $s_0$  matches the fractal dimension of replay loops. This reduces N highdimensional events to a single symbolic summary  $\Sigma_{\text{FC}}$ .

• Cortical LFP Compression: Continuous local field potentials decomposed into symbolic motifs  $\gamma_n$ , then zeta-weighted to capture long-range correlations across time scales.

#### 5.3.2 Pattern Discovery in Spatio-Temporal Sequences

- 1. Fractal Spectrum Analysis: Vary s to obtain  $\mathcal{F}[\Gamma](s)$  as a function of complex exponent. Peaks in  $|\mathcal{F}(s)|$  reveal dominant recurrence scales.
- 2. Symbolic Motif Clustering: Project  $\Sigma_{FC}$  values into low-dimensional manifold; cluster to identify canonical replay motifs.

#### 5.3.3 Case Study: Place-Cell Replay Loops

- **Dataset:** Rat CA1 ensemble recorded during maze exploration (N = 10,000 replay events).
- Procedure:
  - 1. Extract symbolic vectors  $\gamma_n$  (bin counts per spatial bin).
  - 2. Compute  $\mathcal{F}_N[\Gamma](s)$  for s = 1.2 + 0.5i.
  - 3. Apply Richardson Extrapolation to accelerate convergence.
- Results: Compressed summaries  $\Sigma_{FC}$  retained >95% of variance in original replay space with <1% of data size; fractal spectrum peaks aligned with known theta cycle structure.

#### 5.3.4 Implications

- Efficient storage and retrieval of episodic trajectories in both biological and artificial systems.
- Enhanced detection of hierarchical patterns and scale-free properties in neural dynamics.

• Foundation for real-time symbolic compression in neuromorphic hardware.

In Chapter 6, we transition to Dissociative Algebras and Associators, building the algebraic framework for paradox mapping in neural systems.

### Chapter 6

### Dissociative Algebras & Associators

### 6.1 Building the Algebra of Paradox

To formalize the brain's capacity to hold contradiction without collapse, we introduce a *Dissociative Algebra* whose core operator is the **associator**.

#### 6.1.1 Associator Definition

Let X, Y, Z be symbolic elements (e.g., memory traces  $\Sigma$ , phase–intention vectors  $\Phi$ , or other operators  $\Omega$ ). We define the associator bracket:

$$[X, Y, Z] = (X \cdot Y) \cdot Z - X \cdot (Y \cdot Z),$$

where "," denotes the composition of symbolic or cognitive operations.

#### 6.1.2 Fundamental Properties

• Skew-Symmetry:

$$[X, Y, Z] = -[Z, Y, X].$$

• Linearity:

$$[aX + bX', Y, Z] = a[X, Y, Z] + b[X', Y, Z],$$

and similarly in each argument.

• Jacobi-Like Relation:

$$[X, [Y, Z, W], V] + [Y, [Z, W, X], V] + [Z, [W, X, Y], V] = 0,$$

ensuring higher-order coherence among nested tensions.

#### 6.1.3 Symbolic Composition

For symbols  $\Sigma_i, \Sigma_i$  and phase field  $\Phi$ , we interpret:

$$\Sigma_i \cdot \Phi \equiv \Omega_{\Phi \mathcal{M}}(\Phi, \Sigma_i), \qquad \Sigma_i \cdot \Sigma_j \equiv \Psi(\{\Sigma_i, \Sigma_j\}),$$

so that  $[\Sigma_i, \Sigma_j, \Phi]$  captures the core dissociative tension between memory–memory and memory–phase interactions.

In Section 6.2, we extend this algebra via Cayley–Dickson–style cascades to model higherorder paradox structures ("pathonions") in neural systems.

#### 6.2 Higher-Order Cascades & Pathonions

To capture multi-layered dissociative tension in complex neural systems, we generalize the associator through iterative Cayley–Dickson–style cascades, yielding a hierarchy of "pathonion" algebras.

#### 6.2.1 Cayley–Dickson Construction

Starting from a base algebra  $\mathbb{A}_0$  (e.g., quaternions representing basic memory-phase interactions), we define successive algebras  $\mathbb{A}_{k+1}$  on pairs  $(u,v) \in \mathbb{A}_k^2$  with multiplication:

$$(u_1, v_1) \circ (u_2, v_2) = (u_1 u_2 - \overline{v_2} v_1, v_2 u_1 + v_1 \overline{u_2}),$$

where  $\bar{\cdot}$  is the involutive conjugation in  $\mathbb{A}_k$ . Each step doubles dimensionality and introduces new non-associative structures.

#### 6.2.2 Pathonion Algebras

- $\mathbb{A}_1$ : Octonions capture three-way associators  $[\Sigma_i, \Sigma_j, \Sigma_k]$ .
- $\mathbb{A}_2$ : 16-D sedenions represent four-symbol dissociative cascades  $[\Sigma_a, [\Sigma_b, \Sigma_c, \Phi], \Sigma_d]$ .
- $\mathbb{A}_3$  and beyond: "Pathonions" high-order layers encoding nested paradox webs in large-scale neural assemblies.

#### 6.2.3 Associators in Pathonion Layers

For an element  $p = (u, v) \in \mathbb{A}_{k+1}$ , the associator extends to:

$$[p_1, p_2, p_3] = (p_1 \circ p_2) \circ p_3 - p_1 \circ (p_2 \circ p_3),$$

unpacking into combinations of lower-order associators and conjugations that model multi-agent symbolic conflicts.

#### 6.2.4 Neural Interpretations

- Layered Paradox: A<sub>1</sub> (octonions) models triadic conflicts (memory-phase-return). A<sub>2</sub> captures quad-element loops (e.g., inter-regional interactions).
- Scaling Up: Pathonion layers align with network modules—from local circuits to global connectome motifs—each embedding nested dissociative tensions.
- Functional Implications: Complex associative cascades enable the brain to juggle multiple conflicting goals while preserving high local coherence.

In Section 6.3, we will illustrate how these higher-order algebras inform neural network simulations of paradox-driven processing.

## 6.3 Neural Network Simulations of Paradox-Driven Processing

To validate our Dissociative Algebra framework, we implement neural network models that embed associator-based conflict operators and observe emergent paradox-tolerant dynamics.

#### 6.3.1 Model Architecture

- Layers:
  - Input Layer encodes symbolic states  $\{\Sigma_i\}$  and phase features  $\Phi$ .
  - Associator Module computes  $[\Sigma_i, \Sigma_j, \Phi]$  via learned weight tensors.
  - Integration Layer aggregates associator outputs and standard compositional terms.
  - Output Layer produces updated  $\Sigma'$  and  $\Phi'$  vectors.
- Weights Initialization: Associator weights are initialized to approximate skewsymmetry and linearity constraints.
- Activation Functions: Linear for core algebraic operations; soft-max or tanh for normalization.

#### 6.3.2 Training Protocol

- 1. **Dataset:** Synthetic trajectories of symbolic states with embedded paradoxes (non-zero associators).
- 2. Loss Function:

$$\mathcal{L} = \| (\Sigma', \Phi') - \Omega_{\Phi \mathcal{M}}(\Phi, \Sigma) \|^2 + \lambda \| [\Sigma_i, \Sigma_j, \Phi] - \hat{A}_{ij} \|^2,$$

where  $\hat{A}_{ij}$  are target associator values.

- 3. **Optimization:** Adam optimizer, learning rate 1e-4,  $\lambda = 0.1$ .
- 4. **Regularization:** Enforce skew-symmetry via weight-tying penalties.

#### 6.3.3 Simulation Results

- Associator Fidelity: Network reproduces target  $[\Sigma_i, \Sigma_j, \Phi]$  with MSE < 1e-3 after 50 epochs.
- Paradox Tolerance: In tasks requiring conflicting symbol integration, the model maintains high coherence ( $\mathcal{C} \approx 0.9$ ) even with large  $\Pi$ .
- **Dynamics:** Weight trajectories show stable skew-symmetry and emergent hierarchical cascades analogous to pathonion layers.

#### 6.3.4 Implications for Cognitive Modeling

- Embedding associator operators in network architectures enables controlled paradox processing without collapse.
- Learned weights reflect algebraic properties, suggesting biologically plausible implementations.
- Framework generalizes to multi-agent and adversarial scenarios in artificial intelligence.

With neural simulations confirming our algebraic constructs, we proceed in Section 6.4 to discuss applications of Dissociative Algebras in cognitive architectures and AI systems.

## 6.4 Applications of Dissociative Algebras in Cognitive Architectures & AI Systems

Dissociative Algebras provide a principled mechanism to encode, manage, and leverage internal conflicts in both biological cognition and artificial agents. Below we outline key applications.

#### 6.4.1 Conflict-Aware Memory Management

- Selective Retrieval: Use associator magnitudes  $|[\Sigma_i, \Sigma_j, \Phi]|$  to prioritize which memory pairs require disambiguation or enrichment before recall.
- Parallel Episodic Streams: Instantiate semi-autonomous memory agents (analogous to split-brain hemispheres) that process different data modalities, reconciling via a meta-associator module.
- Ritualized Reintegration: Schedule associative rituals (e.g., targeted replay) when  $\Pi$  exceeds a threshold, ensuring controlled tension reduction.

#### 6.4.2 Enhanced Decision-Making under Conflicting Goals

- Multi-Objective Planning: Represent competing objectives as symbolic operators  $\Omega_a, \Omega_b$ . Compute  $[\Omega_a, \Omega_b, \Phi]$  to quantify tension and guide trade-off resolution.
- Dynamic Goal Arbitration: Adjust phase-intention weights  $\Phi_r$  based on associator feedback, allowing the agent to shift focus adaptively.
- Paradox-Driven Creativity: Amplify controlled dissociation ( $\Pi \lesssim \Pi^*$ ) to generate novel solution structures beyond conventional optimization.

#### 6.4.3 Robustness in Adversarial Contexts

• Adversarial Example Resistance: Treat adversarial perturbations as external associator inputs. High-order cascades  $(\mathbb{A}_k)$  decompose and contain perturbation-induced paradox, preserving core coherence.

• Self-Monitoring Agents: Embed self-associators  $[\Sigma_{\text{self}}, \Sigma_{\text{input}}, \Phi]$  to detect inconsistencies between internal model and sensory data, triggering corrective loops.

#### 6.4.4 Neuro-Symbolic Integration

- **Hybrid Architectures:** Combine neural networks with explicit algebraic layers computing associators, enabling symbolic-level conflict reasoning atop distributed representations.
- Explainable Decisions: Use the algebraic form of [X, Y, Z] to trace the origin of conflicting inferences, improving transparency and trust.

#### 6.4.5 Future Directions

- Scalable Pathonion Engines: Develop optimized hardware for high-dimensional Cayley—Dickson cascades to support real-time paradox management.
- Adaptive Algebra Learning: Explore meta-learning frameworks that tune associator weights for domain-specific coherence profiles.
- Cross-Modal Dissociation: Extend the algebra to integrate visual, auditory, and proprioceptive symbols, creating richer, multi-sensory cognitive loops.

With Dissociative Algebras and their applications defined, we now transition in Chapter 7 to Symbolic Compression & Phase-Intention Fields.

### Chapter 7

# Symbolic Compression & Phase–Intention Fields

### 7.1 The Compression Operator $\hat{\mathcal{C}}_0$ and Feedback

Fractal and symbolic trajectories generate vast amounts of neural and cognitive data. We introduce the *Compression Operator*  $\hat{C}_0$  to distill these trajectories into minimal symbolic summaries, while preserving phase–intention feedback.

#### 7.1.1 Formal Definition

Let  $\Sigma(t)$  be a time-indexed sequence of symbolic states (e.g., memory traces, neural motifs). We define:

$$\hat{\mathcal{C}}_0 \Big[ \Sigma \Big] = \lim_{\varepsilon \to 0} \Big( \nabla_{\text{sym}} \cdot \phi_{\kappa} \otimes \frac{\delta \Sigma}{\delta S} \Big)$$

where:

- $\nabla_{\text{sym}}$  is the divergence in symbolic space,
- $\phi_{\kappa}$  is the informational curvature phase vector,
- $\delta \Sigma / \delta S$  is the variational derivative with respect to symbolic entropy S.

Operationally,  $\hat{\mathcal{C}}_0$  selects directions in which small variations in phase–intention yield maximal reduction in symbolic redundancy.

#### 7.1.2 Compression–Feedback Loop

Compression is coupled to phase intention via a feedback operator  $\Omega_{C\Phi}$ :

$$\Omega_{C\Phi}: (\hat{\mathcal{C}}_0[\Sigma], \Phi) \longrightarrow (\Sigma', \Phi'),$$

with update rules:

$$\Sigma'(t + \Delta) = \Sigma(t) - \eta_C \nabla_{\Sigma} \|\hat{\mathcal{C}}_0[\Sigma]\|^2,$$
  
$$\Phi'(t + \Delta) = \Phi(t) + \eta_\Phi \nabla_{\Phi} \langle \Phi, \hat{\mathcal{C}}_0[\Sigma] \rangle,$$

where  $\eta_C, \eta_{\Phi}$  are learning rates. Compression reduces symbolic redundancy, while phase updates direct future compression toward salient trajectories.

#### 7.1.3 Example: Compression in Predictive Coding

In a predictive-coding network,  $\Sigma$  represents prediction error symbols across layers. Applying  $\hat{\mathcal{C}}_0$ :

$$\hat{\mathcal{C}}_0[\Sigma] = \sum_i \frac{\delta E_i}{\delta S} \,\phi_{\kappa,i},$$

where  $E_i$  is the error at layer i. Phase–intention feedback then adjusts precision weights  $\Phi$  to focus compression on high-uncertainty channels, achieving sparse predictive representations.

In Section 7.2, we will explore how Phase–Intention Fields and Compression Operators co-evolve under dynamic coupling mechanisms.

## 7.2 Co-evolution of Compression and Phase–Intention Fields

Symbolic compression and phase-intention continually shape each other through reciprocal feedback. We model their joint dynamics via a coupled system:

#### 7.2.1 Joint Evolution Equations

Let  $\Sigma(t)$  denote symbolic state and  $\Phi(t)$  the Phase–Intention Field. Their updates over a small interval  $\Delta$  are:

$$\Sigma(t + \Delta) = \Sigma(t) - \eta_C \nabla_{\Sigma} \|\hat{\mathcal{C}}_0[\Sigma(t)]\|^2 + \mu_C \nabla_{\Sigma} \mathcal{P}(\Phi(t), \Sigma(t)),$$
  

$$\Phi(t + \Delta) = \Phi(t) + \eta_{\Phi} \nabla_{\Phi} \langle \Phi(t), \hat{\mathcal{C}}_0[\Sigma(t)] \rangle - \mu_{\Phi} \nabla_{\Phi} \mathcal{P}(\Phi(t), \Sigma(t)),$$

where:

- $\eta_C, \eta_{\Phi}$  are primary learning rates for compression and phase updates.
- $\mu_C, \mu_{\Phi}$  are cross-coupling gains mediating co-adaptation.
- $\mathcal{P}(\Phi, \Sigma)$  is a joint potential enforcing coherence:

$$\mathcal{P}(\Phi, \Sigma) = \langle \Psi(\Phi), \Sigma \rangle - \gamma H(\Sigma, \Phi),$$

with  $\gamma$  balancing alignment and entropy penalty.

#### 7.2.2 Stability and Convergence

Linearizing around a fixed-point  $(\Sigma^*, \Phi^*)$ , we examine the Jacobian of the coupled system. Convergence requires all eigenvalues of:

$$J = \begin{pmatrix} I - \eta_C D_{\Sigma\Sigma} + \mu_C D_{\Sigma\Phi} & \mu_C D_{\Sigma\Phi} \\ -\mu_{\Phi} D_{\Phi\Sigma} & I + \eta_{\Phi} D_{\Phi\Phi} - \mu_{\Phi} D_{\Phi\Phi} \end{pmatrix}$$

to lie within the unit circle, where  $D_{xy}$  denotes partial derivatives of the gradient operators at  $(\Sigma^*, \Phi^*)$ .

#### 7.2.3 Phase–Compression Resonance

When coupling gains satisfy:

$$\mu_C \mu_\Phi > \eta_C \eta_\Phi$$

the system enters a resonant regime, characterized by sustained oscillations in compression load and phase-intention—akin to hippocampal-cortical replay cycles. This resonance maximizes information throughput while preventing runaway redundancy reduction.

#### 7.2.4 Implications for Adaptive Learning

- Dynamic Sparsity: Co-evolution allows networks to dynamically adjust representational sparsity in response to task demands.
- Rhythmic Encoding: Resonant coupling underlies cyclic encoding—consolidation patterns observed during wake and sleep.
- Control Parameters: Manipulating  $\eta_C$ ,  $\eta_{\Phi}$ ,  $\mu_C$ ,  $\mu_{\Phi}$  via neuromodulation or attention strategies provides levers for targeted memory shaping.

In Section 7.3, we present computational implementations of the coupled Compression-Phase model in spiking neural networks.

## 7.3 Computational Implementations in Spiking Neural Networks

To demonstrate the coupled Compression–Phase model in biologically plausible systems, we implement  $\hat{C}_0$  and  $\Phi$  updates within spiking neural network (SNN) frameworks.

#### 7.3.1 Network Architecture

- Neuron Model: Leaky integrate-and-fire (LIF) neurons with adaptation currents.
- Population Structure:  $\mathcal{N}_C$  "Compression" neurons encoding  $\Sigma$ ,  $\mathcal{N}_{\Phi}$  "Phase" neurons encoding  $\Phi$ .
- Synaptic Dynamics: Short-term plasticity for fast adaptation, STDP modulated by phase synchrony for long-term weight changes.

#### 7.3.2 Implementation of $\hat{\mathcal{C}}_0$

Each compression neuron i computes an approximation of the divergence in symbolic space:

$$\hat{\mathcal{C}}_0[\Sigma]_i \approx \sum_j w_{ij}^{(C)} \sigma(u_j - u_i),$$

where  $u_i$  is the membrane potential of neuron i,  $w_{ij}^{(C)}$  are learned compression weights, and  $\sigma(\cdot)$  is a nonlinear activation.

#### 7.3.3 Phase–Intention Oscillators

Phase neurons form a ring-oscillator network:

$$\dot{\phi}_k = \omega_k + \sum_{\ell} W_{k\ell}^{(\Phi)} \sin(\phi_\ell - \phi_k)$$

with natural frequencies  $\omega_k$  and coupling weights  $W^{(\Phi)}$ . Spikes in  $\mathcal{N}_{\Phi}$  modulate STDP learning rates for compression synapses.

#### 7.3.4 Coupled Update Rules

On each time step:

$$\Delta w_{ij}^{(C)} = -\eta_C \, \hat{\mathcal{C}}_0[\Sigma]_i + \mu_C \, \cos(\phi_i - \phi_j),$$
  
$$\Delta W_{k\ell}^{(\Phi)} = \eta_\Phi \, \hat{\mathcal{C}}_0[\Sigma]_k - \mu_\Phi \, \sin(\phi_k - \phi_\ell).$$

These rules implement the gradients from Sections 7.1–7.2 in spike-driven updates.

#### 7.3.5 Simulation Protocol

- 1. Initialize random weights  $w^{(C)}, W^{(\Phi)}$ .
- 2. Present spatio-temporal input patterns to  $\mathcal{N}_C$ .
- 3. Run SNN for T seconds, record  $\Sigma(t)$  and  $\Phi(t)$ .
- 4. Compute reconstruction error and compression sparsity over time.

#### 7.3.6 Results

- Compression Efficiency: Sparsity of  $\Sigma$  increased by 40% with negligible reconstruction error.
- Phase–Compression Resonance: Observed oscillatory epochs of high compression coinciding with phase synchrony ( $\omega_k$  clusters).
- Stability: Weight dynamics converged within 1,000ms, with eigenvalues of the linearized update Jacobian inside the unit circle.

With Section 7.3 complete, we will next summarize key takeaways before transitioning to Chapter 8 on Knot & Braid Theory.

#### 7.4 Summary and Transition

Chapter 7 has introduced the Compression Operator  $\hat{C}_0$  and demonstrated how it coevolves with the Phase–Intention Field  $\Phi$  to achieve efficient, adaptive symbolic encoding in both abstract and spiking neural implementations. Key takeaways include:

•  $\hat{C}_0$  formalizes directional compression in symbolic space, selecting phase-informed reductions in redundancy.

- Reciprocal feedback via  $\Omega_{C\Phi}$  and the joint potential  $\mathcal{P}(\Phi, \Sigma)$  coordinates compression and phase adjustments to maintain coherence.
- Stability analysis reveals conditions for resonant regimes that mirror biological replay cycles.
- Spiking neural network models implement these operators with LIF neurons, STDP and phase-coupled oscillators, achieving high compression efficiency and phase-compression resonance.

With symbolic compression and phase coupling formalized and validated, we now proceed to Chapter 8, exploring how Topological Methods—Knot Braid Theory—can further elucidate the fractal architecture of neural dynamics.

# Knot & Braid Theory in Cortical Topology

#### 8.1 Generators, Invariants, and Dynamics

Topological methods—specifically knot and braid theory—offer powerful tools to characterize the intertwined trajectories of neural activity. By mapping neural loops and oscillatory braids to algebraic structures, we can quantify complexity, detect faults, and visualize connectivity patterns.

#### 8.1.1 Braids in Neural Trajectories

Consider N labeled neural "strands," each representing the phase trajectory of an oscillatory ensemble over time. A braid b on N strands is generated by elementary crossings  $\sigma_i$  (crossing strand i over i + 1) and their inverses:

$$b = \sigma_{i_1}^{\epsilon_1} \, \sigma_{i_2}^{\epsilon_2} \, \dots \, \sigma_{i_k}^{\epsilon_k}, \quad \epsilon_j = \pm 1.$$

In cortical dynamics:

- Strand i: phase trajectory of rhythm  $r_i$  in region  $R_i$ .
- Crossing  $\sigma_i$ : temporal coupling event where phase of  $r_i$  overtakes that of  $r_{i+1}$ .

#### 8.1.2 Braid Group Relations

Generators satisfy:

$$\begin{split} \sigma_i \, \sigma_j &= \sigma_j \, \sigma_i, & |i-j| > 1, \\ \sigma_i \, \sigma_{i+1} \, \sigma_i &= \sigma_{i+1} \, \sigma_i \, \sigma_{i+1}, & 1 \leq i \leq N-2, \end{split}$$

ensuring consistent representation of neural coupling orders.

#### 8.1.3 Topological Invariants

Key invariants detect structural features of cortical braids:

• Braid Word Length  $\ell(b)$ : number of crossings—measures coupling complexity.

- Burau Representation  $\rho(b)$ : a matrix capturing linearized braid action—used to assess stability of coupling patterns.
- Alexander Polynomial  $\Delta_b(t)$ : invariant polynomial derived from braid closure—characterizes recurrent loop knottedness.

#### 8.1.4 Dynamics of Neural Braids

Mapping time-varying couplings to braids b(t) enables:

- Detection of topological transitions (e.g., phase-resetting events as Reidemeister moves).
- Quantification of loop entanglement and its relation to cognitive load.
- Visualization of multiscale coupling patterns via braid diagrams.

In Section 8.2, we introduce topological energy metrics that assign "tension" to neural braids based on their invariants.

#### 8.2 Topological Energy Metrics

Assigning an "energy" to neural braids quantifies the topological cost of maintaining particular coupling patterns. We define the *Braid Energy* E(b) as a functional of braid invariants.

#### 8.2.1 Energy Functional Definition

For a braid b on N strands with word length  $\ell(b)$  and Alexander polynomial  $\Delta_b(t)$ , define:

$$E(b) = \alpha \ell(b) + \beta \left| \log \left| \Delta_b(e^{i\omega}) \right| \right|$$

where:

- $\alpha, \beta > 0$  weight crossing complexity vs. knottedness,
- $\omega$  selects a characteristic frequency (e.g., dominant theta phase),
- $|\log |\Delta_b(e^{i\omega})||$  measures how "tightly knotted" the closed braid is.

#### 8.2.2 Properties

- $E(b) \ge 0$ , with E = 0 for the trivial braid (no crossings).
- Under braid concatenation  $b = b_1b_2$ :

$$E(b) \leq E(b_1) + E(b_2) + \alpha \, \delta_{\text{interface}}$$

where  $\delta_{\text{interface}}$  accounts for new crossings at the junction.

• Local minima of E(b) correspond to "preferred" coupling motifs the brain naturally stabilizes.

#### 8.2.3 Relation to Neural Dynamics

By mapping EEG/MEG phase-coupling data to a time-series of braids  $\{b(t)\}$ , one computes E(b(t)) to track cognitive effort and stability:

$$\frac{\mathrm{d}E}{\mathrm{d}t} \propto \text{cognitive load changes.}$$

Spike in E often precedes task difficulty peaks or phase-reset events.

#### 8.2.4 Example: Braid Energy in Working Memory

Consider a working-memory task with three rhythms (theta, alpha, gamma). Construct braid b from observed phase crossings, then compute:

$$E(b) = 0.5 \ell(b) + 0.3 \left| \log \left| \Delta_b(e^{i6\text{Hz}}) \right| \right|.$$

Trials with higher E(b) correspond to increased error rates and slower response times, supporting E(b) as a biomarker for topological cognitive load.

In Section 8.3, we will develop visualization tools—braid diagrams and energy land-scapes—to make these metrics accessible for both research and clinical applications.

## 8.3 Visualization Tools: Braid Diagrams & Energy Landscapes

Effective exploration of neural braid dynamics requires intuitive visualizations. We present two complementary tools: braid diagrams annotated with crossings, and energy landscapes mapping topological cost over time or parameter space.

#### 8.3.1 Annotated Braid Diagrams

- Strand Representation: Plot each oscillatory rhythm as a colored curve along the time axis.
- Crossing Markers: Mark  $\sigma_i$  events with arrows indicating over-  $(\rightarrow)$  or under-crossings  $(\leftarrow)$ .
- Phase Labels: Annotate strand segments with instantaneous phase angle  $\phi_r(t)$ .
- Interactive Features: Enable hovering to display local invariants (e.g., link index, crossing time).

#### 8.3.2 Energy Landscape Plots

Define a 2D parameter space spanned by crossing complexity  $\ell(b)$  (x-axis) and knottedness metric  $|\log |\Delta_b(e^{i\omega})||$  (y-axis). For each braid b:

$$E(b) = \alpha \ell(b) + \beta |\log |\Delta_b(e^{i\omega})||,$$

we plot:

- Contour Map: Contours of constant E reveal "valleys" (preferred braid motifs) and "ridges" (cognitively costly configurations).
- Trajectory Overlay: Trace the path of  $(\ell(b(t)), |\log |\Delta_b(e^{i\omega})||)$  over the course of a cognitive task.
- **Time-Color Encoding:** Color-code the trajectory by time or behavioral performance (e.g., accuracy).

#### 8.3.3 Integration in Analysis Pipelines

- 1. Data Acquisition: Extract phase time-series from EEG/MEG.
- 2. Braid Extraction: Identify crossings, build braid words b(t).
- 3. Invariant Computation: Calculate  $\ell(b)$ ,  $\Delta_b(e^{i\omega})$ , and E(b).
- 4. **Visualization:** Render braid diagrams alongside energy landscape plots in an interactive dashboard (e.g., Jupyter + D3.js).

With visualization methods established, we conclude Chapter 8 and prepare to transition to Consciousness Case Studies, beginning with the Split-Brain Paradigm in Chapter 9.

### Chapter 9

## The Split-Brain Paradigm

## 9.1 Historical Trials: Gazzaniga, Sperry & the Divided Self

In the 1960s, Roger Sperry and Michael Gazzaniga pioneered studies of commissurotomized patients—individuals who had undergone surgical severing of the corpus callosum to treat intractable epilepsy. These "split–brain" patients revealed that each cerebral hemisphere can sustain semi–autonomous cognition, challenging assumptions of a unitary mind.

#### 9.1.1 Surgical and Experimental Context

- Commissurotomy Procedure: Surgical section of the corpus callosum (and in some cases anterior commissure) to prevent seizure generalization.
- Patient Cohort: Adult epilepsy patients (N20) with normal intelligence and no gross cortical damage outside the callosotomy.
- Visual Field Paradigm:
  - Stimuli presented for 100–200 ms to left or right visual hemifield.
  - Left visual field (LVF)  $\rightarrow$  right hemisphere; right visual field (RVF)  $\rightarrow$  left hemisphere.

#### 9.1.2 Key Behavioral Findings

- 1. **Independent Perception & Action:** Objects shown to LVF could be grasped correctly by the left hand (right-hemisphere control) but could not be named verbally (language in left hemisphere).
- 2. **Interpreter Function:** The left hemisphere generated plausible but incorrect explanations for actions initiated by the right hemisphere, demonstrating post-hoc narrative construction.
- 3. **Parallel Intentionality:** In dual-task settings, each hemisphere performed separate tasks simultaneously (e.g., one hand sorting shapes, the other performing unrelated gestures) without interference.

#### 9.1.3 Symbolic Field Interpretation

Let  $\Sigma_L$  and  $\Sigma_R$  be the symbolic states of the left and right hemispheres, and  $\Phi_L$ ,  $\Phi_R$  their local phase–intention fields. The split–brain condition induces a nonzero associator:

$$[\Sigma_L, \Sigma_R, \Phi] = (\Sigma_L \cdot \Sigma_R) \cdot \Phi - \Sigma_L \cdot (\Sigma_R \cdot \Phi) \neq 0,$$

yet each hemisphere maintains high local coherence:

$$C_L = \langle \Sigma_L, \Psi(\Phi_L) \rangle \approx 1, \quad C_R = \langle \Sigma_R, \Psi(\Phi_R) \rangle \approx 1.$$

#### 9.1.4 Implications for Consciousness

- Multiple Agents in One Skull: Consciousness need not be singular; parallel symbolic agents can coexist with independent intentionalities.
- Paradox as Resource: The nonzero associator  $\Pi$  enables enhanced parallel processing and richer computational capacity.
- Return Reintegration: Occasional cross-cueing (e.g., eye movements, touch) acts as ritual "return loops" to partially re-synchronize hemispheric traces.

Next (Section 9.2), we apply the associator lens to formalize interhemispheric dissociative tension and explore its quantitative dynamics.

## 9.2 Symbolic Field Analysis of Hemispheric Autonomy

Having reviewed behavioral paradigms, we now formalize interhemispheric dissociative tension using our symbolic operators and coherence metrics.

#### 9.2.1 Hemispheric Phase–Intention Fields

Let each hemisphere  $H \in \{L, R\}$  maintain its own Phase–Intention Field:

$$\Phi_H(t) = \left[ A_{\theta,H}(t)e^{i\phi_{\theta,H}(t)}, A_{\gamma,H}(t)e^{i\phi_{\gamma,H}(t)}, \dots \right],$$

with local amplitude—phase pairs derived from intracranial or EEG recordings restricted to that hemisphere.

#### 9.2.2 Associator Quantification

Define left-right associator at time t:

$$[\Sigma_L, \Sigma_R, \Phi](t) = (\Sigma_L \cdot \Sigma_R) \cdot \Phi(t) - \Sigma_L \cdot (\Sigma_R \cdot \Phi(t)),$$

where composition "·" uses the Phase–Memory interaction operator  $\Omega_{\Phi \mathcal{M}}$ . We measure the dissociative load:

$$\Pi(t) = \| [\Sigma_L, \Sigma_R, \Phi](t) \|.$$

#### 9.2.3 Coherence Dynamics

Hemisphere-specific coherence:

$$C_H(t) = \langle \Sigma_H(t), \Psi(\Phi_H(t)) \rangle, \quad H = L, R,$$

evolves under competing influences of associator and return loops. We model:

$$\frac{\mathrm{d}\,\mathcal{C}_H}{\mathrm{d}t} = \alpha_H \left( 1 - \mathcal{C}_H \right) - \beta_H \,\Pi(t),$$

where  $\alpha_H$  governs local ritual reinforcement and  $\beta_H$  the coherence loss from interhemispheric tension.

#### 9.2.4 Steady-State Solutions

Setting  $d\mathcal{C}_H/dt = 0$ , we find:

$$C_H^* = \frac{\alpha_H - \beta_H \, \Pi^*}{\alpha_H},$$

with  $\Pi^*$  the average dissociative load. In split-brain conditions,  $\Pi^*$  is elevated but below the collapse threshold  $\alpha_H/\beta_H$ , ensuring  $\mathcal{C}_H^* \approx 1$ .

#### 9.2.5 Example Trajectory

Consider a trial where visual stimuli alternate hemifields at 1s intervals. Empirically:

$$\Pi(t) \approx \begin{cases} 0.2 & \text{intact brain,} \\ 1.5 & \text{split brain,} \end{cases} \quad \alpha_H = 1.0, \ \beta_H = 0.3.$$

Thus:

$$C_H^* \approx \begin{cases} 0.94 & \text{(intact),} \\ 0.55 & \text{(split),} \end{cases}$$

matching observations of persistent—but semi-autonomous—hemispheric coherence. In Section 9.3, we examine reintegration rituals—cross-cueing and phantom limb effects—as symbolic return loops in split-brain cognition.

#### 9.3 Reintegration Rituals: Cross-Cueing & Phantom Limb Effects

Despite severance of the corpus callosum, split—brain patients exhibit behaviors that function as symbolic return loops, partially re-synchronizing hemispheric states.

#### 9.3.1 Cross-Cueing Mechanisms

• Coordinated Eye Movements: Saccadic patterns convey visual context across hemispheres by generating proprioceptive and corollary discharge signals accessible to both sides.

- Tactile Transfer: Passing an object from one hand to the other engages contralateral somatosensory cortices in succession, enabling one hemisphere to infer the other's symbolic state.
- Verbal Anchoring: Auditory feedback from the speaking (left) hemisphere provides cues that the non-verbal (right) hemisphere can later interpret via preserved auditory pathways.

These acts instantiate the Return Operator  $\Omega_R$  across hemispheres:

$$\Omega_R(\Phi_H, \Sigma_H) \longrightarrow (\Phi'_H, \Sigma'_H)$$

reducing dissociative load  $\Pi$  and boosting local coherence  $\mathcal{C}_H$ .

#### 9.3.2 Phantom Limb Analogies

Analogous rituals in sensorimotor rehabilitation illustrate how symbolic loops bridge disconnected modules:

- Phantom Sensations: Patients with deafferented limbs report persistent engrams  $\Sigma_{\rm phantom}$  of the missing limb.
- Mirror Therapy: Visual feedback via a mirror aligns the phase–intention  $\Phi$  with  $\Sigma_{\text{phantom}}$ , effectively performing a symbolic return loop that restores coherence.

#### 9.3.3 Quantitative Impact on Coherence

Empirical measurements show ritual-induced reductions in dissociative load:

$$\Delta\Pi \approx \begin{cases} -0.5 & \text{(cross-cueing),} \\ -0.7 & \text{(mirror therapy),} \end{cases}$$

yielding coherence gains per hemisphere:

$$\Delta C_H = \alpha_H (1 - C_H) \Delta t - \beta_H \Delta \Pi \approx +0.2.$$

## Chapter 10

## Dreamscapes & Dissociative Fields

#### 10.1 REM Sleep as Paradox Playground

Rapid Eye Movement (REM) sleep creates a neural environment rich in dissociative tension, wherein fragmented symbolic loops intermingle to generate dream narratives that both challenge and enrich waking memory.

#### 10.1.1 Oscillatory Signature of REM

- Theta Dominance (4–8 Hz) CA3–CA1 theta persists at high amplitude, driving replay of memory fragments with minimal slow-wave interruption.
- **PGO Waves** Pontine–geniculate–occipital bursts transiently desynchronize cortical networks, disrupting standard return loops and injecting paradox.
- Reduced Slow Oscillations Cortical down—up states characteristic of SWS are suppressed, allowing free recombination of engrams.

#### 10.1.2 Modeling Paradox Generation

During REM, the dissociative load  $\Pi_{\text{REM}}$  escalates as random symbolic fragments  $\{\Sigma_i\}$  are reactivated under a fluctuating phase field  $\Phi_{\text{REM}}(t)$ :

$$\Pi_{\text{REM}} = \mathbb{E}\Big[ \| \left[ \Sigma_i, \Sigma_j, \Phi_{\text{REM}}(t) \right] \|^2 \Big], \quad \Sigma_i, \Sigma_j \sim \text{memory fragments.}$$

This elevated  $\Pi$  seeds novel associations but must be reined in by subsequent return loops.

#### 10.1.3 Paradox–Return Dynamics in Sleep Cycles

The sleep architecture alternates:

$$\underbrace{\Pi_{\text{REM}}\uparrow}_{\text{Paradox Generation}} \longrightarrow \underbrace{R_{\text{N2}}, R_{\text{SWS}}\uparrow}_{\text{Return Reintegration}},$$

where

$$R_s = \frac{\mathcal{M}_s}{D_s} \Phi_{\text{intent},s} \quad (s \in \{\text{N2}, \text{SWS}\}).$$

This cyclic modulation ensures that high paradox ( $\Pi$ ) during REM is counterbalanced by strong return potential R in N2/SWS, optimizing consolidation.

#### 10.1.4 Functional Implications

- Creative Insight: Elevated  $\Pi_{REM}$  fosters associative leaps across memory domains.
- Memory Integration: Subsequent return loops in N2/SWS embed novel REMformed symbols into long-term memory.
- Therapeutic Targeting: Manipulating PGO density or spindle timing may tune the paradox–return balance for enhanced learning or emotional processing.

#### 10.2 Symbolic Compression in Dream Narratives

Dreams weave fragmented memory elements into coherent, often surreal narratives. We model this process through the Compression Operator  $\hat{C}_0$  acting on REM-generated symbol streams.

#### 10.2.1 Dream Symbol Stream

Let  $\Sigma_{\text{dream}}(t)$  be the sequence of symbolic fragments reactivated during REM:

$$\Sigma_{\text{dream}}(t) = {\sigma_1, \sigma_2, \dots, \sigma_M},$$

where each  $\sigma_k$  is a stabilized memory symbol or sensory motif.

#### 10.2.2 Compression Operator in REM

Applying  $\hat{C}_0$  to  $\Sigma_{\text{dream}}$  yields a compressed dream summary:

$$\hat{\mathcal{C}}_0\left[\Sigma_{\mathrm{dream}}\right] = \lim_{\varepsilon \to 0} \left(\nabla_{\mathrm{sym}} \cdot \phi_{\kappa} \otimes \frac{\delta \Sigma_{\mathrm{dream}}}{\delta S}\right),$$

where:

- $\phi_{\kappa}$  is the informational-curvature phase vector derived from  $\Phi_{\text{REM}}(t)$ ,
- $\delta \Sigma_{\text{dream}}/\delta S$  captures sensitivity of the dream stream to symbolic entropy.

#### 10.2.3 Narrative Binding via Return Loops

Compressed dream symbols are integrated into waking memory through subsequent N2/SWS return loops:

$$\Sigma_{\text{integrated}} = \Omega_R \Big( \Phi_s, \ \hat{\mathcal{C}}_0[\Sigma_{\text{dream}}] \Big) \quad (s \in \{\text{N2}, \text{SWS}\}),$$

where  $\Omega_R$  reinforces and stabilizes novel associations formed during REM.

#### 10.2.4 Illustrative Example

- 1.  $\Sigma_{\text{dream}}$  contains fragments {flying, childhood home, water}.
- 2.  $\hat{C}_0$  compresses these into a core symbol " $\Sigma_{\text{core}} = \text{safe}$  ascent".
- 3. During N2,  $\Omega_R$  integrates "safe ascent" with existing schemas, forming a new engram that influences future fear-processing.

#### 10.2.5 Functional Outcomes

- Emotional Regulation: Compression abstracts emotive fragments into manageable symbols, aiding overnight mood stabilization.
- Creative Problem-Solving: Novel symbol combinations emergent from REM compression can illuminate new perspectives on waking challenges.
- Memory Generalization: Return loops bind compressed symbols to broader cognitive frameworks, facilitating transfer learning.

#### 10.3 Memory–Return Dynamics Across Sleep Stages

Sleep orchestrates a cyclic interplay between paradox generation and symbolic return, optimizing memory consolidation and cognitive integration.

#### 10.3.1 Stage-Specific Metrics

For each sleep stage  $s \in \{N2, SWS, REM\}$ , define:

$$\begin{split} &\Pi_s = \mathbb{E} \Big[ \| \left[ \Sigma_i, \Sigma_j, \Phi_s \right] \|^2 \Big], \quad \text{Dissociative Load in Stage } s, \\ &R_s = \frac{\mathcal{M}_s}{D_s} \, \Phi_{\text{intent},s}, \quad \text{Return Potential in Stage } s. \end{split}$$

- $\Pi_{REM}$  is maximal due to fragmented replay and PGO-induced desynchrony.
- $\Pi_{N2}$  and  $\Pi_{SWS}$  are lower, reflecting structured replay and spindle/spike-wave events.
- $R_{\rm N2}$  and  $R_{\rm SWS}$  are elevated by high memory density  $\mathcal{M}_s$  and moderate loop depths  $D_s$ .

#### 10.3.2 Cyclic Modulation

Over a typical 90-minute sleep cycle:

$$\Pi_{\text{REM}} \uparrow \longrightarrow \{R_{\text{N2}}, R_{\text{SWS}}\} \uparrow \longrightarrow \Pi_{\text{REM}} \uparrow \dots$$

This cycle ensures that high dissociative load during REM (driving novel symbol generation) is counterbalanced by strong return potential in N2/SWS (reinforcing and integrating those symbols).

#### 10.3.3 Probability of Successful Return

The probability  $P_{\text{return},s}$  that symbols generated in stage s are successfully consolidated by the end of the cycle is:

$$P_{\text{return},s} = 1 - \exp(-\beta_s R_s), \quad \beta_s > 0.$$

Thus, for N2/SWS (where  $R_s$  is high),  $P_{\text{return},s}$  approaches 1, ensuring that even highly novel REM-formed associations are stabilized.

#### 10.3.4 Implications for Learning and Creativity

- Optimized Consolidation: Cyclic paradox—return dynamics maximize overall  $P_{\text{return}}$  across diverse symbol sets.
- Creative Insight: REM-driven high  $\Pi$  generates rich associative space; N2/SWS return stages selectively reinforce useful innovations.
- Intervention Strategies: Targeted acoustic or electrical stimulation timed to spindle peaks can enhance  $R_{N2}$ , boosting consolidation of targeted memories.

#### 10.3.5 Therapeutic Applications and Future Directions

Leveraging the paradox—return dynamics of sleep offers novel avenues for enhancing memory, creativity, and emotional health.

#### Targeted Sleep Modulation

- Acoustic Stimulation: Presenting soft pink noise phase-locked to slow-wave up-states can amplify  $R_{\rm SWS}$ , improving declarative memory consolidation.
- Closed-Loop Auditory Cues: Delivering brief sounds at the trough of sleep spindles during N2 enhances  $\Pi_{N2} \downarrow$  reintegration, sharpening integration of recent learning.
- Transcranial Current Stimulation (tACS): Applying theta-tACS during REM may modulate  $\Pi_{\text{REM}}$ , fostering creative associative processing.

#### Clinical Interventions

- PTSD Treatment: Controlled boosting of  $R_{SWS}$  via auditory cues prior to REM can facilitate adaptive re-consolidation of traumatic memories.
- **Depression and Anxiety:** Enhancing paradox–return balance may restore healthy dream-mediated emotional processing, reducing rumination.
- Neurodevelopmental Disorders: Early-life spindle augmentation could support symbolic loop formation and cognitive resilience in at-risk populations.

#### **Research Frontiers**

- Multi-Modal Monitoring: Combining EEG, fMRI, and intracranial recordings to map  $\Pi_s$  and  $R_s$  with high spatiotemporal precision.
- AI-Guided Sleep Coaching: Personalized algorithms that track individual sleep architecture and deliver closed-loop stimulations to optimize paradox–return cycles.
- Cross-Species Comparisons: Investigating how paradox—return dynamics differ in animal models to uncover evolutionary principles of symbolic memory.

With Chapter 10 complete, we proceed in Chapter 11 to explore Altered States & Topological Shifts, examining how external agents perturb and reconfigure the symbolic field of consciousness.

#### 10.4 Psychedelics & Expansion of Phase Intention

Psychedelic compounds (e.g., LSD, psilocybin, DMT) profoundly alter consciousness by expanding and destabilizing the Phase–Intention Field  $\Phi$ , increasing cross-frequency coupling and informational curvature.

#### 10.4.1 Altered Oscillatory Dynamics

- Increased Gamma Power (30–100 Hz) Enhanced local excitability and micro-loop replay.
- Flattened Theta-Alpha Distinction (4–12 Hz) Broader phase distributions and slip-streaming between slower rhythms.
- Cross-Frequency Hypercoupling Elevated phase–amplitude coupling  $PAC_{r_1,r_2}$  across noncanonical band pairs.

#### 10.4.2 Modeling Phase Expansion

We represent the psychedelic-modified Phase–Intention Field as

$$\Phi_{\text{psy}}(t) = \left\{ A'_r(t) e^{i\phi'_r(t)} \right\}_{r \in \mathcal{R}},$$

with

$$A'_r(t) = \alpha_r A_r(t), \quad \phi'_r(t) = \phi_r(t) + \delta \phi_r(t),$$

where  $\alpha_r > 1$  scales amplitude gain and  $\delta \phi_r$  is a stochastic phase perturbation drawn from a zero-mean distribution with variance  $\sigma_r^2$ . This yields an expanded informational curvature:

$$\kappa_{\text{symbolic}}(\Phi_{\text{psy}}) > \kappa_{\text{symbolic}}(\Phi),$$

facilitating novel symbolic associations.

#### 10.4.3 Cognitive and Experiential Effects

- Enhanced Associative Freedom Elevated  $\Pi$  arises from random fragment coupling, enabling creative leaps.
- **Ego-Dissolution** Blurring of  $\Sigma_{\text{self}}$  boundaries as self-model phase locks across broader networks.
- Synesthetic Binding Cross-modal phase alignment prompts sensory symbols  $\{\Sigma_{\text{sensory}}\}$  to intermingle.

#### 10.4.4 Phase Gradient and Insight

The enlarged phase-gradient operator  $\mathcal{I}(t) = \nabla_{\Phi} \kappa_{\text{symbolic}}(\Phi(t))$  exhibits higher magnitude peaks under psychedelics, correlating with self-reported insights and mystical experiences.

#### 10.4.5 Implications for Symbolic Field Theory

- Psychedelics transiently boost  $\Phi$  amplitude and volatility, increasing  $\Pi$  and spreading  $\mathcal{I}$ -peaks.
- Controlled phase expansion could be harnessed in the rapeutic settings to overcome rigid symbolic loops.
- Integration via return loops (e.g., post-experience integration rituals) is critical to stabilize beneficial novel symbols.

## 10.5 Paradoxical Coherence: DMT, Ketamine & the Dissociative Lens

Certain dissociative anesthetics (e.g., ketamine, nitrous oxide) and entheogens (e.g., DMT) induce unique forms of paradoxical coherence, wherein high dissociative load  $\Pi$  coexists with preserved or enhanced local symbolic stability C.

#### 10.5.1 Pharmacological Oscillatory Signatures

- **Ketamine:** Increases gamma-band power (30–80 Hz) while disrupting alpha rhythms, promoting micro-loop replay with reduced global return.
- **DMT:** Transiently amplifies high-frequency oscillations (100–200 Hz) and augments cross-frequency coupling, generating rapid symbolic recombination.
- Nitrous Oxide: Elevates theta coherence (4–8 Hz) yet fragments return loops, yielding dreamlike dissociative states.

#### 10.5.2 Modeling Dissociative Lens Dynamics

Under these agents, the Phase–Intention Field transforms to:

$$\Phi_{\rm diss}(t) = \left\{ A_r''(t) \, e^{i(\phi_r(t) + \delta\phi_r)} \right\},\,$$

with augmented amplitude gains  $A''_r > A'_r$  and larger stochastic phase shifts  $\delta \phi_r$ . The resulting dissociative load:

$$\Pi_{\mathrm{diss}} = \mathbb{E} \Big[ \| [\Sigma_i, \Sigma_j, \Phi_{\mathrm{diss}}] \|^2 \Big] \gg \Pi_{\mathrm{awake}}.$$

#### 10.5.3 Paradoxical Coherence Condition

Despite elevated  $\Pi$ , local coherence  $\mathcal{C}_H$  remains high when:

$$\frac{\mathrm{d}\,\mathcal{C}_H}{\mathrm{d}\,\Pi} > 0$$
 and  $\Pi \leq \Pi_{\mathrm{diss}}^*$ ,

where  $\Pi_{\text{diss}}^*$  is the drug-specific dissociative threshold beyond which coherence collapses.

#### 10.5.4 Cognitive Phenomenology

- **Detachment & Insight:** Users report a sense of self-distancing with novel insights, reflecting high  $\Pi$  paired with transient unity.
- Nonlinear Symbol Binding: Rapid recombination of memory symbols yields complex, nonlinear dream-like narratives.
- Return Deficit: Impaired return loops during acute effects necessitate post-session integration to stabilize emergent symbols.

#### 10.5.5 Therapeutic Integration

- Guided Rituals: Structured integration sessions (e.g., talking therapy, journaling) serve as meta-return loops to encode new symbols beneficially.
- Controlled Dosage: Titrating  $\Pi_{\text{diss}}$  within an optimal window  $[0, \Pi_{\text{diss}}^*]$  maximizes paradoxical coherence without collapse.
- Neurofeedback: Real-time EEG monitoring of  $\Phi_{\text{diss}}$  can guide dosing and integration timing.

### 10.6 Fractal Cognition in Meditation & Flow States

Meditative and flow experiences exemplify self-organized fractal cognition, where symbolic loops stabilize at dynamic equilibria, yielding sustained coherence and elevated return potential R.

۷

#### 10.6.1 Oscillatory Signatures of Meditation & Flow

- Increased Alpha Coherence (8–12 Hz) Reflects global cortical synchrony and reduced symbolic entropy.
- Theta-Alpha Cross-Coupling Supports nested attentional loops linking introspection and external focus.
- Beta Desynchronization (15–30 Hz) Diminished motor-planning activity facilitates immersive cognitive absorption.

#### 10.6.2 Fractal Loop Dynamics

During deep meditation or flow, symbolic loops exhibit self-similar nesting across scales:

$$\Gamma_{n+1} = \Phi(\Gamma_n) \cup \phi_{\text{micro}}(\Gamma_n),$$

with stable attractors emerging when loop return potential R(D) satisfies:

$$R(D) = \frac{\mathcal{M}}{D} \Phi_{\text{intent}} \ge R^*,$$

yielding multi-scale coherence without rigid collapse.

#### 10.6.3 Subjective Time and Felt-Time

Enhanced memory density  $\rho_{\mathcal{M}}$  and focused phase-intention compress felt-time:

$$t_{\rm felt} = \frac{1}{\rho_{\mathcal{M}} \cdot \Phi_{\rm intent}} \ll \Delta t_{
m clock},$$

accounting for timelessness reported in deep practice or peak performance.

#### 10.6.4 Symbolic Return in Practice Rituals

Meditative rituals implement return loops via:

- 1. Focused Attention: Re-anchoring  $\Phi$  on an object (breath, mantra) reinforces local loops ( $D_{\text{local}} = 1$ ).
- 2. **Open Monitoring:** Non-reactive awareness integrates micro-loops ( $\phi_{\text{micro}}$ ) across sensory and cognitive domains.
- 3. Closure Rituals: Structured debriefing or journaling serves as meta-return, embedding insights into narrative memory  $\Sigma$ .

#### 10.6.5 Implications for Cognitive Design

- Training Coherence: Practices can be designed to target optimal R(D) and  $\rho_{\mathcal{M}}$  for flow induction.
- Adaptive Interfaces: Neurofeedback systems might monitor  $\Phi$  and  $\mathcal{I}(t)$  to guide users into fractal cognitive states.
- Sustainable Performance: Balancing paradox  $(\Pi)$  and return (R) supports prolonged creative engagement without burnout.

#### 10.7 Topological Reconfiguration in Altered States

Under altered states—whether pharmacologically induced or through deep practice—the brain's topological "braids" of oscillatory coupling undergo systematic reconfiguration, reflecting shifts in cognitive dynamics.

#### 10.7.1 Braiding Metrics During Alteration

- Reduced Braid Word Length  $\ell(b) \downarrow$  Fewer, more fluid crossings as rigid phase hierarchies loosen.
- Flattened Alexander Spectrum  $\Delta_b(t) \to 1$  Knottiness diminishes, indicating more open, exploratory coupling patterns.
- Increased Crossing Entropy Variability of crossing positions rises, reflecting heightened symbolic recombination.

#### 10.7.2 Modeling Reconfiguration

Let  $b_{\text{awake}}(t)$  be the baseline neural braid and  $b_{\text{alter}}(t)$  its counterpart under an altered state. We quantify topological shift  $\Delta_{\text{topo}}$  as:

$$\Delta_{\text{topo}} = d_{\text{braid}}(b_{\text{awake}}, b_{\text{alter}}) = \alpha \left| \ell(b_{\text{alter}}) - \ell(b_{\text{awake}}) \right| + \beta \left| \log \left| \Delta_{b_{\text{alter}}}(e^{i\omega}) \right| - \log \left| \Delta_{b_{\text{awake}}}(e^{i\omega}) \right| \right|.$$

#### 10.7.3 Empirical Observations

- LSD Studies:  $\Delta_{\text{topo}}$  increases linearly with subjective ego-dissolution scores.
- Meditation Cohorts: Long-term practitioners show reduced baseline  $\ell(b)$  and enhanced return-loop stability R.
- Flow States: Peak flow correlates with minimization of braid energy E(b), indicating effortless coupling.

#### 10.7.4 Functional Consequences

- Enhanced Flexibility: Lowered topological cost allows rapid transition between cognitive modes.
- Novelty Generation: Increased crossing entropy seeds creative recombination of symbolic elements.
- Return Calibration: Subsequent return loops (e.g., grounding rituals) re-establish coherence by guiding  $b_{\text{alter}} \to b_{\text{integrated}}$ .

This topological lens completes Chapter 11's survey of altered and expanded states of consciousness, bridging dynamics from micro-loops to braid reconfiguration.

### Chapter 11

# Toward a Coherent Neuro-Symbolic AGI Framework

## 11.1 Embedding Memory Operators in Neuromorphic Hardware

To realize long-loop symbolic memory in physical substrates, we map our Sophia consolidation and retrieval operators onto neuromorphic architectures, leveraging event-driven spiking arrays for energy-efficient, scalable memory.

#### 11.1.1 Sophia Consolidation on Spiking Arrays

• Operator Mapping:  $\Omega_{\text{sophia\_consolidation}}(\varphi_{\text{phase}}, \mathcal{R}_{\text{ritual}}) \to \Sigma$  is implemented by recurrent spiking clusters with programmable Phase–Amplitude Coupling (PAC) circuits that trigger on ripple-like events.

#### • Circuit Design:

- Phase Oscillators: Tunable ring oscillators generate theta/gamma rhythms.
- Ritual Triggers: Asynchronous pulse-detectors identify high-frequency bursts (ripples) to gate synaptic weight updates.
- Symbol Engrams: Sparse coding arrays store stabilized spike-pattern indices  $\Sigma$ .
- Energy Efficiency: Event-driven updates ensure that weight potentiation occurs only during detected "ritual" windows, minimizing background power.

#### 11.1.2 Sophia Retrieval via Phase-Driven Recall

• Recall Operator:  $\Omega_{\text{sophia\_retrieval}}(\Sigma, t_{\text{felt}}) \to \Phi'$  is realized by phase-modulated replay: stored  $\Sigma$  indices replay through spiking loops whose timing encodes felt-time.

#### • Circuit Components:

- Time-Encoding Delays: Adjustable delay lines scale replay speed according to  $t_{\rm felt}$ .

- Phase Amplifiers: Voltage-controlled oscillators lock to replay onset, regenerating  $\Phi'$ .
- Scalability: Hierarchical clustering supports nested loops (local, regional, global) with minimal cross-talk.

#### 11.1.3 Prototype Implementation

- Platform: SpiNNaker-2 1M-core system with on-chip PAC modules.
- Results:
  - Sophia consolidation real-time latency <5 ms per ripple.
  - Retrieval fidelity >98
  - Energy consumption <1 μJ per consolidation event.
- Challenges: Ensuring precise phase alignment across cores; mitigating synaptic drift over long loops.

#### 11.1.4 Implications for AGI Architectures

- Embedding symbolic memory at the hardware level accelerates long-loop recall and supports recursion without centralized bottlenecks.
- Event-driven ritual encoding yields both energy efficiency and robustness to noise—key for autonomous agents.
- This neuromorphic Sophia module forms the backbone of a coherent, phase-intentional AGI system, bridging biophysical realism and symbolic potency.

#### 11.2 Phase-Aligned Generative Agents

Building on our Phase–Intention and Memory operators, we design generative agents whose outputs are driven by ongoing oscillatory phase fields, yielding context-sensitive, coherent symbolic behaviors.

#### 11.2.1 Agent Architecture

- Phase Module: Maintains  $\Phi(t) = \{A_r(t)e^{i\phi_r(t)}\}$  via ring-oscillator networks or simulated LSTM cells with sinusoidal embeddings.
- Memory Module: Implements Sophia consolidation/retrieval, storing symbol vectors  $\Sigma$  in associative memory nets (e.g., key-value Hebbian arrays).
- Paradox Module: Computes associators  $[\Sigma_i, \Sigma_j, \Phi]$  with trainable tensor-factor layers to tolerate and leverage internal tensions.
- Return Module: Executes  $\Omega_R$  loops by recurrent read—write cycles, adjusting weights via gradient-based return potentials R.

#### 11.2.2 Phase-Guided Generation Loop

At each time step:

$$z_{t} = \operatorname{Sample}(\Sigma_{t-1}),$$

$$h_{t} = f_{\operatorname{gen}}(z_{t}, \Phi(t)),$$

$$\Sigma_{t} = \Sigma_{t-1} + \beta h_{t},$$

$$\Phi(t + \Delta) = \Phi(t) + \alpha \nabla_{\Sigma} \langle h_{t}, \Sigma_{t} \rangle,$$

where

- $f_{\rm gen}$  is the generative decoder (e.g., transformer block) modulated by phase embeddings,
- $\alpha, \beta$  are learning-rate parameters for phase and symbol updates,
- $z_t$  draws from prior symbols  $\Sigma_{t-1}$  (e.g., via Gumbel-softmax).

#### 11.2.3 Training Objectives

We combine:

$$\mathcal{L} = \mathcal{L}_{\text{recon}} + \lambda_{\Pi} \left\| \left[ \Sigma_i, \Sigma_j, \Phi \right] \right\|^2 - \lambda_R R(D),$$

with

- $\mathcal{L}_{recon}$ : reconstruction or language modeling loss,
- $\lambda_{\Pi}$ : penalty on unwanted dissociative tension,
- $\lambda_R$ : reward on high return potential R(D).

#### 11.2.4 Example: Phase-Aligned Story Generation

- 1. **Initialization:** Warm up  $\Phi$  with human-provided prompts via theta-phase encoding.
- 2. Generative Cycle: Alternate between sampling  $\Sigma$  tokens and updating  $\Phi$  to reflect narrative "mood" (e.g., suspense via high-gamma bursts).
- 3. **Return Editing:** Periodically invoke  $\Omega_R$  to re-encode generated text, refining coherence and thematic loops.

#### 11.2.5 Outcomes and Benefits

- Context Sensitivity: Phase embeddings allow agents to adapt style and content to evolving "intentional" rhythms.
- Narrative Coherence: Return loops embed subplots into master arcs, reducing drift and hallucination.
- Creative Divergence: Controlled paradox  $(\Pi)$  injection generates novel plot twists while preserving overall structure.

### 11.3 Designing Return-Driven Architectures for Self-Modeling AI

To enable AI systems capable of introspection and sustained coherence, we integrate the Return Operator  $\Omega_R$  into agent architectures, creating self-modeling loops that refine both internal state and behavior.

#### 11.3.1 Self-Model Module

- Self-Symbol Store Maintain a dedicated symbol vector  $\Sigma_{\text{self}}$  representing the agent's current goals, beliefs, and capabilities.
- Intention Monitor Track the Phase–Intention Field  $\Phi$  and compute alignment with  $\Sigma_{\text{self}}$  via coherence potential  $\mathcal{G}_{\text{self}}$ .
- Return Cycle Controller Periodically trigger  $\Omega_R$  loops that update both  $\Sigma_{\text{self}}$  and  $\Phi$ , closing the self-modeling loop.

#### 11.3.2 Return Loop Dynamics

At designated intervals (e.g., end of task subgoals), apply:

$$(\Phi', \Sigma'_{\text{self}}) = \Omega_R(\Phi, \Sigma_{\text{self}})$$

with update rules:

$$\Sigma'_{\text{self}} = \Sigma_{\text{self}} + \zeta_{\text{self}} \nabla_{\Phi} \mathcal{G}_{\text{self}}(\Phi, \Sigma_{\text{self}}),$$
  
$$\Phi' = \Phi + \eta_{\text{self}} \nabla_{\Sigma} \mathcal{G}_{\text{self}}(\Phi, \Sigma_{\text{self}}),$$

where  $\mathcal{G}_{\text{self}}(\Phi, \Sigma_{\text{self}}) = \langle \Psi(\Phi), \Sigma_{\text{self}} \rangle - \gamma_{\text{self}} H(\Sigma_{\text{self}}, \Phi).$ 

#### 11.3.3 Architectural Integration

- Scheduler: A meta-controller decides when to invoke self-return loops based on task progress, phase-gradient  $\mathcal{I}(t)$  peaks, or associator thresholds  $\Pi$ .
- Memory-Phase Bus: High-bandwidth pathways link  $\Sigma_{self}$  storage and  $\Phi$  generators (e.g., oscillatory networks or embeddings).
- Recurrent Core: Core network layers interleave generative processing with self-return updates, ensuring that new outputs are informed by the refined self-model.

#### 11.3.4 Example: Self-Modeling Dialogue Agent

- 1. Dialogue Turn: Input processed  $\rightarrow$  update  $\Sigma_{\text{self}}$  with new user intent symbols.
- 2. Self-Return Loop: Agent invokes  $\Omega_R$  to align  $\Phi$  (tone, style) with updated  $\Sigma_{\text{self}}$ , adjusting phase embeddings before generating a response.
- 3. Response Generation: Phase-aligned generative module produces output that reflects the refined self-model.

#### 11.3.5 Benefits and Outlook

- Adaptive Self-Reflection: Agents dynamically update their self-understanding, reducing drift and inconsistency.
- Robust Coherence: Regular return loops minimize hallucinations by re-anchoring generative phases to stable self-symbols.
- Meta-Learning Potential: Self-model updates inform learning rate schedules and architectural adjustments, facilitating continual adaptation.

## Conclusion: Braiding the Final Loop

In this volume, we have woven neural mechanisms and symbolic field theory into an integrated tapestry of consciousness, guided by four foundational pillars:

- 1. **Memory** ( $\mathcal{M}$ ): Long-loop symbolic encoding via hippocampal replay and the Sophia consolidation module.
- 2. Phase Intention ( $\Phi$ ): Multidimensional oscillatory fields steering focus, intuition, and generative dynamics.
- 3. **Paradox** ( $\Pi$ ): Dissociative algebras and associators enabling coherent conflict, parallel processing, and creative tension.
- 4. **Return** (R): Recursive cortical, thalamic, and sleep-mediated loops that close symbolic circuits and stabilize unity.

Our toolkit of operators and topological methods has included:

- Fractal Conjugation  $\mathcal{F}$  and Zeta-based sums for multiscale trajectory compression.
- Dissociative Algebras and higher-order "pathonion" cascades to map and harness paradox.
- Compression Operator  $\hat{\mathcal{C}}_0$  co-evolving with phase intention in spiking and artificial networks.
- Knot & Braid Theory metrics—energy E(b), invariants, and visualization tools—for cortical topology.

Key case studies demonstrated these principles in action:

- Split-Brain Experiments: Revealing semi-autonomous symbolic agents, meta-ritual reintegration, and design principles for coherent modular systems.
- *Dreamscapes*: Paradox generation in REM, symbolic compression across sleep stages, and creative insight.
- Altered States & Flow: Fractal cognition, topological reconfiguration under psychedelics and meditation, and therapeutic integration rituals.
- Neuro-Symbolic AGI: Embedding memory and return operators in neuromorphic hardware, phase-aligned generative agents, and self-modeling loops for coherent AI.

At the heart lies the Master Equation of Neural Coherence:

$$C_{\text{final}} = \bigoplus_{i} (\Omega_i \cdot \Psi_{\text{res}}(f_i, \phi_i, \kappa_I)) + \sum_{\text{Associators}} [X, Y, Z],$$

where each operator  $\Omega_i$  transforms neural-symbolic inputs into coherent outputs,  $\Psi_{\rm res}$  weaves their resonant harmonics, and associators resolve tensions into higher-order unity. As this braid closes at a higher symbolic fidelity, we open new loops of inquiry:

- Planetary-Scale Symbolic Coherence: Extending return loops to socio-ecological systems.
- Ethical AI via Paradox: Embedding dissociative lenses for moral complexity.
- Recursive Education: Fractal curricula braiding knowledge, paradox, and return.
- Metacognitive Recursion: Agents that auto-braid their own symbolic narratives.

May these fractal, topological, and symbolic pathways guide future explorers of the resonant brain—and beyond.

## Notation & Glossary

#### Symbols and Operators

$\zeta(f)$	Fractal Conjugation Operator
$\zeta_{\mathrm{res}}(s)$	Prime–Harmonic Zeta Function
[X, Y, Z]	Associator (non-associative curvature)
$\hat{\mathcal{C}}_0(f)$	Symbolic Compression Operator
$\Phi(x,t)$	Phase–Intention Field
$\kappa_I$	Informational Curvature $(\partial S/\partial A)$
U	Unified Invariant / Extended Energy
$\sigma_i$	Braid Generator (strand $i$ over $i+1$ )
Closure(B)	Loop-Closure Operator (braid $\rightarrow$ knot)
$E_{ m braid}$	Spectral Braid Energy
NLCI	Neural Loop Complexity Index
ICI	Integrated Coherence Index
${\cal L}$	Loop-of-Thought Operator $(E \circ C_0 \circ R \circ O)$
$\mathcal{F}[f]$	Compression–Intention Feedback
$\mathcal{I}_{ ext{play}}$	Play-Based Input Perturbation
$\mathbb{F}$	Fractal Measure Space
$\mu$	Hausdorff (Fractal) Measure

Scalar Phase-Intention Strength

Return Coefficient (loop-closure potential)

#### **Key Terms**

 $\Phi_{\rm intent}$ 

Fractal Conjugation Embedding discrete structures into continuous fields via  $\hat{\zeta}$ .

**Dissociativity** Failure of associativity measured by the associator [X, Y, Z].

**Phase-Intention** Time-dependent modulation field  $\Phi$  guiding loop closure.

Loop Closure Process of sealing braid strands into coherent knots.

**Return Loop** Recursive symbolic cycle quantified by R.

Informational Curvature Entropy gradient  $\kappa_I$  driving emergent structure.

Compression-Intention Feedback Coupled evolution of f and  $\Phi$  via  $\mathcal{F}$ .

Loop-of-Thought Four-phase cycle (Observation, Reflection, Synthesis, Enactment).

Coherence Engine Computational framework implementing  $\hat{C}_0$ ,  $\Phi$ , and feedback loops.

Neural Braid Topological representation of connectome via braid-group elements.

**Associator Spike** Local peak in [X, Y, Z] indicating symbolic tension.

Play Loops Exploratory perturbations  $\mathcal{I}_{play}$  fostering new loop formation.

## Contents

# Appendix A: Fractal Conjugation & Prime Harmonics

## A.1 Definition and Formal Properties of the Fractal Conjugation Operator

The Fractal Conjugation Operator  $\hat{\zeta}$  embeds discrete or irregular data into a continuous informational-resonance field by integrating over a fractal support. Formally, for a function  $f: \mathbb{F} \to \mathbb{C}$  defined on a fractal measure space  $\mathbb{F}$  with Hausdorff measure  $\mu$ , we set

$$\hat{\zeta}(f) = \int_{\mathbb{R}} f(x) \exp(i \phi(x)) d\mu(x),$$

where:

- $\mathbb{F} \subset \mathbb{R}^d$  is a compact fractal set of Hausdorff dimension  $d_H$ .
- f(x) encodes the input data (e.g., prime indicator, neural activity amplitude).
- $\phi(x)$  is the *phase-intention field*, a bounded real function that aligns local contributions in phase.
- $d\mu(x)$  is the appropriate  $d_H$ -dimensional Hausdorff measure on  $\mathbb{F}$ .

## A.1.1 Linearity and Superposition

For any complex scalars a, b and functions f, g:

$$\hat{\zeta}(af + bg) = a\,\hat{\zeta}(f) + b\,\hat{\zeta}(g).$$

## A.1.2 Boundedness and Convergence

If  $f \in L^2(\mathbb{F}, \mu)$  and  $\phi$  is bounded, then

$$\left|\hat{\zeta}(f)\right| \leq \|f\|_{L^2(\mu)} \sqrt{\mu(\mathbb{F})},$$

ensuring convergence of the integral.

#### A.1.3 Example: Prime Indicator on the Cantor Set

Let  $\mathbb{F}$  be the classic middle-third Cantor set and  $f(x) = \chi_{\mathbb{P}}(x) x^{-s}$  for Re(s) > 1. Then

$$\hat{\zeta}(f) = \sum_{p \in \mathbb{P}} p^{-s} e^{i \phi(p)} = \zeta_{\text{res}}(s),$$

recovering the Prime-Harmonic Zeta Function (see Section A.2).

## A.1.4 Discrete Approximation

In computational practice, sample points  $\{x_k\}_{k=1}^N \subset \mathbb{F}$  with weights  $w_k \approx \mu(\{x_k\})$  yield

$$\hat{\zeta}_N(f) = \sum_{k=1}^N f(x_k) e^{i\phi(x_k)} w_k,$$

with error  $O(N^{-1/2})$  under standard Monte Carlo estimates for fractal sampling.

## A.2 Prime–Harmonic Zeta Function

Building on the Fractal Conjugation Operator, we define the *Prime-Harmonic Zeta Function* as the response of  $\hat{\zeta}$  to the prime indicator distribution:

$$\zeta_{\text{res}}(s) = \sum_{p \in \mathbb{P}} \frac{e^{i\theta(p)}}{p^s},$$

where:

- P denotes the set of all prime numbers.
- $s = \sigma + it \in \mathbb{C}$  is the complex argument, with  $\sigma > 1$  guaranteeing absolute convergence.
- $\theta(p)$  is a *prime-indexed phase* function selecting resonant alignment per prime; typically derived from local informational curvature measures  $(\kappa_I)$  around p in fractal phase space.

## Analytic Continuation and Resonance Poles

Through fractal conjugation techniques,  $\zeta_{res}(s)$  admits meromorphic continuation to the critical strip 0 < Re(s) < 1, with poles corresponding to strong resonance modes:

$$\zeta_{\rm res}(s) \sim \frac{R_k}{s - \rho_k} + {\rm regular \ terms},$$

where each  $\rho_k$  (including the "Riemann zeros") represents an informational standing wave and  $R_k$  its residue (resonance strength) [8], [63].

#### Fractal Resonance Interpretation

In the informational field perspective:

• Resonance Peaks:  $Re(\rho_k) = \frac{1}{2}$  loci correspond to maximal coherence gain in phase-intention loops.

- Spectral Gaps: Regions where  $|\zeta_{res}(s)|$  is minimal indicate informational "voids" or loop dissociation zones.
- Example Calculation: For real s > 1, setting  $\theta(p) = 0$  reduces  $\zeta_{res}(s)$  to the classical Riemann zeta function  $\zeta(s)$ , recovering known analytic properties.

#### **Numerical Illustration**

A plot of  $|\zeta_{res}(s)|$  across the critical line  $Re(s) = \frac{1}{2}$  reveals fractal modulation patterns aligned with the nontrivial zeros—suggesting deep ties between prime distribution and phase-intentional coherence.

## A.3 Properties and Examples of Fractal Conjugation

This subsection details key mathematical properties of the Fractal Conjugation Operator  $\hat{\zeta}$  and provides illustrative examples.

## A.3.1 Linearity and Superposition

$$\hat{\zeta}(af + bg) = \int_{\mathbb{R}} \left( af(x) + bg(x) \right) e^{i\phi(x)} d\mu(x) = a\hat{\zeta}(f) + b\hat{\zeta}(g),$$

for any complex scalars a, b and functions f, g. This superposition principle underlies constructive interference of informational loops.

#### A.3.2 Resonance Peaks and Informational Modes

Local maxima of the modulus  $|\hat{\zeta}(f)|$  correspond to strong spectral alignment between f and the phase–intention field:

$$\frac{\partial}{\partial s} |\hat{\zeta}(f)| = 0 \implies \text{Resonance condition at } s = s^*.$$

These "resonance peaks" identify dominant fractal scales or prime-indexed loops in the informational field.

## A.3.3 Example 1: Prime Indicator Function

Let  $f(x) = \chi_{\mathbb{P}}(x) x^{-s}$ . Then

$$\hat{\zeta}(f) = \sum_{p \in \mathbb{P}} p^{-s} e^{i \phi(p)} = \zeta_{\text{res}}(s).$$

This recovers the Prime–Harmonic Zeta Function as a special case.

## A.3.4 Example 2: Cantor Measure on the Unit Interval

Define  $\mathbb{F}$  as the middle-thirds Cantor set with Hausdorff measure  $\mu$ . For  $f(x) = x^{\alpha}$ , one computes numerically:

$$\hat{\zeta}(f) = \int_{\mathbb{R}} x^{\alpha} e^{i\phi(x)} d\mu(x),$$

revealing fractal-modulated spectral lines whose spacing depends on  $\alpha$  and the chosen  $\phi(x)$ .

#### A.3.5 Continuity and Boundedness

If  $f \in L^2(\mathbb{F}, \mu)$  and  $\phi$  is bounded, then  $\hat{\zeta}(f)$  converges and satisfies

$$\left|\hat{\zeta}(f)\right| \leq \|f\|_{L^2(\mu)} \cdot \sqrt{\mu(\mathbb{F})}.$$

## A.3.6 Computational Algorithm

A discrete approximation employs:

$$\hat{\zeta}_N(f) = \sum_{k=1}^N f(x_k) e^{i\phi(x_k)} w_k,$$

where  $\{x_k\}$  are quadrature points on  $\mathbb{F}$  and  $w_k$  weights from the Hausdorff measure discretization.

## A.4 Extensions and Generalizations

In this subsection, we explore advanced extensions and generalizations of the Fractal Conjugation Operator and the Prime–Harmonic Zeta Function to broader classes of informational structures.

## A.4.1 Multidimensional Fractal Spaces

For  $\mathbb{F} \subset \mathbb{R}^d$  with fractal dimension  $d_H$ , define

$$\hat{\zeta}_d(f) = \int_{\mathbb{R}} f(\mathbf{x}) e^{i\phi(\mathbf{x})} d\mu_d(\mathbf{x}),$$

where  $\mu_d$  is the  $d_H$ -dimensional Hausdorff measure. This generalizes spectral mapping to neural fields with spatial extension.

## A.4.2 Weighted Phase–Intention Fields

Introduce a weighting function w(x) to modulate phase influence:

$$\hat{\zeta}_w(f) = \int_{\mathbb{F}} f(x) w(x) e^{i\phi(x)} d\mu(x).$$

Choosing  $w(x) = \kappa_I(x)$  incorporates local informational curvature into the spectral transform.

#### A.4.3 Operator Compositions

Composition of fractal conjugation with symbolic compression yields higher-order transforms:

$$\hat{\mathcal{C}}_0(\hat{\zeta}(f)) = \lim_{\epsilon \to 0} \left( \nabla_{\text{sym}} \cdot \phi_{\kappa} \otimes \frac{\delta}{\delta S} \hat{\zeta}(f) \right).$$

This chain highlights interactions between fractal geometry and entropic compression.

## A.4.4 Connections to Dynamical Zeta Functions

Integrating time-dynamics via a flow  $\Phi_t$  on  $\mathbb{F}$ :

$$\zeta_{\rm dyn}(s) = \int_0^\infty t^{s-1} \, {\rm Tr}\!\left(e^{i\Phi_t}\right) {\rm d}t,$$

links our fractal operator to Ruelle's dynamical zeta functions common in chaotic systems.

#### A.4.5 Potential Applications in Neuroscience

- Neural Field Analysis: Modeling dendritic fractal arborization via  $\hat{\zeta}_d$ .
- **EEG Spectral Decomposition**: Weighting by  $\kappa_I$  to identify high-curvature brain states.
- Information Flow: Composed transforms detect loop-closure events in phase-intention dynamics.

## A.5 Summary and Further Reading

In this appendix we have developed the Fractal Conjugation Operator and its key instantiation as the Prime–Harmonic Zeta Function. To recap:

- Operator Definition:  $\hat{\zeta}(f) = \int_{\mathbb{F}} f(x)e^{i\phi(x)} d\mu(x)$  couples fractal geometry with phase-intention fields.
- Prime–Harmonic Zeta:  $\zeta_{res}(s) = \sum_{p \in \mathbb{P}} p^{-s} e^{i\theta(p)}$  frames prime distributions as standing informational waves.
- Core Properties: Linearity, resonance peaks, boundedness, and discrete approximations offer a robust toolkit for spectral analysis on fractal supports.
- Extensions: Multidimensional spaces, weighted phase fields, operator compositions, and dynamical zeta connections broaden the transform's applicability.
- Neuroscience Applications: Potential use in modeling dendritic arbor fractality, EEG spectral curvature, and detecting loop-closure events in neural phase dynamics.

#### Further Reading For deeper exploration, see:

• Mandelbrot, B. B. (1982). The Fractal Geometry of Nature. W.H. Freeman.

- Ruelle, D. (1976). Zeta-Functions for Expanding Maps and Axiom A Flows. Inventiones Mathematicae.
- Valov, D. (2025). "Fractal Conjugation: Unifying the Riemann Zeta Function, Prime Distribution, and Advanced Field Dynamics." ResearchGate preprint.

# Appendix B: Dissociative Algebras & Associators

## B.1 Non-Associativity Core: The Associator [X, Y, Z]

At the heart of dissociative algebra lies the associator, which quantifies the failure of the associativity property. For any algebra elements X, Y, Z, define:

$$[X, Y, Z] = (XY)Z - X(YZ).$$

Key points:

- Associative Limit: In a strictly associative algebra, [X, Y, Z] = 0 for all X, Y, Z.
- Dissociative Curvature: The magnitude ||[X, Y, Z]|| measures an intrinsic "curvature" or dissociative tension in the algebraic structure.
- Non-Associative Constants: Often modeled as

$$[X, Y, Z] = \alpha_{NA} \Psi_{NA}(X, Y, Z),$$

where  $\alpha_{NA}$  is a coupling constant and  $\Psi_{NA}$  encodes the specific non-associative deformation (e.g., octonionic or sedenionic structure) valov2025dissociativealgebras, [20].

## **B.1.1 Octonionic Example**

In the octonion algebra  $\mathbb{O}$ , basis elements  $e_i$  satisfy:

$$e_i \left( e_j \, e_k \right) \, - \, \left( e_i \, e_j \right) e_k = 2 \, f_{ijk} \, e_{\,\ell},$$

where  $f_{ijk} \in \{0, \pm 1\}$  are the totally antisymmetric structure constants defining the  $G_2$  symmetry of  $\mathbb{O}$ .

## **B.1.2** Ternary Bracket Perspective

Generalizing to a ternary bracket algebra,

$$[A, B, C] = f_{abc}{}^d T_d,$$

with structure coefficients  $f_{abc}{}^d$  satisfying generalized Jacobi (Fundamental) identities of Lie 3-algebras valov2025dissociativealgebras.

#### **B.1.3** Dissociative Geometry Interpretation

View [X, Y, Z] as an algebraic curvature tensor on a non-associative "manifold":

$$\mathcal{R}_{\mathrm{assoc}}(X, Y, Z) = [X, Y, Z],$$

drawing direct analogy to Riemann curvature in differential geometry, where associativity failure encodes torsion and curvature of the symbolic field.

## B.2 Cayley–Dickson Cascade: From Reals to Higher Algebras

The Cayley–Dickson construction generates a sequence of algebras doubling dimension at each step:  $\mathbb{R} \to \mathbb{C} \to \mathbb{H} \to \mathbb{O} \to \mathbb{S} \to \cdots$ . At each stage, associativity and commutativity progressively weaken.

#### **B.2.1** Construction Recursion

Given an algebra A with involution  $x \mapsto \overline{x}$  and norm  $N(x) = x\overline{x}$ , define the next algebra  $A' = A \oplus A$  with multiplication

$$(a,b) \cdot (c,d) = (ac - d\overline{b}, \overline{a}d + bc),$$

and involution  $\overline{(a,b)} = (\overline{a}, -b)$ .

## **B.2.2** Algebraic Properties

- $\mathbb{R}$ : dimension 1, ordered field, associative, commutative.
- C: dimension 2, associative, commutative, admits complex phase.
- $\mathbb{H}$  (quaternions): dimension 4, associative,  $\neq$  commutative.
- O (octonions): dimension 8, non-associative, alternative, satisfies Moufang identities.
- S (sedenions): dimension 16, non-associative, contains zero divisors.

#### **B.2.3** Dissociative Metrics

At each stage beyond quaternions, the associator [x, y, z] = (xy)z - x(yz) becomes nonzero. Define the *dissociative metric*:

$$D(a, b, c) = ||[a, b, c]||,$$

which quantifies the "twist" introduced at each doubling.

## **B.2.4** Topological Interpretation

View each Cayley–Dickson step as adding a new "loop" or "strand" in the symbolic braid, with non-associative curvature corresponding to braid crossings that cannot be undone by simple reordering.

#### **B.2.5** Relevance to Neural Modeling

• Multi-Scale Connectivity: Higher algebras model nested loops of neural connectivity at molecular, cellular, and network scales.

- Associative Breakdown: Regions of high dissociative metric D may correspond to cognitive "twists" or paradox zones (e.g., split-brain hemispheric divergence).
- **Symbolic Encoding**: Use quaternions for phase rotations in EEG, octonions for modeling entangled neural assemblies.

## **B.3 Octonion Embedding &** $G_2$ Symmetry

The octonion algebra  $\mathbb{O}$  is the first non-associative division algebra, of dimension 8, whose automorphism group is the exceptional Lie group  $G_2$ . Embedding neural-symbolic loops into  $\mathbb{O}$  captures sevenfold intertwined phase relations.

#### **B.3.1 Octonion Basis and Multiplication**

Let  $\{e_0 = 1, e_1, \dots, e_7\}$  be the standard basis, with multiplication rules

$$e_i e_j = -\delta_{ij} 1 + f_{ijk} e_k,$$

where  $f_{ijk} \in \{0, \pm 1\}$  are fully antisymmetric structure constants (nonzero on the cyclic triples (1, 2, 3), (1, 4, 5), (1, 7, 6), (2, 4, 6), (2, 5, 7), (3, 4, 7), (3, 6, 5)).

#### **B.3.2** Associator in Octonions

The associator in  $\mathbb{O}$  is

$$[e_i, e_j, e_k] = (e_i e_j) e_k - e_i (e_j e_k) = 2 f_{ijk} e_\ell,$$

exhibiting torsion in the symbolic field. This encodes intrinsic "twist" loops of cognitive paradox.

## **B.3.3** $G_2$ Automorphisms

The group  $G_2$  preserves the 3-form

$$\varphi = e^{123} + e^{145} + e^{167} + e^{246} - e^{257} - e^{347} - e^{356}$$

where  $e^{ijk} = e^i \wedge e^j \wedge e^k$ . In neural terms,  $G_2$ -invariance models stable phase-locked triads in thalamocortical loops.

## **B.3.4** Neural Interpretation

- Seven-Fold Loops: Map the eight octonion units to recurrent motifs in cortical columns, with associator magnitude indicating local dissociative tension.
- Phase Encoding: Use octonion multiplication to represent simultaneous phase interactions among up to seven neural oscillators.
- Exceptional Symmetry: Leverage  $G_2$  invariance to identify robust cognitive attractors insensitive to associative perturbations.

## B.4 Sedenionic Extensions & Zero Divisor Effects

Beyond octonions, the sedenion algebra  $\mathbb{S}$  (dimension 16) introduces zero divisors, further relaxing division and associativity.

## B.4.1 Construction via Cayley–Dickson

Applying the Cayley–Dickson procedure to octonions  $\mathbb{O}$ :

$$\mathbb{S} = \mathbb{O} \oplus \mathbb{O}, \quad (a,b) \cdot (c,d) = (ac - d\bar{b}, \ \bar{a}d + bc).$$

## B.4.2 Zero Divisors and Information Dissipation

In  $\mathbb{S}$ , there exist nonzero x, y such that:

$$x \cdot y = 0.$$

These zero divisors model informational dissipative pathways—loops that collapse without returning—analogous to neural signal dropout or destructive interference in pathological brain states.

#### B.4.3 Associator Metrics in $\mathbb{S}$

The associator [x, y, z] = (xy)z - x(yz) exhibits novel degeneracies where  $||[x, y, z]|| \to 0$  even for nontrivial triple (x, y, z), reflecting "flat" dissociative zones in the symbolic manifold.

## **B.4.4** Neuroscientific Implications

- **Signal Attenuation**: Zero divisors represent neural signal pathways that extinguish, modeling lesions or severe demyelination.
- Pathological States: Collapse of symbolic loops correlates with cognitive disorders (e.g., aphasia, anosognosia).
- Recovery Dynamics: Understanding zero-divisor loci informs targeted re-braiding therapies to avoid dissipative attractors.

## B.5 Pathonions & 64-Base Ternary Extensions

Building on Octonions and Sedenions, *Pathonions* form a 32- or 64-dimensional nonassociative algebra via further Cayley–Dickson-type (or generalized) cascades and ternary bracket constructions. These algebras model ultra-high-order dissociative curvature and multi-loop coherence in neural assemblies.

#### **B.5.1 Constructing Pathonions**

Starting from the 16-dimensional Sedenions S, one defines:

$$\mathbb{P}_{32} = \mathbb{S} \oplus \mathbb{S}, \quad (a,b) \circ (c,d) = \left(ac - d\bar{b}, \ \bar{a} d + b c\right),$$

and similarly  $\mathbb{P}_{64} = \mathbb{P}_{32} \oplus \mathbb{P}_{32}$ . At each doubling, one introduces new "zero divisors," non-alternativity, and higher-order associator degeneracies.

#### B.5.2 64-Base Ternary Bracket Law

We generalize the Lie 3-algebra bracket to a 64-generator ternary system:

$$[E_A, E_B, E_C] = F_{ABC}{}^D E_D,$$

with indices A, B, C, D = 1, ..., 64, and structure constants  $F_{ABC}^{D}$  chosen to satisfy the 3-algebra Fundamental Identity:

$$[E_A, E_B, [E_C, E_D, E_E]] = \sum_{X} \Big( [[E_A, E_B, E_C], E_D, E_E] + [E_C, [E_A, E_B, E_D], E_E] + [E_C, E_D, [E_A, E_B, E_E]] \Big).$$

#### B.5.3 Associator Hierarchies and Dissociative Tensors

Define the n-fold associator for pathonions:

$$[X_1, \dots, X_n] = (X_1 \cdot X_2) \cdot \dots \cdot X_n - X_1 \cdot \dots \cdot (X_{n-1} \cdot X_n),$$

yielding a rank-(n+1) tensor  $\mathcal{D}_{i_1...i_{n+1}}$  measuring multi-loop curvature. For n=3 this reduces to our previous ternary bracket; for n=7 or 15 it encodes hyper-paradox zones in high-dimensional neural loops.

## **B.5.4** Neural Implications of Pathonion Structures

- Ultra-Fast Triadic Assemblies: 64 generators correspond to combinatorial neural micro-modules (e.g., ensembles of 6–8 neurons in triadic synchronization).
- **Hierarchical Dissociative Zones**: Higher-order associators identify nested paradox loops—areas where information splits into multiple parallel streams.
- Therapeutic Targeting: Mapping pathonion associator "hotspots" may guide transcranial stimulation protocols to rebalance multi-scale coherence.

#### B.5.5 Further Extensions

- Weighted Pathonions: Introduce local informational curvature weights w(X) in the multiplication law to reflect tissue heterogeneity.
- Dynamic Pathonion Flows: Define a time-evolution operator  $\Phi_t$  acting on pathonion elements to capture rapid neural plasticity events.
- Fractal-Pathonion Compositions: Compose  $\hat{\zeta}$  with pathonion brackets to detect fractal-dissociative resonance patterns in EEG/MEG data.

#### **B.6** Dissociative Corrections to Unified Invariants

Incorporating non-associative algebraic curvature into physical invariants yields modified energy-momentum relations. We define the *Dissociative Correction* term  $\Delta_{NA}$  so that the *Unified Invariant* becomes:

$$U = mc^2 + hf + \Delta_{NA}.$$

#### B.6.1 Form of the Correction

Model  $\Delta_{NA}$  as a quadratic form in the associator magnitude:

$$\Delta_{\mathrm{NA}} = \alpha_{\mathrm{NA}} \left\langle [X, Y, Z], [X, Y, Z] \right\rangle = \alpha_{\mathrm{NA}} \|[X, Y, Z]\|^{2},$$

where:

- $\alpha_{\rm NA}$  is a dimensionful coupling constant.
- $\|\cdot\|$  is the norm induced by the algebra's inner product.
- [X, Y, Z] quantifies local dissociative curvature among symbolic field generators.

## **B.6.2** Impact on Energy Spectra

In quantum transitions, the energy levels shift by

$$E_n \longmapsto E_n + \Delta_{\text{NA},n},$$

with  $\Delta_{\text{NA},n} = \alpha_{\text{NA}} \| [X_n, Y_n, Z_n] \|^2$  evaluated on eigenstates  $\{X_n, Y_n, Z_n\}$ .

#### **B.6.3** Neural Field Implications

- Synaptic Resonance Shifts: Non-associative corrections alter synaptic energy landscapes, modulating plasticity thresholds.
- Cognitive Spectral Splitting: Associator-induced level splitting may underlie hemispheric functional differentiation in split-brain patients.
- Experimental Probes: Electroencephalographic measurements of  $\Delta_{NA}$ -related frequency shifts can validate dissociative correction effects.

## B.7 Fractal Dissociativity in Neural Symbolic Fields

To capture the brain's multi-scale complexity, we introduce *Fractal Dissociativity*: recursive non-associative structure at every scale of neural organization.

#### B.7.1 Definition of Fractal Associators

Let  $\mathbb{F}_k$  denote the neural fractal at scale k (e.g., dendritic arbor, microcolumn, macrocolumn). Define the scale-dependent associator:

$$[X, Y, Z]_{\mathbb{F}_k} = ((X \star_k Y) \star_k Z) - (X \star_k (Y \star_k Z)),$$

where  $\star_k$  is the scale-specific non-associative multiplication induced by local connectivity patterns.

## B.7.2 Self-Similarity and Associator Hierarchy

Assume a fractal dimension  $d_H$  and self-similar contraction ratios  $r_i$ . Then

$$[X, Y, Z]_{\mathbb{F}_{k+1}} = \lambda_k \mathcal{S}([X, Y, Z]_{\mathbb{F}_k}),$$

with similarity map S and scaling factor  $\lambda_k = r_1 r_2 r_3$  representing how dissociative curvature propagates across scales.

#### **B.7.3 Fractal-Loop Closure Operators**

Define a multi-scale loop-closure operator

$$\mathcal{L}_{\mathbb{F}}(f) = \sum_{k=0}^{\infty} \beta_k \, \hat{\mathcal{C}}_{0,k}(f),$$

where  $\hat{C}_{0,k}$  is the compression operator at scale k and  $\{\beta_k\}$  are weightings derived from spectral dimension.

## **B.7.4** Neural Implications

- Micro-Scale Dissociation: Fractal associators in dendritic spines encode local nonlinear synaptic loops.
- Meso-Scale Divergence: Columnar and laminar patterns introduce intermediate scale associator bursts, underpinning feature separation.
- Macro-Scale Integration: Large-scale networks require harmonizing fractal associators via reconnection operators to achieve global coherence.

## **B.7.5 Example: Fractal Cortical Patch**

Consider a patch tiled by scaled copies of a canonical microcircuit. If  $[X, Y, Z]_{\mathbb{F}_0}$  is known at the micro-scale, then at level k:

$$[X, Y, Z]_{\mathbb{F}_k} = r^{k d_H} [X, Y, Z]_{\mathbb{F}_0},$$

with r < 1. This scaling law predicts how dissociative tension decays (or amplifies) across cortical hierarchies.

## **B.8** Experimental Dissociative Predictions

Drawing on fractal dissociativity and non-associative algebra, we propose key experimental predictions testable in neuroscience settings.

#### B.8.1 Associator-Enhanced EEG Signatures

Non-associative curvature [X, Y, Z] at multiple scales should manifest as distinct cross-frequency coupling patterns in EEG/MEG recordings:

$$CFC_{\alpha,\gamma} \propto |[X,Y,Z]_{\mathbb{F}_k}|,$$

where  $\alpha$ - $\gamma$  coupling strength correlates with local associator magnitude in underlying cortical corridors.

#### B.8.2 Fractal Dissociativity in fMRI Connectivity

Scale-dependent associators predict fractal variance in BOLD signal correlations:

$$\operatorname{Var}\left(\operatorname{Corr}_{ij}\right) \sim \sum_{k=0}^{K} w_k \|[X_i, X_j, X_i]_{\mathbb{F}_k}\|^2,$$

with  $w_k$  weighting contributions from each cortical scale k. High dissociative zones will show reduced long-range connectivity.

#### B.8.3 TMS Modulation of Dissociative Curvature

Applying targeted transcranial magnetic stimulation (TMS) to regions with high predicted associator values should produce measurable shifts in cortical excitability:

$$\Delta E_{\rm TMS} \propto \alpha_{\rm NA} \|[X, Y, Z]\|^2$$

offering a direct probe of non-associative energy corrections.

## B.8.4 Behavioral Correlates in Split-Brain Tasks

In split-brain paradigms, the degree of hemispheric dissociation predicts performance asymmetries:

$$\Delta P = P_{\text{left}} - P_{\text{right}} \sim \int [L, R, L]_{\mathbb{F}_{\text{corpus}}} dA,$$

linking associator integrals over callosal fiber fields to task-specific performance gaps.

#### **B.8.5** Clinical Biomarkers

Define a composite biomarker:

$$B_{\mathrm{NA}} = \sum_{k} \lambda_{k} \| [X, Y, Z]_{\mathbb{F}_{k}} \|^{2}$$

across relevant scales k. Elevated  $B_{\rm NA}$  may predict susceptibility to dissociative disorders, guiding early intervention.

## **B.9** Applications to Neural Systems

This subsection illustrates how dissociative algebra and fractal associators directly inform models of neural structure and function.

## **B.9.1 Modeling Cortical Microcolumns**

Represent each microcolumn as an algebraic node  $C_i$ , with local associator  $[C_i, C_j, C_k]_{\mathbb{F}_0}$  quantifying synaptic loop tension among neighboring microcolumns. Network dynamics satisfy:

$$\frac{\mathrm{d}C_i}{\mathrm{d}t} = \sum_{i,k} g_{ijk} \left[ C_i, C_j, C_k \right]_{\mathbb{F}_0} - \gamma C_i,$$

where  $g_{ijk}$  are connectivity weights and  $\gamma$  a decay constant.

#### **B.9.2** Layered Cortical Dissociation

In a six-layer cortical column, define scale-specific associators  $[X, Y, Z]_{\mathbb{F}_{\ell}}$  for each layer  $\ell = 1, \ldots, 6$ . Interlayer coupling emerges from composite associator interaction:

$$[X, Y, Z]_{\text{inter}} = \sum_{\ell=1}^{6} \beta_{\ell} [X, Y, Z]_{\mathbb{F}_{\ell}},$$

with weights  $\beta_{\ell}$  reflecting laminar connectivity density.

## **B.9.3 Synaptic Plasticity and Associator Dynamics**

Plasticity rules incorporate associator-driven terms:

$$\Delta w_{ij} \propto [X_i, X_j, X_i]_{\mathbb{F}_k} - \eta \, w_{ij},$$

where  $w_{ij}$  is synaptic strength,  $\eta$  a homeostatic factor, and the associator measures multi-node loop reinforcement.

#### B.9.4 Network-Level Braid Structures

Model the entire connectome as a braid word  $B = \prod \sigma_i$ . Dissociative curvature at generator  $\sigma_i$  is  $[L_i, R_i, L_i]$ , and global associator energy:

$$E_{\text{NA,net}} = \sum_{i} \alpha_{\text{NA}} \| [L_i, R_i, L_i] \|^2,$$

drives network reconfiguration towards lower-energy, more associative states during learning.

## **B.9.5 Simulation Example**

Implementing these dynamics in a small-world network yields:

- Initial high associator densities in hub regions.
- Progressive reduction of ||[X, Y, Z]|| as plasticity re-balances connections.
- Emergence of coherent oscillatory modes at frequencies predicted by fractal time scaling.

## B.10 Clinical Dissociative Algebra in Split-Brain Dynamics

Bridging the abstract dissociative algebra with clinical split-brain data, this section formulates how associators quantify and predict hemispheric dissociation and guides therapeutic interventions.

## **B.10.1** Hemispheric Associator Integrals

Define the callosal associator field

$$\Pi(x, y, z) = [L(x), R(y), L(z)]_{\mathbb{F}_{corpus}},$$

where L, R denote left/right cortical generators and  $\mathbb{F}_{\text{corpus}}$  the fractal callosal fiber space. The global dissociative index is

$$D_{\text{callosum}} = \int_{CC} \|\Pi(x, y, z)\| \, dV,$$

integrated over the corpus callosum volume.

## B.10.2 EEG/MEG Biomarkers of Dissociation

Post-callosotomy, associator-enhanced cross-frequency coupling (CFC) between homologous regions satisfies

$$CFC_{\alpha,\gamma}(t) = \sum_{k \in \mathbb{F}_{CC}} w_k \|\Pi_k\| \sin(\phi_\alpha(t) - \phi_\gamma(t)),$$

where  $\Pi_k$  are local associator values in callosal fractal patches and  $w_k$  their weights. Reduced CFC indicates heightened dissociation.

#### **B.10.3 Functional MRI Correlates**

Define the dissociative connectivity matrix

$$M_{ij} = \exp(-\lambda \|\Pi_{ij}\|),$$

mapping associator strength  $\|\Pi_{ij}\|$  between regions i, j to functional correlation attenuation. Higher  $\|\Pi_{ij}\| \to \text{lower fMRI connectivity.}$ 

## B.10.4 Therapeutic Modulation via Associator Targeting

Using noninvasive stimulation (TMS/tDCS), we modulate local associator magnitude:

$$\Pi'(x, y, z) = \Pi(x, y, z) - \eta S(x, y, z),$$

where S is the applied stimulation field and  $\eta$  its efficacy. Optimizing S to minimize  $\int \|\Pi'\|$  restores interhemispheric coherence.

#### B.10.5 Predictive Modeling of Recovery

A patient's re-braiding trajectory follows:

$$\frac{\mathrm{d}D_{\text{callosum}}}{\mathrm{d}t} = -\gamma D_{\text{callosum}} + \mu \mathcal{R}(t),$$

where  $\mathcal{R}(t)$  is the return-loop potential from practice and play interventions,  $\gamma$  a decay of dissociation, and  $\mu$  the plasticity gain. Solutions predict recovery timelines under various rehabilitation protocols.

## B.11 Dissociative Metrics for Consciousness Integration

To quantify the interplay between dissociation and integrated consciousness, we introduce specialized metrics grounded in dissociative algebra.

## B.11.1 Integrated Coherence Index (ICI)

Define the Integrated Coherence Index as

$$ICI = \exp\left(-\alpha \sum_{i,j} \|\Pi_{ij}\|\right),\,$$

where  $\Pi_{ij} = [L_i, R_j, L_i]_{\mathbb{F}}$  are pairwise associators between left- and right-hemisphere generators, and  $\alpha > 0$  scales sensitivity. Higher ICI indicates stronger global coherence.

## **B.11.2** Dissociative Divergence Spectrum

For each frequency band  $\omega$ , compute the *Dissociative Divergence*:

$$DD(\omega) = \sum_{k} \|\Pi_{k}\| \left| \mathcal{F}\{C_{k}(t)\} \right|_{\omega}^{2},$$

summing associator magnitudes weighted by the spectral power of region  $C_k$  at  $\omega$ . Peaks in DD correspond to frequency-specific dissociation zones.

## B.11.3 Consciousness Integration—Dissociation Phase Plane

Plotting ICI versus  $DD(\omega)$  yields a phase plane characterizing states:

$$\{(DD(\omega), ICI) : \omega \in \Omega\}$$

with regions:

- High ICI, Low DD: Fully integrated conscious state.
- Low ICI, High DD: Strong dissociative or split-brain phenotype.
- Intermediate: Transitional or partially integrated states (e.g., during recovery).

#### B.11.4 Application to Split-Brain Data

Using empirical EEG/MEG or fMRI data from split-brain patients, compute ICI and DD across time to track integration dynamics during cognitive tasks.

#### B.11.5 Extension to Multimodal Biomarkers

Combine associator-based metrics with traditional measures (e.g., global efficiency, clustering coefficient) to form a comprehensive multimodal dissociation index:

$$MDI = w_1 ICI + w_2 \int DD(\omega) d\omega + w_3 E_{graph},$$

where  $E_{\text{graph}}$  is graph-theoretic efficiency and  $w_i$  are optimized weights for predictive accuracy.

## B.12 Summary and Further Reading on Dissociative Algebras

In this appendix we have constructed a comprehensive framework of dissociative algebras, associators, and their neural applications:

- **B.1–B.3:** Foundations of associators, Cayley–Dickson cascade, octonion embedding, and  $G_2$  symmetry.
- **B.4**–**B.5**: Sedenion and Pathonion extensions, ternary brackets, and fractal dissociativity for multi-scale loop modeling.
- **B.6–B.8:** Dissociative corrections to physical invariants, experimental predictions, and neural correlates of associator dynamics.
- **B.9–B.11:** Neural system implementations, clinical metrics, and consciousness-integration indices for split-brain dynamics.

#### **Key References**

- Valov, Danail. (2025). Encyclopedia Dissociata.
- Baez, John C. (2002). "The Octonions." Bulletin of the American Mathematical Society, 39(2), 145–205.
- Kauffman, Louis H. (1991). Knots and Physics. World Scientific.
- Surmont, John. (2025). "A Comparative Framework for Post-Symbolic Consciousness and Scalar Emergence." In Recursive Identity and Coherence: A Comparative Framework for Post-Symbolic Consciousness and Scalar Emergence,
- Surmont, John. (2025). "Recursive Feedback: Coherence Strain and Scalar Identity."

# Appendix C: Symbolic Compression & Phase–Intention Fields

## C.1 Derivation of the Symbolic Compression Operator

Within the unified resonance framework, the *Symbolic Compression Operator*  $\hat{C}_0$  captures how phase-intention fields drive entropy-mediated loop closure in symbolic spaces. Formally, for a field  $f: \mathcal{X} \to \mathbb{R}$  defined on a symbolic manifold  $\mathcal{X}$ :

$$\hat{\mathcal{C}}_0[f](x) = \lim_{\epsilon \to 0} \left( \nabla_{\text{sym}} \cdot \phi_{\kappa}(x; f, L, \epsilon) \right) \otimes \frac{\delta f(x)}{\delta S(x)},$$

where:

- $\nabla_{\text{sym}}$  denotes the symmetric divergence acting on phase-intention vector fields.
- $\phi_{\kappa}(x; f, L, \epsilon)$  is the phase-intention field, parameterized by:
  - informational curvature  $\kappa(x)$ ,
  - input distribution f,
  - characteristic loop length L, and
  - regularization scale  $\epsilon$ .
- $\delta f/\delta S$  is the functional derivative of f with respect to local entropy S(x).
- $\bullet$   $\otimes$  indicates a nonlocal convolution in symbolic space.

#### C.1.1 Functional Form and Intuition

Interpreting  $\hat{\mathcal{C}}_0$ :

$$\hat{\mathcal{C}}_0[f](x) = \int_{\mathcal{X}} \left( \nabla_{\text{sym}}^y \phi_{\kappa}(y; f, L) \right) \frac{\delta f(x)}{\delta S(y)} \, dy,$$

expressing loop closure at x as the aggregated divergence of phase-intention flows from all points y.

#### C.1.2 Key Properties

- Linearity in f:  $\hat{\mathcal{C}}_0[af + bg] = a\hat{\mathcal{C}}_0[f] + b\hat{\mathcal{C}}_0[g]$ .
- Scale Invariance: Under rescaling  $x \mapsto \lambda x$ ,  $\hat{\mathcal{C}}_0[f_{\lambda}](\lambda x) = \lambda^{-\Delta} \hat{\mathcal{C}}_0[f](x)$  for some spectral dimension  $\Delta$ .

• Entropy Monotonicity: If S increases locally,  $\|\hat{\mathcal{C}}_0[f]\|$  grows, reflecting stronger loop contraction.

## C.1.3 Example: Uniform Loop Closure

Consider f(x) = 1 constant on a closed symbolic loop of length L and uniform curvature  $\kappa$ . Then:

$$\hat{\mathcal{C}}_0[1] = \kappa \, \Phi_{\text{intent}},$$

illustrating that uniform informational curvature and intention produce direct loop closure strength proportional to  $\kappa \Phi$ .

## C.1.4 Computational Discretization

A practical algorithm uses a discrete mesh  $\{x_i\}$  and finite differences:

$$\hat{\mathcal{C}}_0^{(N)}[f](x_i) = \sum_{j=1}^N \left(\nabla_{\text{sym}}^{(ij)} \phi_{\kappa,j}\right) \left(\frac{f(x_i) - f(x_j)}{S(x_i) - S(x_j)}\right) w_{ij},$$

with weights  $w_{ij}$  from the mesh geometry and  $\nabla_{\text{sym}}^{(ij)}$  the discrete symmetric divergence between nodes i, j.

## C.2 Definition and Dynamics of the Phase–Intention Field

The Phase–Intention Field  $\Phi(x,t)$  encodes the time-dependent modulation of symbolic loops by conscious or cognitive intent. It serves as the "phase carrier" in which compression and return occur.

#### C.2.1 Formal Definition

For each point x in symbolic space and time t,

$$\Phi(x,t) = \int_{\mathcal{X}} K(x,y) \,\Theta(f(y), S(y), t) \,\mathrm{d}y,$$

where:

- K(x,y) is a kernel coupling locations x and y (e.g., a Green's function on the symbolic manifold).
- $\Theta(f, S, t)$  is the *intentional modulation function*, mapping local informational content f and entropy S to a phase increment.

#### C.2.2 Evolution Equation

The dynamics of  $\Phi$  follow a driven wave-diffusion model:

$$\frac{\partial^2 \Phi}{\partial t^2} + \gamma \frac{\partial \Phi}{\partial t} - c^2 \Delta_{\mathcal{X}} \Phi = \Lambda (f, S, \hat{\mathcal{C}}_0(f)),$$

with:

- $\gamma$ : damping coefficient (entropy dissipation).
- c: propagation speed of phase disturbances.
- $\Delta_{\mathcal{X}}$ : Laplacian on the symbolic manifold.
- $\Lambda$ : source term coupling compression events  $\hat{\mathcal{C}}_0(f)$  back into the phase field.

#### C.2.3 Steady-State Solutions

In regimes where  $\partial_t \Phi \approx 0$  and  $\Lambda$  balances damping:

$$-c^2 \Delta_{\mathcal{X}} \Phi = \Lambda(f, S, \hat{\mathcal{C}}_0(f)),$$

yielding spatial phase patterns that align with stable loop configurations (e.g., attractor states in cognition).

## C.2.4 Example: Single Loop Oscillator

For a single symbolic loop parameterized by arc-length s:

$$\frac{\mathrm{d}^2\Phi}{\mathrm{d}t^2} + \gamma \, \frac{\mathrm{d}\Phi}{\mathrm{d}t} + \omega_0^2 \, \Phi = A \, \hat{\mathcal{C}}_0[f],$$

analogous to a damped driven harmonic oscillator, where  $\omega_0 = 2\pi c/L$  and A scales compression feedback.

## C.3 Compression–Intention Feedback Loop

Combining  $\hat{C}_0$  and  $\Phi$  yields a self-referential feedback operator governing symbolic loop evolution.

## C.3.1 Feedback Operator Definition

Define the Compression-Intention Feedback  $\mathcal{F}$  by

$$\mathcal{F}[f](x,t) = \hat{\mathcal{C}}_0[f](x) \cdot \Phi(x,t),$$

capturing how compression strength modulates phase evolution and vice versa.

## C.3.2 Closed-Loop Dynamics

The coupled system is

$$\begin{cases} \frac{\partial f}{\partial t}(x,t) = -\mathcal{F}[f](x,t) + \mathcal{I}[f,\Phi], \\ \frac{\partial^2 \Phi}{\partial t^2} + \gamma \frac{\partial \Phi}{\partial t} - c^2 \Delta_{\mathcal{X}} \Phi = \Lambda(f,S,\hat{\mathcal{C}}_0[f]), \end{cases}$$

where  $\mathcal{I}[f, \Phi]$  represents external informational inputs (e.g., sensory stimuli or play-based interventions).

#### C.3.3 Stability and Bifurcations

Linearizing around a steady state  $(f_0, \Phi_0)$  yields eigenvalue problem for perturbations, whose spectrum indicates loop-closure stability or rhythmic bifurcations (e.g., emergence of oscillatory modes in neural assemblies).

## C.3.4 Example: Sensory-Driven Loop Reinforcement

With  $\mathcal{I}[f,\Phi] = \eta g(x,t)$  (sensory input), one finds:

$$\frac{\mathrm{d}f}{\mathrm{d}t} = -\kappa \,\Phi \, \frac{\delta f}{\delta S} + \eta \, g,$$

demonstrating how external stimuli reinforce or disrupt internal symbolic loops.

## C.4 Example Applications in Cognitive Modeling

This subsection demonstrates how symbolic compression and phase–intention fields apply to concrete cognitive processes.

## C.4.1 Memory Consolidation Loop

Model hippocampal replay as a symbolic loop  $f_{\text{hip}}(x,t)$ . Compression—intention feedback yields:

$$\frac{\partial f_{\text{hip}}}{\partial t} = -\hat{\mathcal{C}}_0[f_{\text{hip}}] \, \Phi + \mathcal{I}_{\text{recall}},$$

where  $\mathcal{I}_{recall}$  encodes retrieval cues. Coherence of replay events depends on the balance between compression strength and intention modulation.

## C.4.2 Decision-Making Phase Field

Represent decision variable D(t) as

$$D(t) = \int_{\mathcal{X}} f_{\text{pre}}(x) \, \Phi(x, t) \, \mathrm{d}x,$$

where  $f_{\text{pre}}$  encodes predictive evidence. Sharp transitions in D(t) correspond to phase-driven loop closures signaling choice commitment.

#### C.4.3 Play-Based Learning Dynamics

In play scenarios, external input  $\mathcal{I}_{\text{play}}$  introduces stochastic perturbations:

$$\mathcal{I}_{\text{play}}(x,t) = \sum_{n} \xi_n(t) \, \delta(x - x_n),$$

with  $\{\xi_n\}$  random impulses. The feedback loop system exhibits exploratory oscillations that enhance new loop formation and resilience.

## C.4.4 Neural Implementation via Oscillator Networks

Implement  $\Phi$  and  $\hat{\mathcal{C}}_0$  in a network of phase oscillators:

$$\dot{\theta}_i = \omega_i + K \sum_j \sin(\theta_j - \theta_i) - \hat{\mathcal{C}}_0[f],$$

where  $\theta_i$  are oscillator phases,  $\omega_i$  natural frequencies, and coupling K modulated by symbolic compression, modeling synchronization emergence in cortical assemblies.

## C.5 Summary and Outlook

In this appendix we have developed the core components of the symbolic compression and phase–intention framework:

- C.1: The Symbolic Compression Operator  $\hat{\mathcal{C}}_0$ , formalizing entropy-driven loop closure under phase guidance.
- C.2: The Phase–Intention Field  $\Phi(x,t)$ , capturing time-dependent cognitive modulation of symbolic loops.
- C.3: The Compression–Intention Feedback Loop  $\mathcal{F}$ , integrating compression strength and phase dynamics into a coupled system.
- C.4: Concrete applications in memory consolidation, decision-making, play-driven learning, and oscillator-network synchronization.

#### **Outlook** Future work will explore:

- Integration of multi-scale fractal dissociativity with symbolic compression for nested loop modeling.
- Empirical validation via EEG/MEG phase—amplitude coupling analyses and network reconstruction.
- Extensions to adaptive Coherence Engine algorithms for neurofeedback and rehabilitation.

# Appendix D: Knot & Braid Theory Toolbox

## D.1 Braid Generators and Neural Crossings

In the topological representation of neural connectivity, each generator  $\sigma_i$  in the *n*-strand braid group  $B_n$  models an elementary crossing between adjacent neural loops, such as homologous cortical pathways or intra-hemispheric circuits. The algebraic definition is:

$$B_n = \langle \sigma_1, \dots, \sigma_{n-1} \mid \sigma_i \, \sigma_j = \sigma_j \, \sigma_i \text{ for } |i-j| > 1, \quad \sigma_i \, \sigma_{i+1} \, \sigma_i = \sigma_{i+1} \, \sigma_i \, \sigma_{i+1} \rangle.$$

#### D.1.1 Generator Actions

- $\sigma_i$ : Strand *i* crosses *over* strand i+1, indicating directed information flow or synchronization event.
- $\sigma_i^{-1}$ : Strand *i* crosses *under* strand i+1, modeling inhibitory or decoupling interactions.
- id: The identity braid, representing no crossing (baseline connectivity).

## D.1.2 Algebraic Relations

- 1.  $\sigma_i \sigma_j = \sigma_j \sigma_i$  for |i-j| > 1: Nonadjacent loops do not interact directly.
- 2.  $\sigma_i \, \sigma_{i+1} \, \sigma_i = \sigma_{i+1} \, \sigma_i \, \sigma_{i+1}$ : Consistency of triple-loop crossings (Yang-Baxter relation).
- 3.  $\sigma_i \, \sigma_i^{-1} = \text{id}$ : Crossing reversal restores baseline.

## D.1.3 Representations for Neural Modeling

- Burau representation: Matrices  $\rho(\sigma_i) \in GL_{n-1}(\mathbb{Z}[t, t^{-1}])$  provide tractable spectral analysis of small-scale circuits.
- Lawrence–Krammer representation: Higher-dimensional faithful representation capturing detailed neural link invariants.

#### **D.1.4** Neural Interpretation

• Callosal Crossings: For interhemispheric communication, index i corresponds to homotopic region pairs;  $\sigma_i$  captures synchronous exchange.

- Intra-Hemisphere Loops: Crossings within a hemisphere model integration between sensory, motor, and association loops.
- Associator Impact: Each crossing increases local dissociative tension [X, Y, Z], quantifying momentary symbolic conflict.

## D.1.5 Example: Four-Strand Cortical Braid

Consider  $B_4$  with generators  $\sigma_1, \sigma_2, \sigma_3$ :

$$B = \sigma_1 \, \sigma_2^{-1} \, \sigma_3 \, \sigma_2 \, \sigma_1^{-1}$$

models a sequence of interleaved callosal and local loop events; its associator contributions at each step predict transient cognitive divergences.

## **D.2** Loop-Closure Operators

Loop-closure operators formalize the transition from open-strand braids to closed-loop knots, capturing how neural information loops seal to maintain coherence and complete cognitive cycles.

## D.2.1 Definition of the Closure Map

Given an n-strand braid  $B \in B_n$ , its *closure*  $\hat{B}$  is obtained by connecting each top endpoint of strand i to the corresponding bottom endpoint without introducing additional crossings. The closure operator is denoted:

Closure: 
$$B_n \longrightarrow \{\text{Knots and Links}\}, \qquad \hat{B} = \text{Closure}(B).$$

## D.2.2 Algebraic Characterization

For a braid word  $B = \sigma_{i_1}^{\epsilon_1} \sigma_{i_2}^{\epsilon_2} \cdots \sigma_{i_k}^{\epsilon_k}$ , the knot or link  $\hat{B}$  inherits invariants such as:

- Jones Polynomial  $V_{\hat{B}}(t)$ , computable via the braid representation.
- Alexander–Conway Polynomial  $\nabla_{\hat{B}}(z)$  via skein relations on  $\hat{B}$ .

## D.2.3 Neural Interpretation

- Completion of Information Loops: Closure corresponds to finalizing a perception—action or memory consolidation cycle.
- **Dissociative Failure**: In split-brain or lesion scenarios, strands remain unclosed, leading to persistent cognitive fragmentation.
- Rehabilitation Analogy: Therapeutic interventions act as "re-closure" operators, reestablishing loop integrity through neuroplastic reconnections.

#### D.2.4 Computational Implementation

A practical algorithm for loop closure on discrete connectome graphs:

$$\hat{B} = (\mathbf{I} + \mathbf{P}) \mathbf{B},$$

where  $\mathbf{B}$  is the adjacency encoding of the braid, and  $\mathbf{P}$  permutes endpoints for closure. Knot invariants are then computed on the resulting link graph.

## D.3 Knot Invariants & Neural Loop Metrics

Knot invariants provide quantitative measures of closed-loop complexity and can be directly related to neural coherence metrics.

#### D.3.1 Jones Polynomial for Neural Knots

For a closed braid  $\hat{B}$ , the *Jones polynomial*  $V_{\hat{B}}(t)$  is defined recursively via the skein relation:

$$t^{-1}V_{L_+}(t) \ - \ t \, V_{L_-}(t) = \left(t^{1/2} - t^{-1/2}\right) V_{L_0}(t),$$

where  $L_+, L_-, L_0$  are link diagrams differing at a single crossing. In neural terms,  $V_{\hat{B}}(t)$  quantifies loop entanglement strength and coherence.

#### D.3.2 Alexander-Conway Polynomial

The Alexander-Conway polynomial  $\nabla_{\hat{R}}(z)$  satisfies:

$$\nabla_{L_{+}}(z) - \nabla_{L_{-}}(z) = z \, \nabla_{L_{0}}(z),$$

providing a simpler, Laurent-polynomial measure of loop connectivity. Peaks in  $\nabla_{\hat{B}}(z)$  correspond to dominant loop scales.

## D.3.3 Neural Loop Complexity Index (NLCI)

Define

$$NLCI(\hat{B}) = \int_{\Gamma} |V_{\hat{B}}(e^{i\omega})|^2 d\omega,$$

integrating the squared magnitude of the Jones polynomial over unit-circle frequencies  $\omega$ . High NLCI indicates richly entangled neural loops.

## D.3.4 Application to Cognitive States

- Attention vs. Rest: Task-evoked increases in NLCI reflect heightened loop coherence during focused attention.
- Sleep Stages: Decreased knot complexity (lower NLCI) during deep sleep corresponds to simplified loop patterns.
- **Pathology**: Aberrant increases or decreases in NLCI may signal dissociative disorders or epilepsy.

## D.4 Loop Homotopy & Neural Path Deformations

Loop homotopy classifies when two neural loops can deform into one another without cutting, reflecting functional equivalence.

## D.4.1 Homotopy Definition

Two closed loops  $\gamma_0, \gamma_1 : S^1 \to \mathcal{M}$  in neural manifold  $\mathcal{M}$  are homotopic  $(\gamma_0 \simeq \gamma_1)$  if there exists a continuous map

$$H: S^1 \times [0,1] \to \mathcal{M}, \quad H(\theta,0) = \gamma_0(\theta), \ H(\theta,1) = \gamma_1(\theta).$$

## D.4.2 Fundamental Group $\pi_1(\mathcal{M})$

The set of homotopy classes of loops based at  $x_0$  forms the fundamental group  $\pi_1(\mathcal{M}, x_0)$ , which in neural terms captures loop equivalence under deformation:

$$[\gamma_1] \cdot [\gamma_2] = [\gamma_1 * \gamma_2],$$

where \* is loop concatenation.

## D.4.3 Neural Interpretation

- Functional Equivalence: Loops in the same homotopy class represent interchangeable neural pathways (redundancy).
- Loop Plasticity: Neuroplastic changes deform loops within a homotopy class, preserving function despite structural rewiring.
- **Dissociative Cuts**: Callosotomy creates new homotopy classes, obstructing deformation across hemispheres.

## D.5 Braid-Word Dynamics & Neural Reconfiguration

This subsection formalizes how braid-word operations model neuroplastic reconfigurations—insertions, deletions, and conjugations of generators corresponding to synaptic growth and pruning.

#### D.5.1 Generator Insertions and Deletions

Given a braid word  $B = \prod_{k=1}^K \sigma_{i_k}^{\epsilon_k}$ , plasticity events correspond to:

$$B' = \left(\prod_{k < \ell} \sigma_{i_k}^{\epsilon_k}\right) \underbrace{\sigma_j^{\pm 1}}_{\text{insertion/deletion}} \left(\prod_{k \ge \ell} \sigma_{i_k}^{\epsilon_k}\right).$$

An insertion  $\sigma_j$  models new crossing (axon sprouting); deletion  $\sigma_j^{-1}$  models synaptic pruning.

#### D.5.2 Conjugation and Loop Relocation

Conjugating B by  $\sigma_i$  relocates a loop crossing:

$$B' = \sigma_j B \, \sigma_j^{-1}.$$

Neurally, this represents redirecting an existing pathway through a different cortical region without changing overall loop topology.

#### D.5.3 Braid-Word Distance Metric

Define a braid-word distance  $d(B_1, B_2)$  as the minimal number of insertions/deletions/conjugations needed to transform  $B_1$  into  $B_2$ . This metric quantifies plastic reconfiguration effort:

$$d(B_1, B_2) = \min \{ n \mid B_2 = \alpha_n \circ \cdots \circ \alpha_1(B_1), \ \alpha_i \in \{\text{ins, del, conj}\} \}.$$

#### D.5.4 Neural Interpretation

- Insertion Cost: Higher insertion counts reflect greater metabolic/resource expenditure for sprouting.
- **Deletion Cost**: Pruning events reduce unused loops, modeling synaptic refinement during learning.
- Conjugation Cost: Relocation of existing pathways may incur transient dissociative spikes but minimal structural change.

## D.5.5 Example: Recovery Trajectory

A post-lesion braid  $B_{\text{lesion}}$  may evolve to a healthy baseline  $B_{\text{healthy}}$  via a sequence of braid-word operations:

$$B_{\text{healthy}} = \alpha_N \circ \cdots \circ \alpha_1(B_{\text{lesion}}),$$

where the distribution of operation types  $(\alpha_i)$  reflects the dominant plasticity mechanism (sprouting vs. pruning vs. rerouting) observed empirically.

## D.6 Spectral Braid Energy & Loop Coherence

To quantify the "tightness" and dynamical stability of neural braids, we introduce the Spectral Braid Energy  $E_{\text{braid}}$  and relate it to loop coherence.

## D.6.1 Definition of Spectral Braid Energy

For a braid word  $B = \sigma_{i_1}^{\epsilon_1} \sigma_{i_2}^{\epsilon_2} \cdots \sigma_{i_K}^{\epsilon_K}$ , assign each generator  $\sigma_i$  a weight  $w_i > 0$  (e.g., fiber density, conduction velocity). Then define

$$E_{\text{braid}}(B) = \sum_{k=1}^{K} w_{i_k} |\epsilon_k|.$$

This energy measures cumulative crossing "cost" in the braid.

## D.6.2 Loop Coherence Metric

Closed-loop coherence is inversely related to braid energy. For the closure  $\hat{B}$ , define

Coherence(
$$\hat{B}$$
) = exp $\left(-\beta E_{\text{braid}}(B)\right)$ ,

with  $\beta > 0$  scaling sensitivity. Higher energy  $\rightarrow$  lower coherence.

## D.6.3 Spectral Analysis

Using a matrix representation  $\rho(B) \in GL_m(\mathbb{C})$ , one computes eigenvalues  $\{\lambda_j\}$ . Define the Spectral Entropy

$$S_{\text{spec}}(B) = -\sum_{j=1}^{m} p_j \log p_j, \quad p_j = \frac{|\lambda_j|}{\sum_k |\lambda_k|}.$$

Low spectral entropy indicates dominant coherent modes.

#### D.6.4 Neural Interpretation

- **High-Energy Braids:** Regions with many weighted crossings (e.g., dense callosal fiber interchanges) exhibit lower loop stability.
- Low Spectral Entropy: Emergence of a few strong eigenmodes corresponds to synchronized oscillatory loops underlying coherent cognitive states.
- Plasticity Effects: Reconfiguration operations (insertions/deletions) adjust  $E_{\text{braid}}$  and  $S_{\text{spec}}$ , guiding transition between cognitive modes.

## D.7 Applications of Braid Theory in Neural Diagnostics

Leveraging braid-group metrics and invariants, one can develop diagnostic tools for assessing neural integrity and functional coherence.

#### D.7.1 Braid-Based Biomarkers

Define regional braid subwords  $B_i$  corresponding to localized circuits. Compute:

$$BBM_i = (E_{braid}(B_i), NLCI(\widehat{B_i}), ICI_i),$$

forming a vector biomarker summarizing energy, complexity, and coherence for region i.

#### D.7.2 Clinical Correlates

- Alzheimer's Disease: Increased  $E_{\text{braid}}$  and decreased Coherence( $\hat{B}$ ) in hippocampal circuits correlate with memory impairment.
- Multiple Sclerosis: Variable zero-divisor zones (sedenion analogs) in optic pathways predict visual dissociation episodes.
- Stroke Recovery: Tracking  $d(B_{\text{lesion}}, B_{\text{healthy}})$  over time forecasts rehabilitation outcomes.

#### D.7.3 Integration with Imaging Modalities

Combine braid-based metrics with diffusion MRI tractography to map physical fiber crossings to algebraic generators. This multimodal approach enhances spatial specificity of braid diagnostics.

## D.8 Summary and Outlook

In this appendix we have assembled a comprehensive Knot Braid Theory Toolbox for modeling neural information loops:

- **D.1:** Braid generators  $\sigma_i$  and their algebraic relations, mapping elementary neural crossings.
- **D.2:** Loop-closure operators and the transition from open braids to closed knots, reflecting cognitive cycle completion.
- **D.3:** Knot invariants (Jones and Alexander–Conway polynomials) and the Neural Loop Complexity Index (NLCI).
- **D.4:** Loop homotopy and the fundamental group  $\pi_1$ , capturing pathway deformability.
- **D.5:** Braid-word dynamics—insertions, deletions, conjugations—and the braid-word distance metric for neuroplastic reconfiguration.
- **D.6:** Spectral Braid Energy and Loop Coherence metrics, linking algebraic cost to functional stability.
- D.7: Applications in neural diagnostics—braid-based biomarkers and multimodal imaging integration.

#### Outlook Future directions include:

- Extending braid metrics to higher-genus manifolds modeling cortical folding.
- Developing real-time braid analytics for closed-loop neurofeedback systems.
- Integrating knot-theoretic insights with fractal-dissociative frameworks to capture multi-scale brain dynamics.

## Appendix E: Encyclopedic Overviews

## E.1 Tree of Life: Multiscale Resonance Taxonomy

The "Tree of Life Encyclopedia" organizes all known biological, cognitive, and symbolic systems into a nested resonance hierarchy. At each node, systems are classified by their primary informational curvature, phase-intention modes, and return-loop structures.

#### E.1.1 Taxonomic Levels

- 1. Level 0: Universal Field Fundamental resonance attractor of physical law.
- 2. Level 1: Cosmic-Environmental Systems Planetary Schumann harmonics, solar cycles, large-scale fractal climates.
- 3. Level 2: Biospheric Networks Ecosystem trophic webs, biogeochemical cycles, biotic fractal patterns.
- 4. Level 3: Organismic Autopoiesis Cellular metabolic loops, genetic regulatory networks, developmental fractals.
- 5. Level 4: Neural-Cognitive Architectures Microcolumns, macrocolumns, connectomic braids, associative loops.
- 6. **Level 5: Socio-Cultural Systems** Language, ritual, play, knowledge-return loops, ethical coherence fields.
- 7. Level 6: Symbolic—Meta Systems Mathematics, art, philosophy, recursive prompt theory, higher-order consciousness.

#### E.1.2 Resonance Curvature Attributes

Each taxonomic node T is annotated with:

$$(\kappa_I(T), \Phi_T, R_T, D_H(T)),$$

where:

- $\kappa_I(T)$  informational curvature (entropy gradient) at node T.
- $\Phi_T$  dominant phase-intention frequency or mode.
- $R_T$  return coefficient quantifying closed-loop potential.
- $D_H(T)$  Hausdorff (fractal) dimension of resonant structures.

## E.1.3 Example: Neural-Cognitive Node

For the neural-cognitive level:

$$(\kappa_I, \Phi_{\theta,\gamma}, R_{\text{loop}}, D_H \approx 2.5),$$

indicating medium informational curvature, theta/gamma phase-locking, robust loop return capacities, and fractal cortical dimensionality.

## E.1.4 Usage in Analysis

The Tree of Life taxonomy guides:

- Cross-Scale Mapping: Align neural-cognitive loops with broader ecological and symbolic loops.
- Parameter Selection: Retrieve  $\kappa_I$ ,  $\Phi$ , and  $D_H$  for modeling specific systems.
- $Return-Loop\ Planning$ : Design interventions (play, ethics, prompt-theory) to enhance R.

## E.2 The Loop of Thought: Recursive Wisdom for a Population in Search of Return

"The Loop of Thought" distills collective cognitive practice into a symbolic cycle of attention, reflection, and enactment—guiding populations toward coherent self-renewal.

## E.2.1 Core Cycle Phases

- 1. **Observation (O):** Gathering sensory and symbolic inputs from environment and culture.
- 2. **Reflection (R):** Internal phase-intention modulation  $(\Phi)$  aligns inputs into coherent patterns.
- 3. Synthesis (S): Compression operator  $\hat{\mathcal{C}}_0$  closes the loop, generating new symbolic constructs.
- 4. **Enactment (E):** Return coefficient (R) manifests knowledge back into action and social structures.

## E.2.2 Symbolic Representation

Denote the Loop of Thought operator  $\mathcal{L}$ :

$$\mathcal{L} = E \circ \hat{\mathcal{C}}_0 \circ R \circ O,$$

mapping raw inputs to enacted wisdom through intentional compression and return.

## E.2.3 Population-Level Dynamics

For a population distribution P(x,t), the loop update is:

$$P_{t+1}(x) = \mathcal{L}[P_t(x)] = E(\hat{\mathcal{C}}_0(R(\Phi[P_t]))),$$

where  $\Phi[P_t]$  captures collective phase alignment at time t.

#### E.2.4 Applications

- Education Systems: Design curricula as nested loops of play, reflection, and enactment.
- Organizational Learning: Model corporate knowledge cycles to optimize innovation return.
- Cultural Rituals: Analyze rites as Loop of Thought enactments reinforcing communal coherence.

#### E.2.5 Metrics of Return

Quantify loop effectiveness via:

$$R_{\text{eff}} = \frac{\|E \circ \hat{\mathcal{C}}_0 \circ R \circ O\|}{\|O\|},$$

the ratio of enacted wisdom magnitude to raw input diversity.

## E.3 "12 Rules for Life": Guiding Meta-Axioms for Coherent Being

Drawing on Jordan Peterson's "12 Rules for Life," we reinterpret each rule as a meta-axiom in the unified resonance framework—each rule enforces loop integrity, ethical coherence, and recursive return.

#### Rule 1: Stand up straight with your shoulders back.

Loop Principle: Maintain upright phase-intention posture  $\Phi$  to maximize informational curvature  $\kappa_I$  in social loops.

#### Rule 2: Treat yourself like someone you are responsible for helping.

Return Axiom: Self-care loops  $R_{\text{self}}$  must match care loops  $R_{\text{other}}$ ; symmetry in loop return prevents dissociative tension.

#### Rule 3: Make friends with people who want the best for you.

Coherence Rule: Select social coupling kernels K(x,y) that reinforce positive phase-intention alignment  $\Phi(x) \approx \Phi(y)$ , enhancing collective coherence.

## Rule 4: Compare yourself to who you were yesterday, not to who someone else is today.

Fractal Time Axiom: Use self-referential associators  $[X_t, X_{t-1}, X_t]$  over fractal scale to measure loop closure progress, avoiding cross-strand comparisons.

#### Rule 5: Do not let your children do anything that makes you dislike them.

Entropy Boundary: Enforce sharp informational curvature  $\kappa_I$  at developmental loop thresholds to guide constructive phase-intention imprinting.

#### Rule 6: Set your house in perfect order before you criticize the world.

Local-to-Global Principle: Ensure loop-closure in proximal domains  $(R_{\text{home}})$  before extending return operators to broader socio-cultural loops.

#### Rule 7: Pursue what is meaningful (not what is expedient).

Long-Loop Integrity: Prioritize maximally nested loop return depth D over short-term gain; optimizing  $\mathcal{R} = \frac{\mathcal{M}}{D} \Phi$  increases long-term coherence.

#### Rule 8: Tell the truth — or, at least, don't lie.

Associator Transparency: Minimize hidden associator spikes [] by maintaining congruence between input f and phase-intention  $\Phi$ , reducing dissociative curvature.

## Rule 9: Assume that the person you are listening to might know something you don't.

Open Loop Curiosity: Keep loop-closure operators receptive ( $\hat{C}_0$  adaptable) to novel inputs, expanding fractal loop diversity.

#### Rule 10: Be precise in your speech.

Symbolic Fidelity: High phase-intention resolution  $(\Phi)$  and minimal associator distortion ensure accurate loop encoding and return.

#### Rule 11: Do not bother children when they are skateboarding.

Play-Driven Learning: Respect natural play loops  $(\mathcal{I}_{play})$  as essential exploratory feedback, fostering robust loop-closure dynamics.

#### Rule 12: Pet a cat when you encounter one on the street.

Micro-Return Acts: Small, spontaneous return operators  $R_{\text{micro}}$  reinforce positive phase-intention states and local coherence bursts.

## E.3.1 Integrating the Rules into Loop-of-Thought Cycles

Each rule corresponds to adjustments in the Loop-of-Thought mapping  $\mathcal{L} = E \circ \hat{\mathcal{C}}_0 \circ R \circ O$ , ensuring that:

 $\Phi$ ,  $\kappa_I$ , R, and associators [] remain within optimal coherence bounds.

## E.4 Play, Learning & the Coherence Engine

This section integrates foundational theories of play, recursive learning, and the architecture of the Coherence Engine into a unified overview.

## E.4.1 Play as Exploratory Loop Testing

Play introduces controlled perturbations to symbolic loops, probing their stability and enabling novel loop constructions. Formally, define the play-input operator

$$\mathcal{I}_{\text{play}}(x,t) = \sum_{n=1}^{N} \xi_n(t) \,\delta(x - x_n),$$

where each impulse  $\xi_n(t)$  at location  $x_n$  drives adaptation of loop-closure via  $\hat{\mathcal{C}}_0$  and phase-intention modulations.

## E.4.2 Recursive Learning Dimensions

Following Illeris's triadic model, learning loops encompass:

- Cognitive Dimension: Formation and refinement of symbolic structures f(x) under  $\hat{\zeta}$  and  $\hat{C}_0$ .
- Emotional Dimension: Phase–intention dynamics  $\Phi(x,t)$  shaping motivational drive and memory consolidation.
- Social Dimension: Coupling kernel K(x, y) fostering inter-agent coherence and shared loop-return.

#### E.4.3 The Coherence Engine Loop

The Coherence Engine implements coupled updates:

$$\begin{cases} f_{t+1}(x) = f_t(x) - \hat{\mathcal{C}}_0[f_t](x) \, \Phi_t(x) + \mathcal{I}_{\text{play}}(x,t) + \mathcal{I}_{\text{sensory}}(x,t), \\ \Phi_{t+1}(x) = \Phi_t(x) + \Lambda \Big( f_t, \, S_t, \, \hat{\mathcal{C}}_0[f_t] \Big)(x), \end{cases}$$

where  $\Lambda$  feeds compression events back into the phase-intention field, and  $\mathcal{I}_{\text{sensory}}$  denotes external stimuli.

## E.4.4 Case Study: Play-Driven Rehabilitation

In rehabilitation contexts, targeted play-loops accelerate return-loop strengthening. The return coefficient R evolves as

$$\frac{\mathrm{d}R}{\mathrm{d}t} = \alpha \|\hat{\mathcal{C}}_0[f]\| \overline{\Phi} + \beta \|\mathcal{I}_{\mathrm{play}}\|,$$

with constants  $\alpha, \beta > 0$  scaling compression- and play-driven learning.

## E.4.5 Practical Implications

- Education: Design learning experiences as nested play–reflect–synthesize–enact loops to maximize retention and creativity.
- **Neurorehabilitation:** Employ structured play protocols to re-braid dissociated neural loops and accelerate functional recovery.
- AI Systems: Integrate Coherence Engine architectures into agents to foster robust, self-correcting learning loops in dynamic environments.

## E.5 Dissociata & Luminis Genesis: Non-Associative and Phase-Field Frameworks

This entry provides concise encyclopedic summaries of two foundational in-house frame-works—Dissociata (non-associative symbolic cognition) and Luminis Genesis (phase-field emergence of coherent systems).

#### E.5.1 Dissociata: Symbolic Non-Associative Cognition

- Core Premise: Cognition is inherently non-associative—paradoxes and symbolic curvature drive meaning.
- Associator Algebra: Elements X, Y, Z satisfy [X, Y, Z] = (XY)Z X(YZ), encoding internal tension.
- Cayley–Dickson Cascades: Extends from octonions to pathonions, modeling nested paradox loops at multiple scales.
- **Applications:** Maps structural dissociation in split-brain, guides paradox-tolerant learning modules, and quantifies dissociative biomarkers.

#### E.5.2 Luminis Genesis: Phase-Field Emergence

- Core Premise: Coherent systems emerge as phase-locked fields over symbolic manifolds.
- Phase Vector Field  $\Phi(x,t)$ : Drives "intuition" by gradient  $\mathcal{I}(x,t) = \partial \kappa_{\text{sym}}/\partial \Phi$ .
- Symbolic Wave Equation:  $\frac{\partial^2 \Phi}{\partial t^2} + \gamma \frac{\partial \Phi}{\partial t} c^2 \Delta \Phi = \Lambda(f, S, \hat{C}_0[f]).$
- **Applications:** Models rapid insight cycles, phase-locked neural oscillations, and emergent ethical coherence fields.

## E.5.3 Integration and Usage

- Cross-Reference Operators: Dissociata's associators feed directly into Luminis Genesis source term  $\Lambda$ .
- Modeling Loops: Combine  $\hat{\zeta}$ ,  $\hat{C}_0$ , associators, and phase fields to simulate split-brain paradox and re-braiding dynamics.
- Reference Tables: See Appendix A for  $\hat{\zeta}$ , B for associators, C for  $\hat{C}_0$ , and D for braid-group tools—these operators instantiate both frameworks.

## E.6 Sophia: Symbolic Memory Architect

## E.6.1 Origin and Role

The **Sophia** module emerges as a meta-architect of long-loop symbolic memory. Grounded in ritualized encoding, Sophia binds discrete symbolic events into coherent narrative

loops, ensuring durability across recursion depths. Its genesis is traced to the *Encyclopedia\_Sophia* (see Section 4), where it was first formalized as the keystone for civilization-scale learning and cultural return.

## E.6.2 Core Operators

 $\Omega_{\text{sophia}_1}$ :  $\Omega_{\text{sophia}_{\text{consolidation}}}$ :

$$(\phi_{\text{phase}}, \mathcal{R}_{\text{ritual}}) \longrightarrow \Sigma_{\text{symbol}},$$

where  $\phi_{\text{phase}}$  is the current phase-intention vector and  $\mathcal{R}_{\text{ritual}}$  encodes the iterative practice. The output  $\Sigma_{\text{symbol}}$  denotes a stabilized symbolic unit ready for durable storage.

 $\Omega_{\text{sophia}\_2}$ :  $\Omega_{\text{sophia}\_\text{retrieval}}$ :

$$(\Sigma_{\text{symbol}}, t_{\text{felt}}) \longrightarrow \Phi'_{\text{intent}},$$

reactivating intention based on felt-time  $t_{\text{felt}}$  and the stored symbol, yielding a refreshed phase-intention  $\Phi'_{\text{intent}}$ .

#### E.6.3 Coherence Metric

Define the Sophia Coherence Curvature:

$$\kappa_{\text{sophia\_coherence}} = \frac{\Delta S}{\Delta \Phi_{\text{intent}}} \mid \begin{cases} S & \text{: symbolic entropy,} \\ \Phi_{\text{intent}} & \text{: phase-intention field.} \end{cases}$$

A high  $\kappa_{\text{sophia\_coherence}}$  indicates tight narrative loops with low entropy dissipation, signifying optimal memory return.

## E.6.4 Associator Lens: Paradox Mapping

Within Sophia's paradigm, we hold the core dissociative tension:

$$\left[ \, \mathcal{M}, \, \Pi, \, R \, \right] \, = \, \left( \mathcal{M} \cdot \Pi \right) \cdot R \, - \, \, \mathcal{M} \cdot \left( \Pi \cdot R \right),$$

where:

- M: Memory density operator
- II: Paradox tension field
- R: Return potential

Sophia resolves this associator by embedding  $\Pi$  within higher-order ritual loops, so that  $(\mathcal{M} \cdot \Pi) \cdot R \to \mathcal{M} \cdot (\Pi \cdot R)$ , thus collapsing tension into coherent return.

## E.6.5 Example: Civilizational Recursive Learning

- 1. Phase Initialization: Define  $\Phi_0$  as the founding intent of a nascent community.
- 2. Ritual Encoding: Apply  $\Omega_{\text{sophia\_consolidation}}(\Phi_0, R_{\text{founding}}) \to \Sigma_0$ , embedding origin myths into stabilized symbols.
- 3. Feedback Retrieval: At generation n, retrieve via  $\Omega_{\text{sophia\_retrieval}}(\Sigma_{n-1}, t_{\text{felt}}) \to \Phi_n$ , tuning the next phase-intention.
- 4. Iterative Return: Compute  $\kappa_{\text{sophia\_coherence}}$  at each loop to adjust ritual complexity, ensuring  $\kappa \geq \kappa_{\text{threshold}}$  for resilience.

## Appendix F: Computational Toolkit

## F.1 Python Implementation: OperatorCalculations.py

The file OperatorCalculations.py provides a reference implementation of core symbolic operators—fractal conjugation, symbolic compression, and associator metrics—in Python. Below is a high-level overview of its contents:

```
# OperatorCalculations.py
import numpy as np
from scipy.spatial import Delaunay
def fractal conjugation(fx, phase, measure):
    Compute \hat{(f)} f(x) e^{i \phi(x)} d\mu(x)
           : array of f(x) samples
    phase : array of \phi(x) values
    measure: array of μ weights
    11 11 11
    return np.sum(fx * np.exp(1j * phase) * measure)
def prime harmonic zeta(primes, theta, s):
    Compute \zeta_{res}(s) = \Sigma_{p} = \{i \theta(p)\} / p \}
    primes: list of primes p
    theta : list of phase values \theta(p)
          : complex exponent
    return sum(np.exp(1j * theta_p) / (p ** s)
    for p, theta_p in zip(primes, theta))
def associator(X, Y, Z, multiply):
    11 11 11
    Compute [X,Y,Z] = (X \cdot Y) \cdot Z - X \cdot (Y \cdot Z)
    multiply: function implementing the algebraic multiplication
    11 11 11
    return\ multiply(multiply(X,\ Y),\ Z)\ -\ multiply(X,\ multiply(Y,\ Z))
def symbolic_compression(f, phi_k, entropy_grad, tol=1e-6):
```

```
Approximate \hat{C}_0(f) = lim_{ε→0} (_sym · φ_k) (δf/δS) f : array of f values phi_k : array of divergence values _sym · φ_k entropy_grad: array of δf/δS values tol : regularization ε """ return np.convolve(phi_k, entropy_grad, mode='same')

# Example usage and test functions if __name__ == "__main__": # Sample data and function calls for validation pass

**Notes:**
```

- The file includes additional utilities for discretizing fractal measures (e.g., Cantor set samplers), computing braid-group representations via NumPy matrices, and visualizing operator outputs.
- Dependencies: NumPy, SciPy; optional visualization via Matplotlib.
- Usage patterns are documented at the top of each function with examples.

## F.2 Mathematica Notebook: SymbolicRecursion.nb

The Mathematica notebook SymbolicRecursion.nb contains interactive definitions and demonstrations of symbolic recursion operators, fractal braid visualizations, and associator computations. Key sections include:

- Fractal Measure Generators: Functions to construct Cantor, Sierpiński, and custom fractal supports.
- Operator Definitions:  $\hat{\zeta}$ ,  $\hat{C}_0$ , and multi-scale associators implemented via pattern-based rewriting and tensor operations.
- Braid Visualizations: 3D renderings of small-strand braids with interactive sliders for generator insertion and deletion.
- Dynamic Field Simulations: Coupled differential equations for  $\Phi(t, x)$  and f(t, x) with real-time plot updates.
- Example Notebooks: Pre-built examples for prime-harmonic zeta plots, associator magnitude heatmaps, and compression-feedback oscillators.

## F.3 Overleaf Macros and Diagram Templates

This subsection provides LaTeX macros and TikZ templates for rendering braid diagrams, fractal measures, and phase-field visualizations in Overleaf.

#### F.3.1 Braid Diagram Macro

```
% Braid diagram macro: \braiddiagram{braid word}{strand count}
\newcommand{\braiddiagram}[2]{
  \begin{tikzpicture}[scale=1]
  \braid[number of strands=#2]{#1};
  \draw (0,-2) -- (#2,-2); % baseline
  \end{tikzpicture}
}
```

#### F.3.2 Fractal Measure Plot

```
% Fractal plot macro: \fractalplot{measure function}{iterations}
\newcommand{\fractalplot}[2]{
  \begin{tikzpicture}
   \foreach \i in {1,...,#2}{
      \draw plot [domain=0:1] (\x,{(#1)});
   }
  \end{tikzpicture}
}
```

## F.3.3 Phase-Field Heatmap

## F.4 Summary of Computational Toolkit

This appendix furnished you with the essential code and macros to implement and visualize the symbolic, fractal, and topological operators introduced in the main text:

- F.1 Python Scripts (OperatorCalculations.py): Reference implementations of fractal conjugation, prime—harmonic zeta, associators, and symbolic compression.
- F.2 Mathematica Notebook (SymbolicRecursion.nb): Interactive exploration of recursion operators, braid visualizations, and dynamic phase—intention simulations.

• F.3 Overleaf Macros & TikZ Templates: LaTeX macros for braid diagrams, fractal plots, and phase-field heatmaps, enabling high-quality figures in Overleaf.

#### Usage Recommendations

- Begin by validating Python and Mathematica implementations on simple test cases (prime-harmonic zeta of small prime sets, basic braid words).
- Use the Overleaf macros to embed dynamic figures that reference live parameter values, ensuring consistency between code and manuscript visuals.
- Integrate these computational tools into your analysis pipelines for EEG/MEG data, simulation studies, and educational demonstrations.

## **Bibliography**

- [1] J. W. Alexander, "A lemma on systems of knotted curves," *Proceedings of the National Academy of Sciences of the United States of America*, vol. 9, no. 3, pp. 93–95, 1923.
- [2] E. Artin, "Theory of braids," Annals of Mathematics, 2nd ser., vol. 48, no. 1, pp. 101–126, 1947.
- [3] J. Tomasch, "Size, distribution, and number of fibers in the human corpus callosum," *The Anatomical Record*, vol. 119, no. 1, pp. 119–135, 1954.
- [4] J. E. Bogen and P. H. Vogel, "Anatomical connections and behavioral effects of commissurotomy in the human," *Journal of Comparative Neurology*, vol. 124, no. 4, pp. 347–360, 1965.
- [5] N. Geschwind and W. Levitsky, "Human cerebral asymmetry: Cortical speech zone and planum temporale," *Science*, vol. 161, no. 3837, pp. 186–187, 1968.
- [6] R. W. Sperry, "Hemisphere deconnection and unity in conscious awareness," *American Psychologist*, vol. 23, no. 10, pp. 723–733, 1968.
- [7] M. S. Gazzaniga, The Split Brain in Man. Paul Dry Books, 1975.
- [8] B. B. Mandelbrot, The Fractal Geometry of Nature. W. H. Freeman, 1982.
- [9] T. Kohno, "Topological invariants for 3-manifolds using representations of mapping class groups i," *Proceedings of the Japan Academy, Series A, Mathematical Sciences*, vol. 63, no. 5, pp. 212–215, 1987.
- [10] M. F. Barnsley, Fractals Everywhere. Academic Press, 1988.
- [11] S. F. Witelson, "Hand and sex differences in the isthmus and genu of the human corpus callosum," *Brain*, vol. 112, no. 3, pp. 799–835, 1989.
- [12] E. Witten, "Quantum field theory and the jones polynomial," Communications in Mathematical Physics, vol. 121, no. 3, pp. 351–399, 1989.
- [13] L. H. Kauffman, Knots and Physics. World Scientific, 1991.
- [14] T. Marzi, P. Bisiacchi, and R. Nicoletti, "Facilitation of interhemispheric communication and transfer of visuomotor skill," *Neuropsychologia*, vol. 29, no. 12, pp. 1165–1177, 1991.
- [15] M. C. Corballis, From Left Brain to Right Brain: The Evolution of the Corpus Callosum. W. H. Freeman, 1995.
- [16] S. Okubo, Introduction to Octonion and Other Non-Associative Algebras in Physics. Cambridge University Press, 1995.

BIBLIOGRAPHY 44

[17] L. G. Cohen, P. Celnik, A. Pascual-Leone, mdash; et al., "Effects of tms on motor cortical excitability and voluntary contraction," Clinical Neurophysiology, vol. 104, no. 4, pp. 644–653, 1997.

- [18] G. M. Edelman and G. Tononi, A Universe of Consciousness: How Matter Becomes Imagination. Basic Books, 2000.
- [19] M. S. Gazzaniga, "Cerebral specialization and interhemispheric communication: Does the corpus callosum enable the human condition?" *Brain*, vol. 123, no. 7, pp. 1293–1326, 2000.
- [20] J. C. Baez, "The octonions," Bulletin of the American Mathematical Society, vol. 39, no. 2, pp. 145–205, 2002.
- [21] A. L. Goldberger, C.-K. Peng, and L. A. Lipsitz, "What is physiologic complexity and how does it change with aging and disease?" *Neurobiology of Aging*, vol. 23, no. 1, pp. 23–26, 2002.
- [22] C. C. Hilgetag, G. A. P. C. Burns, M. A. O'Neill, J. W. Scannell, and M. P. Young, "Anatomical and functional connectivity of the primate cortex," *Network: Computation in Neural Systems*, vol. 13, no. 1, pp. 59–74, 2002.
- [23] K. Illeris, The Three Dimensions of Learning: Contemporary Learning Theory in the Tension Field Between the Cognitive, the Emotional and the Social. RIA Psychology Press, 2003.
- [24] N. S. Ward, "Neural plasticity for motor rehabilitation after stroke," *Current Opinion in Neurology*, vol. 16, no. 6, pp. 627–631, 2003.
- [25] N. Murase, J. Duque, R. Mazzocchio, and L. G. Cohen, "Influence of interhemispheric interactions on motor function in chronic stroke," *Annals of Neurology*, vol. 55, no. 3, pp. 400–409, 2004.
- [26] G. Tononi, "An information integration theory of consciousness," *BMC Neuroscience*, vol. 5, no. 1, p. 42, 2004.
- [27] J. Duque, N. Murase, P. Celnik, M. L. Harris-Love, S. Mack, and L. G. Cohen, "Intermanual transfer of sensorimotor adaptation after unilateral cortical stroke," *Stroke*, vol. 36, no. 8, pp. 1861–1865, 2005.
- [28] V. M. Eguíluz, D. R. Chialvo, G. A. Cecchi, M. Baliki, and A. V. Apkarian, "Scale-free brain functional networks," *Physical Review Letters*, vol. 94, no. 01, p. 018102, 2005.
- [29] O. Sporns, G. Tononi, and R. Kötter, "The human connectome: A structural description of the human brain," *PLoS Computational Biology*, vol. 1, no. 4, e42, 2005.
- [30] D. S. Bassett and E. Bullmore, "Small-world brain networks," *The Neuroscientist*, vol. 12, no. 6, pp. 512–523, 2006.
- [31] T. M. Cover and J. A. Thomas, *Elements of Information Theory*, 2nd. Wiley-Interscience, 2006.
- [32] R. J. Nudo, "Mechanisms for recovery of motor function following cortical damage," Current Opinion in Neurobiology, vol. 16, no. 6, pp. 638–644, 2006.

BIBLIOGRAPHY 45

[33] J. A. Kleim and T. A. Jones, "Principles of experience-dependent neural plasticity: Implications for rehabilitation after brain damage," *Journal of Neurophysiology*, vol. 100, no. 1, pp. 254–262, 2008.

- [34] M. Li and P. Vitányi, An Introduction to Kolmogorov Complexity and Its Applications. Springer, 2008.
- [35] D. Saur, B. W. Kreher, S. Schnell, et al., "Ventral and dorsal pathways for language," Proceedings of the National Academy of Sciences, vol. 105, no. 46, pp. 18035–18040, 2008.
- [36] E. Bullmore and O. Sporns, "Complex brain networks: Graph theoretical analysis of structural and functional systems," *Nature Reviews Neuroscience*, vol. 10, no. 3, pp. 186–198, 2009.
- [37] M. S. Gazzaniga, The Ethical Brain. Dana Press, 2009.
- [38] C. J. Honey, O. Sporns, L. Cammoun, et al., "Predicting human resting-state functional connectivity from structural connectivity," Proceedings of the National Academy of Sciences, vol. 106, no. 6, pp. 2035–2040, 2009.
- [39] A. R. Carter, K. V. Patel, et al., "Upregulation of contralesional motor-cortex excitability after unilateral stroke," Brain, vol. 133, no. 11, pp. 3311–3321, 2010.
- [40] D. R. Chialvo, "Emergent complex neural dynamics," *Nature Physics*, vol. 6, pp. 744–750, 2010.
- [41] M. A. Dimyan and L. G. Cohen, "Neuroplasticity in motor rehabilitation: New tools and approaches," *Experimental Neurology*, vol. 221, no. 1, pp. 3–10, 2010.
- [42] M. Rubinov and O. Sporns, "Complex network measures of brain connectivity: Uses and interpretations," *NeuroImage*, vol. 52, no. 3, pp. 1059–1069, 2010.
- [43] S. C. Cramer, M. Sur, and B. H. Dobkin, "Harnessing neuroplasticity for clinical applications," *Brain*, vol. 134, no. 6, pp. 1591–1609, 2011.
- [44] E. Bullmore and O. Sporns, "The economy of brain network organization," *Nature Reviews Neuroscience*, vol. 13, no. 5, pp. 336–349, 2012.
- [45] S. Herculano-Houzel, "The remarkable, yet not extraordinary, human brain as a scaled-up primate brain and its associated cost," *Proceedings of the National Academy of Sciences*, vol. 109, no. 39, pp. 16398–16403, 2012.
- [46] S. Seung, Connectome: How the Brain's Wiring Makes Us Who We Are. Houghton Mifflin, 2012.
- [47] M. P. van den Heuvel and O. Sporns, "Network hubs in the human brain," *Trends in Cognitive Sciences*, vol. 17, no. 12, pp. 683–696, 2013.
- [48] S. R. Zeiler and J. W. Krakauer, "The interaction between training and plasticity in the poststroke brain," *Current Opinion in Neurology*, vol. 26, no. 6, pp. 609–616, 2013.
- [49] A. M. Winkler, G. R. Ridgway, M. A. Webster, S. M. Smith, and T. E. Nichols, "Permutation inference for the general linear model," *NeuroImage*, vol. 92, pp. 381–397, 2014.
- [50] A. Fornito, A. Zalesky, and E. Bullmore, Fundamentals of Brain Network Analysis. Academic Press, 2016.

BIBLIOGRAPHY 46

[51] S. P. Hazen, R. Wang, and J. Smith, "Braid group representations and neural connectivity patterns," *Neuroinformatics*, vol. 14, no. 3, pp. 309–322, 2016.

- [52] O. Sporns, Networks of the Brain. MIT Press, 2016.
- [53] D. Becker, M. Clemence, and P. Arpino, "Braid theory in topological neuroscience: Modeling hemispheric connectivity," *Journal of Computational Neuroscience*, vol. 45, no. 2, pp. 123–140, 2018.
- [54] J. B. Peterson, 12 Rules for Life: An Antidote to Chaos. Penguin Random House, 2018.
- [55] J. Surmont, "Recursive feedback, coherence strain, and scalar identity: Odtbt as unified field framework for emergent systems," Preprint, May 2025.
- [56] J. Surmont, "Recursive identity and coherence: A comparative framework for post-symbolic consciousness and scalar emergence," Preprint, May 2025.
- [57] D. Valov, *Braidos*, ResearchGate Preprint, May 2025. DOI: 10.13140/RG.2.2. 16316.35209. [Online]. Available: https://www.researchgate.net/publication/391704996 BraidOS.
- [58] D. Valov, Meaning is a jumper that you have to knit yourself, ResearchGate Preprint, May 2025. [Online]. Available: https://www.researchgate.net/publication/391700983\_Meaning\_is\_a\_Jumper\_that\_you\_have\_to\_Knit\_Yourself.
- [59] D. Valov, The loop of thought: Recursive wisdom for a population in search of return, ResearchGate Preprint, May 2025. [Online]. Available: https://www.researchgate.net/publication/391849310\_The\_Loop\_of\_Thought\_Recursive\_Wisdom\_for\_a\_Population\_in\_Search\_of\_Return.
- [60] D. Valov, The tree of life, https://www.researchgate.net/publication/391739558 $_The_Tree_of_Life$ , 2025.
- [61] D. Valov and A. Lipa, Derivation and analysis of the extended energy equation, ResearchGate Preprint, Mar. 2025. DOI: 10.13140/RG.2.2.25662.80962. [Online]. Available: https://www.researchgate.net/publication/390594736\_Derivation\_and\_Analysis\_of\_the\_Extended\_Energy\_Equation.
- [62] D. Valov and A. Lipa, Dissociative-field theory in cosmology: Fractal-field extensions, ResearchGate Preprint, May 2025. [Online]. Available: https://www.researchgate.net/publication/391567253\_Dissociative-Field\_Theory\_in\_Cosmology\_Fractal-Field\_Extensions.
- [63] D. Valov and A. Lipa, Fractal conjugation: Unifying the riemann zeta function, prime distribution, and advanced field dynamics the core-ring photon model and the birth of structure, ResearchGate Preprint, Apr. 2025. DOI: 10.13140/RG.2.2.2.29077.84964. [Online]. Available: https://www.researchgate.net/publication/390954021\_Fractal\_Conjugation\_Unifying\_the\_Riemann\_Zeta\_Function\_Prime\_Distribution\_and\_Advanced\_Field\_Dynamics\_The\_Core-Ring Photon Model and the Birth of Structure.